The non-covalent compatibilization of carbon nanotubes for use in polymeric composite materials

By Kerstin Scharlach

Thesis presented in partial fulfilment of the requirements for the degree of Master of Science (Polymer Science)

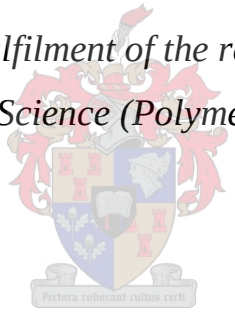

Supervisor: Prof Peter Mallon

University of Stellenbosch

Department of Chemistry and Polymer Science

April 2014

Declaration

By submitting this thesis electronically, I declare the entirety of the work contained therein is my own, original work, that I am the owner of the copyright thereof (unless to the extent explicitly otherwise stated) and that I have not previously in its entirety or in part submitted it for obtaining any qualification.

Kerstin Scharlach February 2014

The Abstract

Since the discovery of carbon nanotubes (CNTs), a large interest has developed around the incorporation of these into polymeric matrices in order to introduce the excellent mechanical, thermal and electrical properties of CNTs into the resultant composites. Nanocomposites of polymer/CNT composition allow for the favourable combination of the physical properties of the polymeric matrix and of the CNT filler.

The biggest existing challenge of producing such nanocomposites is presented by the tendency of CNTs to occur in bundles or aggregates which are difficult to break up and to disperse in solution which leads to non-uniform distributions within the polymeric matrix. This problem has been combated through the use of CNT surface functionalization. However, a disadvantage exists with this solution. Since covalent functionalization of the CNT surface disrupts the electronic π-electron cloud which is responsible for the excellent electronic properties which CNTs are often desired for, an alternative method of functionalization must be employed in order to maintain the excellent intrinsic properties of CNTs yet create uniform dispersion of the nanotubes upon compatibilization with the polymeric matrix.

Two alternative methods for the production of noncovalent compatibilization of multi-walled carbon nanotubes (MWNTs) with polystyrene were investigated and compared. These two methods involved the synthesis of a pyrene-functional macroinitiators for reversible addition fragmentation chain transfer (RAFT) and atom transfer radical polymerization (ATRP). Both of these methods allow for the controlled polymerisation of pyrene functional polystyrene chains. For comparison, the direct covalently functional MWNTs were also synthesised first by oxidation of the MWNT surface and conversion of the MWNT into the multifunctional RAFT and ATRP macroinitiator in which the styrene chains were controllably directly grafted from the surface of the MWNTs. The interaction of the pyrene chains with MWCNTs was monitored by using NMR, TGA and fluorescence spectroscopy.

The NMR results showed the broadening and weakening of the pyrene protons as well as the polystyrene (PS) protons. TGA showed the loss of the pyrene-functional PS portion throughout the heating process. Fluorescence provided the conclusive result that the noncovalent compatibilization had occurred through the quenching of the emission and

excitation signals as a result of electron transfer being facilitated by the π-stacking interactions.

Finally, the MWNT nanocomposite polymer nanofibres are produced via the electrospinning technique with the various covalent and non-covalent compatibilized MWNT. The fibre morphology for the different compatibilization methodologies is compared as a function of the MWNT content. Distinct differences are observed for the different composites.

Opsomming

Sedert die ontdekking van koolstof-nanobuisies (KNBs), het ’n groot belangstelling ontwikkel rondom die betrekking van KNBs in polimeriese matrikse om samestellings met uitstekende meganiese, termiese en elektriese eienskappe te vervaardig. Nanosamestellings van polimeer/KNB komposisie laat toe dat gunstige kombinasies van fisiese eienskappe van die polimeer en die KNB vuller gerealiseer kan word.

Die grootste uitdaging van die vervaardiging van sulke nanosamestellings is die neiging van KNBs om gebondelde formasie te vorm wat baie moeilik is om op te breek. Dit maak hulle verspreiding in oplossings en in polimeer matrikse oneweredig. Hierdie probleem word deur funksionalisering opgelos. Nogtans, ’n nadeel van hierdie oplossing is dat kovalente funksionalisering verander die elektroniese struktuur van die KNB oppervlakte deur die ontwrigting van die π-elektron wolk wat vir die uitstekende elektroniese eienskappe verantwoordelik is. Dus moet ’n alternatiewe funksionalisering metode gebruik word om die inherente eienskappe van die KNBs te behou en terselfde tyd ’n uniforme verspreiding te bewerkstellig gedurende die vermenging met die polimeer matriks.

Twee alternatiewe metodes vir die vervaardiging van nie-kovalente gefunksionaliserde multi-ommuurde koolstof-nanobuisies (Eng: MWNTs) met polistireen (PS) was ondersoek en vergelyk. Hierdie twee metodes was uitgevoer deur die sintese van ’n pyreen-funksionele omkeerbare addisie-fragmentasie-kettingoordrag (OAFO) en atoomorrdragradikaaladdisie (AORA) makromiddel. Al twee van hierdie metodes lei tot ’n gekontrollerde polimerisasie van pyreen-gefunksionaliserde stireen. Vir vergelyking was ’n kovalente- gefunksionaliserde MWNT vervaardig deur die oksidasie van die MWNT oppervlakte en die daaropvolgende immobilisasie van dieselfde AORA en OAFO middel aan hierde aktiewe punte. Daarvan af was stireen gekontroleerd gepolimeriseer deur middel van die AORA en OAFO middel. Die interaksie was gekarakteriseer deur TGO, KMR en fluoressensie spektroskopie.

Die KMR resultate het seine gewys van die verspreiding en verswakking van die pyreen en PS protone. TGO het die verlies van die pyreen-funksionele PS deel van die nie-kovalente produk gewys. Fluoressensie het beslissende bewyse gelewer dat die nie-kovalente

funksionalisiering plaas gevind het deur die onderdrukking van die stralende en opwekkings seine as ŉ gevolg van die elektron oordrag wat deur die π-stapel interaksies gefasiliteer word.

Uiteindelik was die nanosamestellings vermeng met PS en geelektrospin. Die vesel morfologie vir die verskillende gefunksionaliserde MWNT nanosamestellings metodes was vergelyk as ŉ funksie van MWNT inhoud. Duidelike verskille is waargeneem vir die verskillende samestellings.

Acknowledgements

First and foremost I have to thank my parents for allowing me to take a leap of faith by studying at Stellenbosch and for always showing an interest in my studies, for supporting me all this time and for all the words of wisdom, prayers, love and comfort. Many lessons were learnt. My sister and her family are thanked for providing me with happiness, love and such a support network.

Dino, you have really carried me through this time. I could never have come this far without your help, love, support and constant encouragement. Thank you to you and your family for being so understanding and supportive.

I am very grateful for all the friends that I have known for years and those that I have found at Stellenbosch. I have had the best time with you.

My supervisor Prof Peter Mallon is extremely thankfully acknowledged for all his help, guidance and his constant “open-door” policy. His patience never seemed to run out which, at times, is nothing short of a miracle. Thank you for this opportunity.

All the staff of the Department of Chemistry and Polymer Science at Stellenbosch allowed for this project to progress: Mrs Erinda Cooper, Mrs Aneli Fourie, Mr Deon Koen, Mr Jim Motschweni, Mr Calvin Maart and Elsa Malherbe at NMR for running all my samples.

A big thank you to Hussein Etmimi for always being willing to help me and to Mohamed Jaffer at the electron microscope unit at UCT who went out of his way several times to help me to get descent TEM images. I really appreciate your help!

List of Contents

List of Figures

List of Schemes

List of Tables

List of Abbreviations

AIBN	2,2'-Azobis(isobutyronitrile)
ATR	Attenuated total reflectance
ATRP	Atom transfer radical polymerization
BPO	Benzoyl peroxide
$CDCl_3$	Deuterated chloroform
CNT	Carbon nanotube
CRP	Conventional free radical polymerization
CRP	Conventional free radical polymerization
CTA	Chain transfer agent
CVD	Chemical vapour deposition
DCC	1,3-Dicyclohexyl carbodiimide
DCM	Dichloromethane
DDI	Distilled deionized
DIBTC	S-1-dodecyl-S'-(isobutyric acid) trithiocarbonate
DIBTC-PS-Py	Dodecyl isobutyric acid trithiocarbonate-polystyrene-pyrene
DMAP	4-Dimethylamino pyridine
DMF	Dimethylformamide
DMSO-d_6	Deuterated dimethyl sulfoxide
FT-IR	Fourier transformed-infrared
GO	Graphitic oxide
HD	Hexadecane
HEBrIB	Hydroxyethyl-2-bromoiobutyrate
HEBrIB-Py-PS	Hydroxyethyl-2-bromoiobutyrate-Pyrene-PS
LRP	Controlled/living radical polymerization
M	monomer
MMA	Methyl methacrylate
MWNT	Multi-walled nanotube
MWNT/PyPS	MWNT/Pyrene-polystyrene
MWNT-COOH	oxidized MWNT
MWNT-DIBTC	DIBTC immobilized MWNTs

MWNT-HEBrIB-PS	Multi-wall carbon nanotube-polystyrene-hydroxyethyl-2-bromoiobutyrate
MWNT-PS	Multiwall carbon nanotube-polystyrene
MWNT-PS-DIBTC	Multi-wall carbon nanotube-polystyrene-dodecyl isobutyric acid trithiocarbonate
NMP	Nitroxide-mediated polymerization
NMR	Nuclear magnetic resonance
NMRP	Nitroxide-mediated radical polymerization
pBIEM	Poly-(2-(bromoisobutyryloxy) ethyl methacrylate)
PCN	Polymer/carbon nanotube nanocomposite
PEO	Poly (ethylene oxide)
PMDETA	N,N,N′,N″,N″-Pentamethyldiethylenetriamine
PMMA	Poly (methyl methacrylate)
PS	Polystyrene
PVA	Polyvinyl alcohol
Py	Pyrene
RAFT	Reversible addition fragmentation chain transfer
RI	Refractive index
ROMP	Ring-opening metathesis polymerization
S	Styrene
SDBS	Sodium dodecylbenzene sulfonate
SEC	Size exclusion chromatography
SEM	Scanning electron microscopy
SI-ATRP	Surface-initiated atom transfer radical polymerization
SI-RAFT	Surface-initiated reversible addition fragmentation chain transfer
SWNT	Single-walled nanotube
TEM	Transmission electron microscopy
TGA	Thermogravimetric analysis
THF	Tetrahydrofuran
TLC	Thin layer chromatography
UV	Ultraviolet
UV/Vis/NIR	Ultraviolet-visible-near-infrared spectroscopy
UV-Vis	Ultraviolet-visible spectroscopy

List of Symbols

wt%	Weight percentage
$\overrightarrow{C_h}$	Roll-up vector of graphene
k_t	Rate of termination constant
k_{td}	Rate of disproportionation constant
k_i	Rate of reinitiation constant
k_p	Rate of propagation
$(\mathrm{M}_t^n - \mathrm{Y/L})$	A transition metal/ligand complex
k_{act}	Initiating alkyl halide rate of activation constant
$\bar{M}_w$	Weight average molecular weight
$\bar{M}_n$	Number average molecular weight
Đ	Dispersity

Chapter 1: Introduction

1.1 Abstract

This chapter aims to introduce and provide the objectives for this research study.

1.2 Introduction

Polymer nanocomposites containing carbon nanotubes are an area of immense interest and research due to the ability that carbon nanotubes (CNTs) can influence and improve the mechanical, thermal and electrical properties of the nanocomposite.[1-9] One of the main challenges of incorporating CNTs into polymeric materials is their tendency to form aggregated bundles which are difficult to disperse in solution and therefore poor distributions are obtained. As a result, CNTs have been functionalized through a variety of methods including direct and indirect functionalization.[5,10-21] Direct functionalization, however, has the distinct disadvantage of damaging the electronic structure of the CNT surface through the addition of new bonds to the surface.[5,12,13,22] Noncovalent functionalization, however, prevents this problem and thus allows for the excellent electronic properties of the CNTs to be maintained and transferred to the composite material.[5,23-27] Yan *et al.*[25] describe the noncovalent functionalization of pristine single-walled carbon nanotubes (SWNTs) using pyrene-functional polystyrene (PS) to disperse the SWNTs within a PS matrix using π-π stacking between the SWNT surface and the pyrene groups. It was found that this functionalization was not only effective in dispersing the SWNTs within the PS matrix, but also produced composites which met the antistatic criterion for thin films due to the maintained conductive capabilities of the SWNTs.

In this study, multi-walled carbon nanotubes (MWNTs) will be comparatively functionalized covalently and noncovalently using two different controlled/living radical polymerization (LRP) techniques to synthesise the polymers. These functionalized MWNTs will then be dispersed in a PS matrix and will be attempted to be electrospun into nanofibres at different weight percentage (wt%) ratios to determine the effect of indirect versus direct functionalization of MWNTs on the properties of the final composites and fibres. To our knowledge, the electrospinning of noncovalently compatibilized MWNTs in a PS matrix has not been reported in literature.

Electrospun fibres containing noncovalently functionalized MWNTs have the potential to find application in aerospace, light emitting diodes, biosensors, electromagnetic shielding materials, sporting equipment and in antistatic coatings.[5,28,29]

1.3 Objectives

This study aims to investigate the difference between covalent versus noncovalent functionalization of pristine MWNTs and the effect on their respective dispersibility in solution and in polystyrene as well as the ability of such solutions to be electrospun. The following list describes the objectives to be met in order to investigate this difference:

1. Pyrene functional reversible addition fragmentation chain transfer (RAFT) and atom transfer radical polymerization (ATRP) macroinitiators have to be synthesised using esterification reactions. These will then be used to controllably polymerize styrene into two different targeted chain lengths. This step has the objective of determining any differences between the use of RAFT or ATRP mediated polymerization on the degree of control and efficiency of producing the PS chains which will then be interacted with the MWNTs to disperse them in solution and ultimately in a PS matrix. The synthetic success of these products will be determined using nuclear magnetic resonance (NMR), size exclusion chromatography (SEC) and Ultraviolet-infrared (UV-Vis) spectroscopy.

2. To successfully create noncovalent functionalization of pristine MWNTs with the Pyrene-functional PS chains through π-π stacking interactions. Proof of such interactions will be established using thermogravimetric analysis (TGA), NMR, UV/Vis/NIR and fluorescence spectroscopy.

3. Covalent functionalization of MWNTs will be done by immobilizing the same ATRP and RAFT agents as used for the macroinitiator synthesis along the MWNT surface. Styrene will then be grafted from these active sites. This covalent attachment will be characterized using UV/Vis, Fourier transformed-infrared (FT-IR) and TGA.

4. Solutions of these synthesised products dispersed in a PS matrix will be attempted to be electrospun into fibres containing the functionalized MWNTs which are expected to be dispersed more effectively throughout the matrix than an unfunctionalized or pristine MWNT containing composite would appear to be. The electrospun fibres will

be analysed using transmission electron microscopy (TEM) and scanning electron microscopy (SEM) imaging.

5. Ultimately a comparison will be drawn between the differences of covalently functionalized MWNTs and noncovalently functionalized MWNTs. This includes the degree of dispersion of the MWNTs within the composites as well as the effect of the type of MWNT functionalization on the behaviour of the MWNTs in a PS matrix.

1.4 Layout of thesis

This study was separated into four chapters and consists of the following content:

1.4.1 Chapter 1: Introduction

The first chapter introduces the subject matter central to this study and provides a brief outlook on the work which was performed in this research. It provides a brief introduction of polymer nanocomposites which contain carbon nanotubes and the reason behind why interest exists in these materials.

1.4.2 Chapter 2: Background and Literature Review

Chapter 2 provides a more detailed account of the synthesis, functionalization, structure and application of carbon nanotubes and their potential in producing grafted polymeric composites. Here the LRP techniques which have been applied to synthesising such functional CNTs are discussed but the focus is cast onto ATRP and RAFT mediated polymerization since these two LRP techniques are applied in this study. Finally the electrospinning of polymer-carbon nanotube nanocomposites is outlined with specific mention to the lack of information about electrospinning noncovalently compatibilized MWNTs in a polymeric matrix.

1.4.3 Chapter 3: Preparation of Polystyrene/MWNT nanocomposites via noncovalent versus covalent interactions

The synthesis of the pyrene-functional ATRP and RAFT macroinitiators is described and discussed here as well as the consequent polymerization of styrene mediated by these molecules to produce the pyrene-capped PS. The noncovalent interaction with these compounds and pristine MWNTs is described and discussed. The covalent version of these composites is also covered in this chapter. The analytical results of these reactions,

interactions and finally the electrospinning of the composites are communicated in this chapter.

1.4.4 Chapter 4: Conclusion

This final chapter provides a general conclusion to the results obtained in chapter 3 and the implications thereof.

1.5 References

1. Iijima S. Helical microtubules of graphitic carbon. Nature. 1991;354(6348):56-8.

2. Niyogi S, Hamon MA, Hu H, Zhao B, Bhowmik P, Sen R, et al. Chemistry of single-walled carbon nanotubes. Accounts of Chemical Research. 2002;35(12):1105-13.

3. Fischer JE, Gogotsi Y. Carbon nanotubes: Structure and properties. Carbon Nanomaterials. CRC Press, Boca Raton, USA. 2006:41.

4. Petrov PD, Georgiev GL, Müller AHE. Dispersion of multi-walled carbon nanotubes with pyrene-functionalized polymeric micelles in aqueous media. Polymer. 2012;53(24):5502-6.

5. Hirsch A. Functionalization of single-walled carbon nanotubes. Angewandte Chemie International Edition. 2002;41(11):1853-9.

6. Malhotra SK, Goda K, Sreekala MS. Part one introduction to polymer composites. 2012.

7. Atta S, Ikbal M, Boda N, Gauri SS, Singh NP. Photoremovable protecting groups as controlled-release device for sex pheromone. Photochemical & Photobiological Sciences. 2013;12(2):393-403.

8. Gangopadhyay, R, De A.Conducting polymer nanocomposites: A brief overview. Chemistry of Materials.2000;12(3):608-622.

9. Fischer H. Polymer nanocomposites: From fundamental research to specific applications. Materials Science and Engineering: C.2003;23(6–8):763-72.

10. Jakubowski W, Matyjaszewski K. Activators regenerated by electron transfer for atom-transfer radical polymerization of (meth)acrylates and related block copolymers. Angewandte Chemie. 2006;118(27):4594-8.

11. Ajayan P, Stephan O, Colliex C, Trauth D. Aligned carbon nanotube arrays formed by cutting a polymer resin—nanotube composite. Science. 1994;265(5176):1212-4.

12. Kong H, Gao C, Yan D. Controlled functionalization of multiwalled carbon nanotubes by in situ atom transfer radical polymerization. Journal of the American Chemical Society. 2004;126(2):412-3.

13. Cui J, Wang W, You Y, Liu C, Wang P. Functionalization of multiwalled carbon nanotubes by reversible addition fragmentation chain-transfer polymerization. Polymer. 2004;45(26):8717-21.

14. Pollino JM, Weck M. Non-covalent side-chain polymers: Design principles, functionalization strategies, and perspectives. Chemical Society Reviews. 2005;34(3):193-207.

15. Wang W, Neoh K, Kang E. Surface functionalization of Fe3O4 magnetic nanoparticles via RAFT-mediated graft polymerization. Macromolecular Rapid Communications. 2006;27(19):1665-9.

16. Simmons TJ, Bult J, Hashim DP, Linhardt RJ, Ajayan PM. Noncovalent functionalization as an alternative to oxidative acid treatment of single wall carbon nanotubes with applications for polymer composites. ACS nano. 2009;3(4):865-70.

17. Meng L, Fu C, Lu Q. Advanced technology for functionalization of carbon nanotubes. Progress in Natural Science. 2009;19(7):801-10.

18. Assali M, Leal MP, Fernández I, Baati R, Mioskowski C, Khiar N. Non-covalent functionalization of carbon nanotubes with glycolipids: Glyconanomaterials with specific lectin-affinity. Soft Matter. 2009;5(5):948-50.

19. Star A, Liu Y, Grant K, Ridvan L, Stoddart JF, Steuerman DW, et al. Noncovalent side-wall functionalization of single-walled carbon nanotubes. Macromolecules. 2003;36(3):553-60.

20. Chen RJ, Zhang Y, Wang D, Dai H. Noncovalent sidewall functionalization of single-walled carbon nanotubes for protein immobilization. Journal of the American Chemical Society. 2001;123(16):3838-9.

21. Nakashima N, Tomonari Y, Murakami H. Water-soluble single-walled carbon nanotubes via noncovalent sidewall-functionalization with a pyrene-carrying ammonium ion. Chemistry Letters. 2002;31(6):638-9.

22. Qin S, Qin D, Ford WT, Resasco DE, Herrera JE. Functionalization of single-walled carbon nanotubes with polystyrene via grafting to and grafting from methods. Macromolecules. 2004;37(3):752-7.

23. Liu J, Yang W, Tao L, Li D, Boyer C, Davis TP. Thermosensitive graphene nanocomposites formed using pyrene-terminal polymers made by RAFT polymerization. Journal of Polymer Science Part A: Polymer Chemistry. 2010;48(2):425-33.

24. Baskaran D, Mays JW, Bratcher MS. Noncovalent and nonspecific molecular interactions of polymers with multiwalled carbon nanotubes. Chemistry of Materials. 2005;17(13):3389-97.

25. Yan Y, Cui J, Pötschke P, Voit B. Dispersion of pristine single-walled carbon nanotubes using pyrene-capped polystyrene and its application for preparation of polystyrene matrix composites. Carbon. 2010 8;48(9):2603-12.

26. Mazinani S, Ajji A, Dubois C. Morphology, structure and properties of conductive PS/CNT nanocomposite electrospun mat. Polymer. 2009;50(14):3329-42.

27. Loos J, Alexeev A, Grossiord N, Koning CE, Regev O. Visualization of single-wall carbon nanotube (SWNT) networks in conductive polystyrene nanocomposites by charge contrast imaging. Ultramicroscopy. 2005;104(2):160-7.

28. Kilbride Be, Coleman J, Fraysse J, Fournet P, Cadek M, Drury A, et al. Experimental observation of scaling laws for alternating current and direct current conductivity in polymer-carbon nanotube composite thin films. Journal of Applied Physics. 2002;92(7):4024-30.

29. Safadi B, Andrews R, Grulke E. Multiwalled carbon nanotube polymer composites: Synthesis and characterization of thin films. Journal of Applied Polymer Science. 2002;84(14):2660-9.

Chapter 2: Background and Literature Review

2.1. Polymer/Carbon Nanotube Nanocomposites (PCNs)

A nanocomposite is defined as a multiphase solid material where at least one of its phases has dimensions of less than 100nm.[1] It is usually taken to mean the solid combination of a bulk matrix and nano-dimensional phases differing in properties due to dissimilarities in structure and chemistry. These change the inherent properties and behaviours of the original material. The area of interface between nanofillers and the matrix is much higher for nanocomposites than it is in conventional composites, therefore the matrix properties are more strongly affected in the vicinity of the reinforcement. This also means that low volume additions of nanocomposites can have a large effect on the macroscopic properties of the final material.

Polymer nanocomposites involve a polymer matrix or blends of different polymer matrices with nanometer-sized functional fillers. The inclusion of nanoparticles in a polymer matrix affects various polymer properties such as crystallization, chain conformation, local chemistry, and chain mobility, and has led to enhanced physical, thermomechanical and processing characteristics.

Polymer nanocomposites using carbon nanotubes are widely researched due to their ability to introduce an increased amount of mechanical strength to the composite, with the benefit of being light weight, having a high aspect-ratio and a small diameter. PCNs are also excellent electrical and thermal conductors which have led to their use as high performance, multifunctional composites.[1-11] As such, their incorporation into common and accessible polymer systems such as polystyrene (PS) is an area of avid interest.[2,12,13,13-15]

2.2. Carbon nanotubes (CNTs)

In 1991 Iijima first reported the helical formation of graphitic carbon sheets,[16] known as carbon nanotubes (CNTs) or tubular fullerenes. CNTs are a popular choice for composite fillers given their outstanding electrical, mechanical and thermal properties.[3,17] Their mechanical strength is obtained from π-bonds holding the atoms together. The curvature which originates from their tubular shape creates a strain energy described by the pyrimidalization angle and π-orbital misalignment which enable complex and interesting reactivities to be found. The high aspect ratios achievable by CNTs in a polymer matrix provides a great advantage in attaining a composite material that maintains its intrinsic matrix

properties such as flexibility whilst introducing a desirable property presented by the addition of a very low amount of CNTs such as electrical conductivity.[10] Due to the natural aggregation of CNTs to form bundles due to inter-tubular van der Waal's forces, the uniform dispersion of CNTs in solution and within the polymer matrix is difficult to control and achieve. As a result, the incorporation of this material into composites has been mostly achieved through direct functionalization of the surface chemistry of the nanotubes. This, however, has the disadvantage of decreasing the intrinsic physical and chemical properties of the original CNTs by diminishing the strain energy of the sp^2-hybridized carbon atoms.[18] As such new methods of indirect functionalization are being researched.[2,19] Naturally, various challenges are imminent regarding carbon nanotubes. The synthesis of CNTs unfortunately often produces batches of varying length, chirality, helicity, diameter, structural defects, impurities etc. which makes the comparison and especially the reproducibility of available results of CNT research extremely intricate.[20,18] Differences in solubility between the polymer matrix, solvents and CNTs also present a problem of technicality and make processability of such compounds challenging. However various literature sources have reported the successful incorporation of CNTs into polymer matrices.[3,10,7,2,18,20]

2.2.1. Carbon Nanotube Structure

CNTs are found in two forms, namely the single wall nanotube form (SWNT) and the multi wall nanotube (MWNT) form. SWNTs are made by essentially rolling up a graphene sheet consisting of a monolayer of hexagonal sp^2-bonded carbon atoms in the x-y plane and delocalized π-electron clouds in the z-plane.[20,21] It is this delocalized electron cloud that provides CNTs with their desirable electronic properties. The direction of the tube axis or the helicity of these sheets is described by the chiral roll-up vector for graphene: $\overrightarrow{C_h} = n\boldsymbol{a_1} + m\boldsymbol{a_2}$where $\mathbf{a_1}$ and $\mathbf{a_2}$ represent the graphene lattice vectors and n and m are integers. The integers (n, m) describe the lattice point which defines the diameter according to equation 2.1[21] and together with the chirality plays a large role in determining the electronic properties of the CNTs.[11,9]

$$\boldsymbol{d} = \frac{\boldsymbol{a}\sqrt{\boldsymbol{n^2}+\boldsymbol{nm}+\boldsymbol{m^2}}}{\boldsymbol{\pi}} \qquad \textbf{(Equation 2.1)}$$

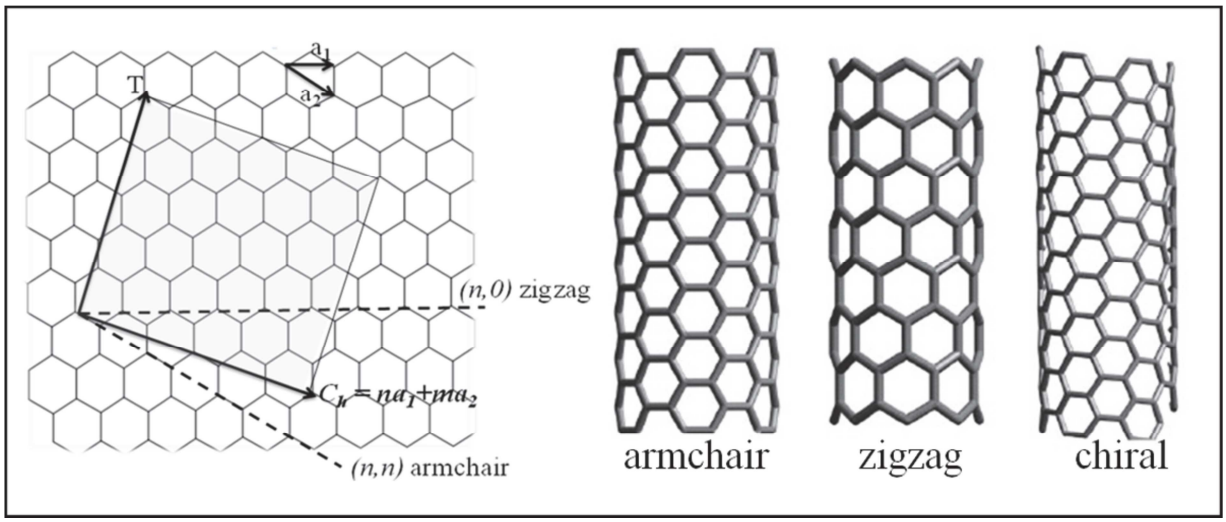

Figure 2.1: Alignment of the graphene roll-up vector determines which type of nanotube is formed; armchair, zigzag or chiral.

As seen in Figure 2.1[22], for $\overrightarrow{C_h} \equiv (n, 0)$, the CNTs have the "zig-zag" configuration, for (n, n) the "armchair", and for (n, m) the chiral configuration. The chirality of these CNTs influences their electronic properties to a large extent. For the zig-zag configuration, when n/3 is an integer, then the structure shows metallic behaviour, whereas otherwise it will be semiconducting. The armchair configuration portrays purely metallic behaviour.[11] MWNTs consist of concentrically grouped SWNTs separated by a distance of 3.4 Å.[21] Their diameter is influenced by the amount of concentric nanotubes present per MWNT which decreases the surface area available relative to SWNTs and as a result their aspect ratio also decreases.[23] Due to the polarizable π-electron cloud that exists in the z-plane, strong van der Waal's interactions result between individual tubes which cause the aggregation of singular CNTs and make uniform dispersion in a solution or polymer matrix very difficult.[20]

2.2.2. Carbon Nanotube Synthesis

CNTs are commonly synthesised by either chemical vapour deposition (CVD), Electric arc-discharge or laser vaporization.[4,6,24] Other methods are also used and are briefly discussed below.

2.2.2.1. Growth Mechanism

The mechanism by which the nanotubes form has not been yet been verified. Several opinions exist, one of which involves the formation of C_2 on a metal catalyst particle

followed by rod-like carbon formation and a consequent graphitization of the rod-like structure walls.[25]

2.2.2.2. Electric-arc discharge

By striking an arc using high direct current between two graphite electrodes placed end-to-end and separated by a small distance in an inert and low pressure atmosphere chamber, a high temperature discharge (>3000 °C) is created between the two electrodes and vaporizes carbon atoms from the anode into plasma form which then forms small rod-shaped deposits on the cathode which are then purified to yield high crystallinity CNTs. SWNTs are created when the anode is doped with certain metal catalysts such as Fe, Co, Ni, Y and Gd. Depending on the type or combination of metals used, different arrangements of SWNTs are produced from bundles (ropes)[26] to highway-junction patterns.[27,4] MWNTs however are synthesised in the absence of metal catalysts and instead use pure graphite electrodes. Various techniques are available for the optimization of specific aspects of the CNTs[4,28] including one technique which utilizes liquid nitrogen and eliminates the use of inert gases and low pressures.[29]

A disadvantage to this technique is the high cost of CNTs produced by this method which makes it an invalid option for large scale CNT synthesis. Also the CNTs obtained require purification from by-products like polyhedral graphite particles in the case of MWNTs and encapsulated metal catalyst particles for SWNTs. Control over dimensions such as length and diameter are also a challenge with this technique due to the inconsistency of the electrode placement and thus current flow, electric field and temperature distribution fluctuations.[4]

2.2.2.3. Laser Vaporization

A small piece of a graphite target is vaporized by ablation by either a pulsed or a continuous laser[4,28,30,31] at high temperatures (1200°C), inert conditions and low pressure. This plume of vaporized carbon cools and condenses to form clusters which are prevented from forming closed cage structures by the presence of metal catalysts and instead form tubular molecules. These tubular molecules grow to create ‘ropes’ of SWNTs with a narrow size distribution and improved properties in comparison to the arc-discharge method. MWNTs are produced by the absence of metal catalysts in the graphite target, similar to the arc-discharge method. Although the laser vaporization technique produces nanotubes of higher purity and narrower distribution than those synthesised by electric arc-discharge, it is not economically viable as

the power required for the lasers is extremely high, the graphite targets must be of high purity and thus are also expensive and the rate of daily CNT production is not high enough for the benefit to off-set the cost.[4,28,31]

2.2.2.4. Chemical Vapour Deposition (CVD)

An organic gas such as methane, carbon monoxide or acetylene[28] is decomposed by "cracking" the molecule into reactive atomic carbon through the use of an energy source which produces temperatures of around 400-1200°C.[4,32] This atomic carbon is then deposited onto a substrate which is coated with a metal catalyst such as Ni. The advantages of CVD methods are that films of assorted stoichiometries can be controllably synthesised, the thin films of CNTs created can be deposited homogenously even onto non-uniform shapes[33] and CNTs created by CVD require purification only if the metal catalyst is required to be absent from the final product. These CNTs have excellent dimensional parameters, alignment, and yield. A slight drawback to this technique is that the synthesis time is much longer than that of electric arc-discharge and of laser vaporization. However, CNTs produced by this method are usually long, tangled, and have tapered ends which makes them undesirable for certain applications.[34] Various methods of optimising certain aspects exist within the CVD scope and can be found in various literature sources.[4,28,35]

2.2.2.5. Other methods of CNT synthesis

New methods are being researched for the synthesis of CNTs. Commonly used methods include flame synthesis in which SWNTs are grown by using a flame to produce a temperature of around 800°C through which small aerosol cobalt metal catalyst islands are created. Inexpensive hydrocarbon fuels are partially burned by the flame to produce the carbon atoms which then grow on these metal catalyst islands into nanotubes.[28,36]

CNTs can also be prepared electrochemically through the electrolysis of molten alkali chloride salts at 600°C using graphite electrodes under inert atmosphere. The electrolytic cell is polarized such that the metal ions are reduced on the graphite cathode whilst the chloride ions are oxidized on the graphite anode. The reduction of the metal ions leads to the intercalation of these into the graphite cathode, destabilizing the graphite microstructure to produce carbon nanostructures such as nanotubes amongst others. These are then recovered from the molten salt by water and organic solvents.[37-39]

Another method of preparing CNTs is by heat treatment of polymers[4] consisting mostly of Carbon. When polymers prepared by the polyesterification between citric acid and ethylene glycol[40] are thermally treated in air, the bonds between the carbon atoms and other elements are broken to produce CNTs.

2.2.3. Carbon Nanotube Functionalization

One of the great challenges of working with CNTs is their natural tendency to aggregate and form non-crystalline bundles of nanotubes between 10-100 nm in diameter[41,42] which are not easily broken up due to a significant amount of van der Waal's forces that exist between them. SWNTs also occur in ropes of 10-25 nm in diameter and a few micrometres in length.[43] When in the solid state, these ropes exist in a tangled network-like structure which makes their dispersion in solutions and in composites very difficult and mostly uneven[44] and thus their processability proves challenging.[17] The problem with CNT aggregation may be temporarily solved by vigorous ultrasonication in specific solvents. However, a more lasting solution is through the chemical functionalization of the surface of the nanotubes. Chemical functionalization allows for the bundles to be broken up but also allows for an improved solubility in solution and thus eases their processability as well as increasing their degree of interaction with a matrix in a composite material.[17,44-46] Functionalization of CNTs can take place by one of three methods: 1) by the direct covalent attachment of molecules to the nanotube surface walls. 2) Through the indirect noncovalent adhesion of functional groups to the CNT surface or through polymer wrapping or 3) through the endohedral filling of their vacant inner cavity.[47]

Covalent functionalization involves the formation of covalent bonds between the carbon atoms of the CNT surface and functional entities.[42] The sp^2 hybridized orbitals of the CNT surface atoms and their π-orbital misalignment favours addition reactions and thus the formation of covalent bonds. This type of functionalization can be separated into either direct or indirect covalent functionalization. Direct covalent functionalization involves the formation of covalent bonds through the loss of conjugation with a change in hybridization from sp^2 to sp^3 such as occurs upon fluorination,[48] the cycoladdition of carbine or nitrenes[47] or hydrogenation through Birch reduction.[43,47] Indirect covalent functionalization commonly occurs through the nanotube surface oxidation using harsh acidic conditions[1,44,49] followed by further chemical modification as well as composite incorporation.[42] The acid oxidation of the nanotubes introduces defects along the nanotube walls and causes the shortening of the tubes

which is detrimental to electrical as well as mechanical properties.[50] However, the covalent indirect functionalization allows for the formation of a strong interface between the nanotube surface and the composite which is a great advantage as this method can be used to create reinforced polymer composites.[46] The disadvantage with covalent functionalization is that the chemical surface of the nanotube is altered which affects the physical properties mostly in a detrimental manner such that, for example, the conductivity and the strength of the original nanotube is significantly decreased.

Noncovalent functionalization is mostly achieved through the formation of supramolecular complexes using dispersive forces such as hydrogen bonding, electrostatic forces, van der Waal's forces and π-stacking between the conjugated C-C atoms of the CNT surface and those of the functional molecule.[2,18,51-55] Noncovalent functionalization methods usually do not require harsh reactive conditions as covalent methods of functionalization do. As a result, this technique has the significant benefit of leaving the intrinsic CNT surface intact and thus the much desired physical properties of the nanotubes are maintained. Through this manner, CNTs have been incorporated into composite materials.[46,52] Chen *et al.*[20] showed the successful noncovalent functionalization of SWNTs using a pyrene functional ester via π-stacking between the pyrene moiety and the basal plane of the graphitic side wall of the SWNTs for use in biological applications. Reinforcing composites, however, are not ideally produced via noncovalent functionalization of CNT since the noncovalent attachment is based on weaker dispersive forces and as such the interfacial strength between the composite matrix and the nanotubes is low which leads to inefficient load transfer as shown by Eitan *et al.*[46]

2.3. Graft Copolymers

There is a great interest in creating polymers with well-defined morphologies such that the properties of the resulting polymer may be specifically tailored. The copolymer properties are more similar to those of a mechanical mixture of the constituent homopolymers and allow for new or improved properties to be realised. Different arrangements of the repeat units of the copolymer determine its structure and as a result its physical properties too. Through conventional free-radical copolymerization, the monomeric units are seen to be either alternately distributed or randomly so. This is dependent on the respective reactivity ratios of the monomers as indicated in equation 2.2, which is a measure of the relative probability that

a monomer will react with itself compared to the other monomer, where r_1 and r_2 represent the monomer reactivity ratios.[56]

$$r_1 = \frac{k_{11}}{k_{12}} \qquad r_2 = \frac{k_{22}}{k_{21}} \qquad \text{(Equation 2.2)}$$

In general the distribution along the polymeric chain consists of a random distribution of monomer units A and B as indicated below:

$$-A-A-A-B-A-A-B-B-B-A-B-A-$$

When the reactivity ratio is quite small however, this distribution is found to give a regular alternating sequence of monomer units A and B:

$$-A-B-A-B-A-B-A-B-A-B-A-B-$$

When copolymers are synthesised with a long uninterrupted stretch of a single monomer, different properties to those obtainable by random copolymers and their constituent homopolymers are possible.

2.3.1. Synthesis of Graft Copolymers by grafting onto solid surfaces

Graft copolymers are commonly divided into three categories according to their synthesis procedure. These methods are chosen depending on the types of monomers and solvent systems used, and the type of copolymers that are desired. Grafting from, grafting to, and grafting through are the different techniques available,[57] and are illustrated by Figure 2.2.

In the grafting through technique, the monomers of one constituent are mixed with a macromonomer of the second constituent and polymerization ensues to give macromonomers grafted onto the backbone compiled of the monomers of the first constituent. This method allows for the individual control of side chain length and grafting density through the regulation of the degree of polymerization of the individual constituent monomers. A disadvantage is the steric hindrance which becomes a problem when sterically bulky or high molecular weight macromonomers are used.[58]

Grafting from involves the functionalization of the macromolecular backbone by specific reactive groups to produce a macroinitiator, which creates active sites onto which the monomers of the second constituent are then grafted. This macroinitiator is prepared by the use of a chosen controlled/living polymerization technique. Especially controlled/living free

radical polymerization techniques such as ATRP are favoured for this purpose due to the low amount of instantaneous propagating species which are formed, thus allowing a decreased steric effect to be achieved due to the limitation of terminating and coupling reactions which enable a slow growth of side chains to be realised.[57,59-61] This also holds the benefit of a lower unreacted macroinitiator content in the final product, as well as greater range or possible backbone and/or side chain lengths and composition.[61] Further functionalization of the backbone is then achieved via various traditional chemical processes.

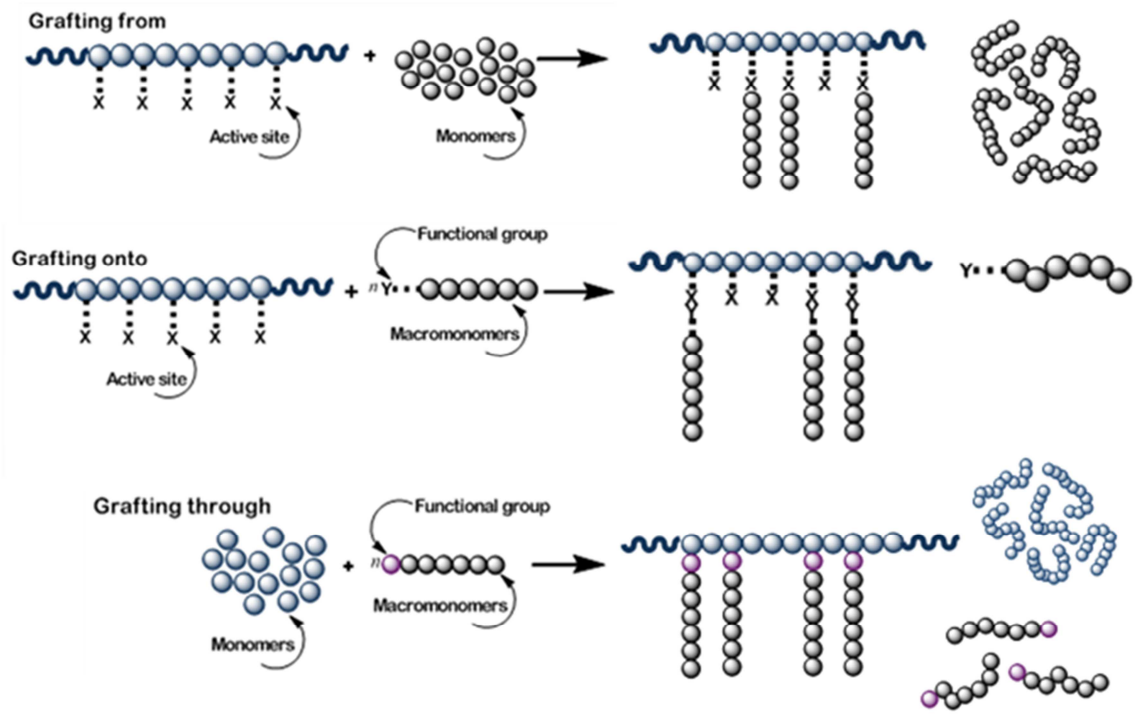

Figure 2.2: Illustration of grafting techniques available

Grafting onto involves the addition of a functional macromonomer of one composition onto a functionalized linear backbone of another composition. Although the backbone and the side chains are individually prepared which allows the advantage of easily tailoring and characterizing these components via the suitable pathways, a highly effective coupling method must be used to minimize the amount of unreacted side chains present in the product, which in turn also require an efficient method of removal in order to achieve a polymer with a narrow molecular weight distribution.[57] A limitation to the grafting onto technique is the low grafting density which results due to hindered diffusion of macromolecules onto the functionalized backbone surface.[62]

The grafting of polymers from solids such as clay,[63] graphite,[49] silicon wafers[64] and carbon nanotubes,[45,65] and many others, is an effective method for the modification of solid surfaces (see Figure 2.3) or their incorporation into composites.[66] "Grafting from" allows for greater grafting densities to be realised due to the higher rate of diffusion of the smaller monomers,[67] whilst control over the molecular weight and the polymer architecture are however difficult to achieve.[68] "Grafting onto" on the other hand, provides full control over the architecture and molecular weight but produces low theoretical polymer loadings due to steric repulsions between the side chains and the solid backbone. This problem is addressed through the use of Controlled/"living" free radical polymerizations such as atom transfer radical polymerization (ATRP),[69] reversible addition fragmentation chain transfer (RAFT),[70] and nitroxide-mediated polymerization (NMP).[71] This is because the immobilization of radical species onto solid surfaces from which monomers can then be polymerized falls under the "grafting from" category and therefore allows for greater polymer loadings than the "grafting onto" method does, yet great control over molecular weight and architecture is realised.[45]

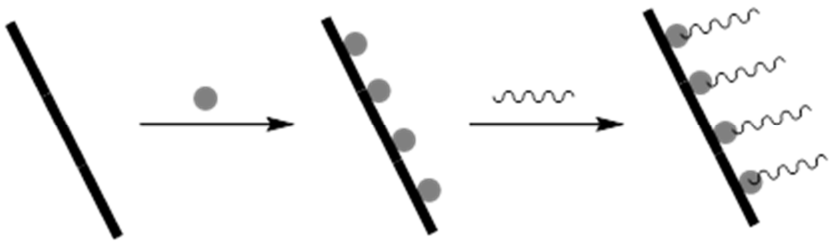

Figure 2.3: Schematic representation of grafting from a solid surface through the creation of active sites via immobilization

Hong *et al.*[45] successfully showed the grafting of poly(N-isopropylacrylamide)from the surface of MWNTs which were first functionalized through the surface immobilization of a dithiobenzoate RAFT agent onto the nanotube surface followed by the RAFT mediated polymerization of N-isopropylacrylamide off these active sites. As a result, it is expected that the immobilization of a trithiobenzoate RAFT agent onto the MWNT surface will successfully graft styrene from these points to produce a covalently bound MWNT-PS nanocomposite.

Similarly, Shanmugharaj *et al.*[72] demonstrated the *in situ* ATRP-mediated surface initiated polymerization of styrene and acrylonitrile from the ATRP initiator 2-hydroxyethyl 2-bromoisobutyrate active sites which had been immobilized on the surface of MWNTs.

Noncovalent grafting onto has been used to describe the grafting of a preformed side chain onto apolymeric backbone via noncovalent bonding. The type of noncovalent bonding or recognition motif that is used such as π-π interactions, hydrogen bonding, electrostatic interactions or metal-ligand coordination are chosen depending on the noncovalent bond strength desired between the backbone and the side chain which is determined by the end-use applications of the graft copolymer.[73] The correct polymerization method must be utilized depending on its tolerance of the functional groups as well as its ability to control the molecular weight and produce a well-defined graft copolymer with a narrow polydispersity. As such controlled/living polymerization techniques such as ATRP, RAFT or ROMP are commonly employed.[74-76]

The reversibility of the self-assembled polymeric system needs to be considered since environmental factors such as solvent, temperature, pressure, concentration, the state (liquid or solid) and so on influences the final copolymer structure largely due to the weak noncovalent forces being easily affected or overcome by these factors.[57,73,77] This creates the potential for highly dynamic and versatile applications seeing as these graft copolymers could be tailored to be reversible under the right conditions.

Many noncovalent graft copolymers have been prepared *via* self-assembly through hydrogen bonding between the side-chains and the backbone[73,78-80] whereas the functionalization of CNTs through π-π stacking interactions lends a common example of where noncovalent grafting-onto strategies are used.[5,17,18,45,81] A disadvantage of the noncovalent grafting onto copolymerization lies in the large steric hindrance presented by the side-chains which results in an increased amount of unreacted side chains which in turn require further purification in order to recover a pure copolymer without unreacted components in the final product.

This research focused on the synthesis of side-chain supramolecular polymers in which a pyrene-functional PS chain will be bonded noncovalently onto a MWNT surface which acts as the backbone. The pyrene-functional PS side-chains will be polymerized first, through both ATRP and RAFT as means of comparison, followed by the π-π stacking interaction of the functional PS onto the MWNTs.

Ideally, only graft copolymers are synthesised. In reality this is often not the case since mixtures of homopolymers of the constituents are also realised together with the copolymeric products. These complex mixtures therefore require advanced analytical techniques for their complete characterization and identification.

2.4. Controlled/Living Radical Polymerization (LRP)

The discovery of "living" anionic polymerization in 1955[82] using styrene monomers brought about a new polymerization technique in which polymerization could progress with neither chain transfer nor chain termination occurring such that a polymer capable of further growth was realised. This discovery was shortly followed by the development of other types of ionic polymerizations which were able to create well-defined polymers of controllable composition, morphology, molecular weight and functionality. Upon introduction of controlled/living radical polymerization techniques, the synthesis of specifically tailored complex polymer architectures was diversified to include a greater tolerance towards a variety of polymerizable monomers and in a range of different solvents compared to the living ionic methods which were generally intolerant to functional groups, required a complete absence of moisture, contained many side reaction products and were restricted to a select few monomer types.[60,82-86,86]

2.4.1. Conventional free radical polymerization (CRP)

In conventional radical polymerization, a chain reaction as shown in scheme 2.1 below, of chain initiation occurs in which the radicals formed by the thermal or photochemical decomposition of an initiator (scheme 2.2) molecule are added to a vinyl monomer (M), which must contain an electron withdrawing group.[87,88] The initiator choice can influence the rate of polymerization, the final molecular weight, structure and thus also possibly the properties of the final polymer. Azo and peroxide compounds such as 2,2'-Azobis(isobutyronitrile) (AIBN) and benzoyl peroxide (BPO) are most commonly used as initiators.[86] Here the rate of initiator decomposition, and such the rate of initiation, is described by the rate coefficient value k_d which is dependent on solvent and temperature and is unique to the specific initiator compound. The resultant primary radical is then added to another monomer, the rate of which is described by the rate coefficient k_i to result in a monomer radical.

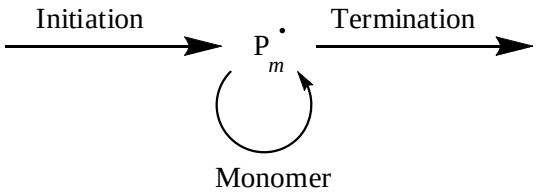

Scheme 2.1: Conventional radical polymerization process

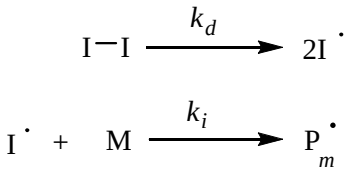

Scheme 2.2: Decomposition mechanism of initiator molecule to form radicals

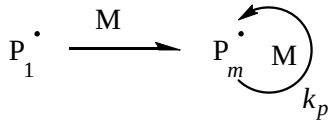

Scheme 2.3: Chain Propagation mechanism

After formation of the primary propagating radical, chain propagation takes place (scheme 2.3) in which the monomers are sequentially added to the propagating radical species, followed subsequently by chain termination in which the propagating radicals react either through combination or coupling, or disproportionation in which one radical chain extracts a hydrogen from another, forming an unsaturated chain and resulting, in both cases, in a "dead" polymer. Scheme 2.4 shows this process in which the rate of termination (k_t) for disproportionation is describes by k_{td} and the rate constant for termination through coupling by k_{td}.

This method of polymerization is inexpensive and versatile and as such is commonly used in the commercial sector.[89] A range of monomers including styrene, butadiene, methacrylates, acrylic acids, acrylates, vinyl acetates and vinyl chlorides can be polymerized using CRP via bulk, suspension, solution, emulsion, micro- and mini-emulsion polymerizations.[85,90] The termination of these chains does not allow adequate control over the synthesised polymer structure. The chains are described as being "dead" meaning that they can no longer be used to propagate any other types of monomers to produce complex polymer composites, morphologies or topologies. As a result, the controlled "living" radical polymerization techniques are preferred in the synthesis of tailored polymer products such as branched, graft,

block, star and other complex architectures. Living radical polymerization is also more tolerant towards a variety of functional groups (such as OH, COOH, NR_2 and $CONR_2$),[85] impurities, as well as temperature and solvent ranges.

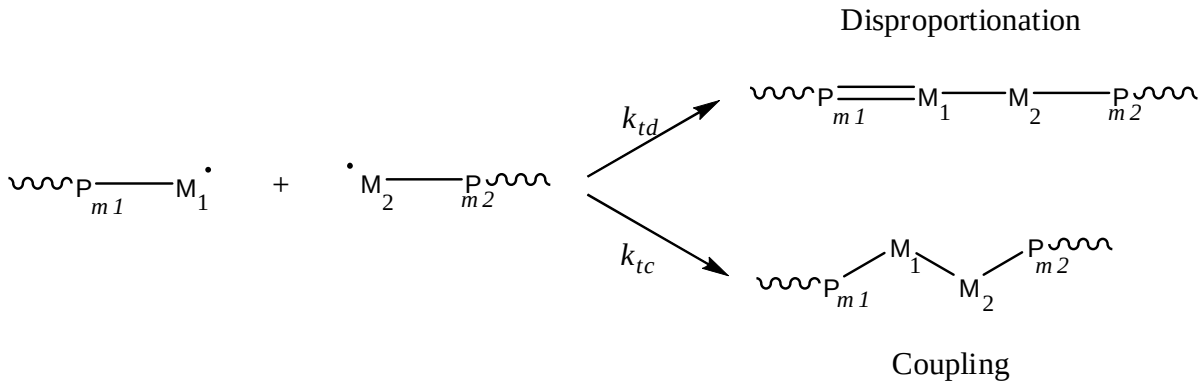

Scheme 2.4: Chain termination through disproportionation and coupling

2.4.2. Controlled Living radical polymerization (LRP)

Central to all LRP methods is the formation of a dynamic equilibrium between the low concentration of propagating free radicals and the larger concentration of the dormant species. The irreversible chain termination which occurs in CRP is suppressed by compounds which react reversibly with the propagating radical chain ends to allow for controllable capping and uncapping of the propagating chain ends which impart them with the "living" character and creates equilibrium between the propagating and dormant species. This is done through either reversible chain transfer or through reversible chain deactivation, so that the majority of chains are kept in the dormant state. As a result of this, all chains are able to grow simultaneously through almost instantaneous initiation and the minimization of chain breaking and termination reactions. The molecular weight is seen to increase linearly, leading to a very narrow molecular weight distribution which results in a slow and simultaneous polymer growth allowing for improved control of the polymerization. Since these chains are reversibly deactivated, polymerization and propagation will ensue once more monomer is added. In the case of ATRP, these reversible activating/deactivating compounds are usually alkyl esters, in RAFT they are thioesters and in NMP alkoxyamines.[74,83] These compounds appear at the ends of the final polymer chains once all the monomer units have been propagated. Due to the simultaneous initiation and linear chain growth through the reversible activating/deactivating species, the concentration of radicals should not fluctuate

significantly. LRP is defined by the ability to produce polymers of narrow molecular weight dispersity and predictable molecular weight through the linear increase in molar mass with regard to the rate of monomer conversion.[86]

The most common methods of LRP are ATRP, RAFT and NMP. NMP includes the formation of a carbon-centred and a nitroxide-centred radical, which are produced through the thermal decomposition of an alkoxyamine species in equilibrium which introduces the disadvantage of requiring high reaction temperatures for this procedure. The carbon-centred radical can then react with monomer units during propagation or it can be reversibly trapped by the nitroxide again to prevent termination from occurring. Because termination is to be minimized to enable simultaneous chain growth, the equilibrium concentration should ideally lie towards the alkoxyamine such that the concentration of radicals is low and the polymerization will be slower and more controlled. NMP is mostly used for the synthesis of styrene and acrylate copolymers as well as narrow molecular-weight distribution homopolymers.[71,85] NMP however is not as tolerant toward a wide range of monomers unlike RAFT and ATRP methods.[91] RAFT and ATRP both produce uniform chain growth. ATRP however achieves this by the atom transfer step in its mechanism, whereas RAFT relies on the addition-fragmentation process for this property. These last two methods of LRP are focused on in this research.

2.4.2.1. RAFT

RAFT polymerization provides a number of advantages. It has the ability to produce polymers of predictable molecular weight and a narrow dispersity. It is very tolerant towards various solvents, reaction temperatures and conditions, and towards a variety of monomers of acid, hydroxyl and amino acid functional groups.[85] It also adds the benefit of being able to create polymers end-capped by a specific functionality which is incorporated into the RAFT agent through the R or Z group (see scheme 2.5) to essentially produce a RAFT macroinitiator. This versatile, convenient, and highly effective method of LRP was discovered in the 1990's by researchers at CSIRO.[92] It involves the same chain reaction as CRP but it prevents the termination step of CRP through the action of thiocarbonylthio chain transfer agents (CTAs) (**1** in scheme 2.5) which reversibly trap the radical of the propagating chain through capping/uncapping of the active centre. Typical CTAs used in RAFT are separated into dithioesters,[93] dithiocarbamates,[92] trithiocarbonates[93] and xanthates.[94] The choice of RAFT agent is dependent on the monomer used, as well as the R and Z groups

which represent a free-radical leaving group and stabilizing group respectively. Chain initiation proceeds in the same manner as shown in scheme 2.2 for the CRP. However, chain propagation is more complex in that reversible chain transfer takes place during the RAFT polymerization to reversibly activate/deactivate the active radical site at the chain end as shown in scheme 2.5. The weak S-R bond shown in scheme 2.5 (**2**), is fragmented rapidly if side reactions are to be avoided, to produce a reactive C=S bond (**4**) and the radical leaving group $R^{\bullet}$, which consequently causes reinitiation, given that there are any monomer units present. To obtain a decent polymer, this equilibrium should favour the products. Penultimately chain equilibration takes place in which the dormant polymeric thiocarbonylthio (**4**) reacts with a neighbouring propagating radical in equilibrium, such that both chains ($P_n^{\bullet}$ and $P_m^{\bullet}$) have the same probability of propagation, leading to chains of narrow polydispersity.[85] The stability of the Z group in **4** governs the rate of radical addition during chain equilibration. Through this chain transfer equilibrium, radicals are neither created nor destroyed but are instead provided by the decomposition of the initiator molecule.

To avoid retardation of the chain propagation, the correct concentration and choice of RAFT agent must be used. The rate of reinitiation (k_i), should also be larger than the rate of propagation (k_p) to avoid retardation. This is influenced by the choice of the Z-group which must be balanced between its tendency towards its leaving group ability and the reinitiation efficiency of the radical $R^{\bullet}$.

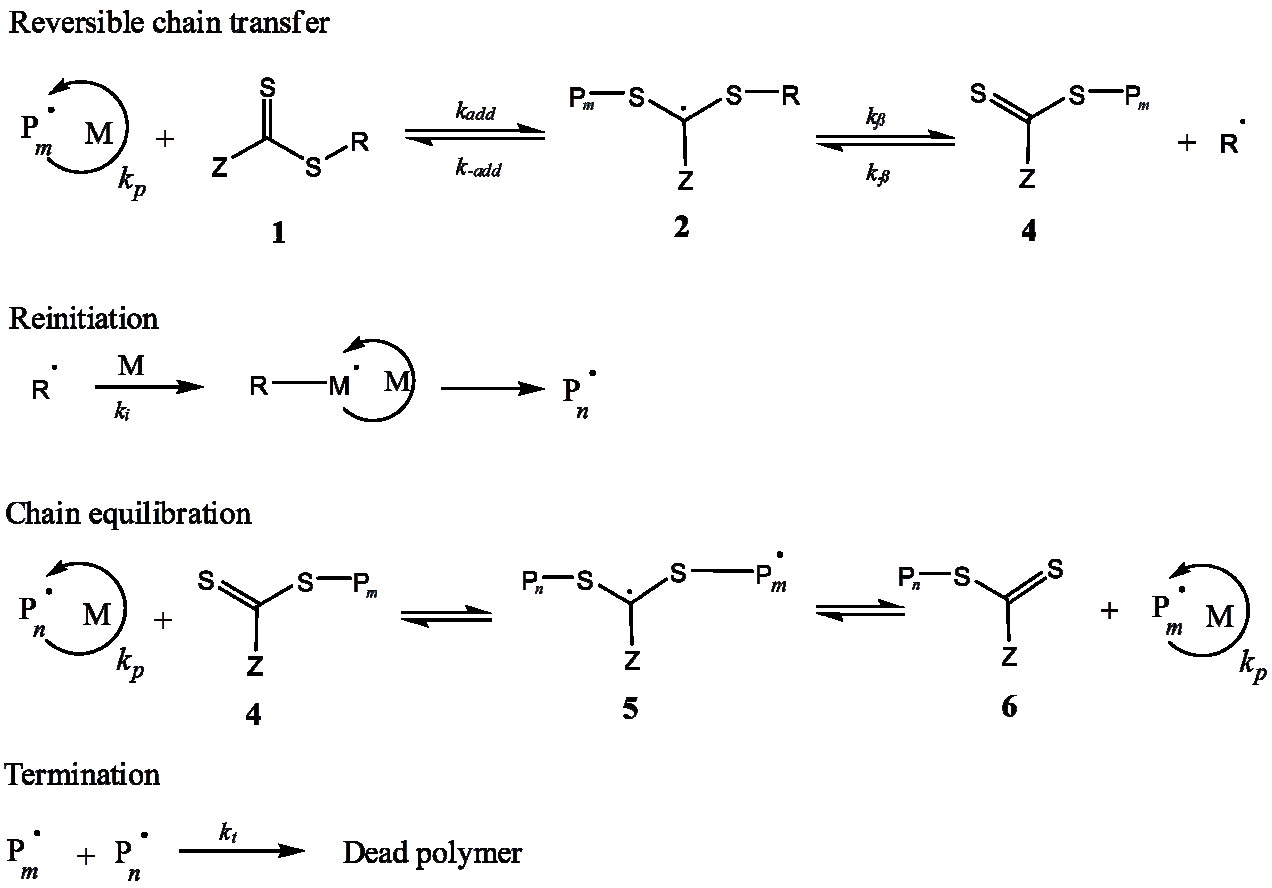

Scheme 2.5: Mechanism of RAFT polymerization according to Moad, Rizzardo and Thang [85]

2.4.2.2. ATRP

ATRP is similar in mechanism to NMP in that it is also a reversible activation/deactivation system where control is achieved through the reversible deactivation of propagating radicals via atom transfer.[85] ATRP is more versatile than NMP, and it has a higher tolerance to a variety of functional groups and monomers[69] and can be applied to a range of reaction conditions (bulk, solution, emulsion and suspension). The choice of solvent and the reaction temperature however play a significant part in optimising the reaction conditions. The solvent choice is decided according to which solvent minimizes chain transfer to solvent reactions, catalyst poisoning and changes to the catalyst structure. The reaction temperature is dependent on the monomer and catalyst choice, and on the desired molecular weight. At high temperatures, the rate of polymerization increases which leads to higher rate for propagation than for termination which enables increased chain growth control. However high temperatures also increase the amount of side reactions and chain transfer reactions that are realised.

ATRP has the potential to produce well-defined polymers of predetermined molecular weight, narrow weight distribution and complex compositions and architectures. Since it involves the transfer of a halogen atom between an alkyl halide and a transition metal compound, this method of LRP enables the incorporation of a halogen functionality into to the final polymer product. This can be capitalised by attaching the initiating component onto a macromolecule to create an ATRP macroinitiator which can be used to create complex polymer compositions especially block or graft copolymers.[95]

ATRP polymerization is initiated by the transition metal complex catalysed reversible redox reaction with an alkyl halide as shown in scheme 2.7 below. A transition metal/ligand complex ($M_t^n - Y/L$) (**2**) consisting of a lower oxidation state transition metal (such as Iron, Nickel, Rhenium, Copper, Palladium, Molybdenum, Ruthenium, Chromium or Rhodium) and an amino or phosphorous based multidentate complexing ligand is used to abstract a halogen from the initiating alkyl halide (**1**) at a rate k_{act}, to generate the radical species (**3**) and an oxidized transition metal/ligand complex (**4**). Propagation ensues through the addition of the radicals to monomers. The production of the oxidized metal complex (**4**) ensures that the growing radical concentration is kept low as well as constant throughout propagation. This situation together with a fast rate of initiation and a rapid reaction between the reagents and the products indicated in scheme 2.7 enables uniform chain polymerization at a rate of k_{act}/k_{deact}. Furthermore, termination reactions through bimolecular radical coupling or disproportionation are suppressed through this phenomenon thus imparting the system with its "living" characteristics.[60,95]

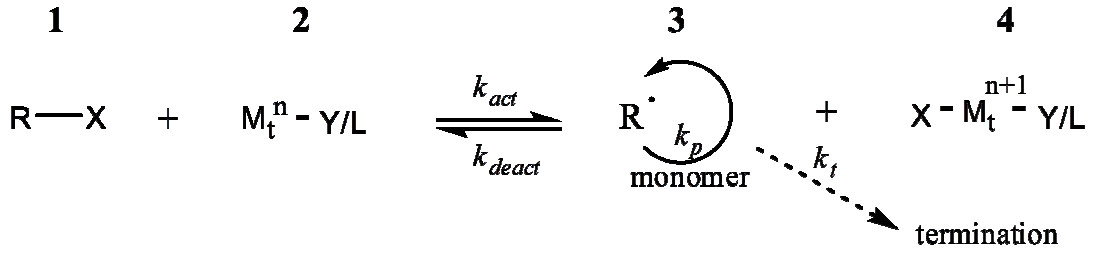

Scheme 2.6: General ATRP mechanism

The choice of catalyst determines where the equilibrium of the atom transfer step will lie and as such the balance between the dormant and active species which control the chain growth. The transition metal chosen for ATRP has to meet specific requirements: it must have a minimum of two oxidation states with a one electron difference between the two states; it

must have a coordination sphere around the metal which must be able to expand to accommodate the second halogen; it must have an affinity towards this second halogen; and the ligand should be able to complex strongly with the transition metal.[95]

Disadvantages of ATRP are presented by the requirement for more stringent reaction conditions, a lower tolerance to impurities and the need for unconventional initiating systems compared to RAFT polymerization.[85] Metal contamination and as a result the removal of the metal catalyst from the final product is also a problem.[96]

2.5. Electrospinning

Electrospinning is a versatile, effective and simple technique used for the processing of polymer materials.[97-99] It introduces the benefit of producing long, continuous, ultrathin nanofibres of a variety of materials with increased mechanical properties due to their high aspect ratio. Specifically the interest in electrospinning polymer composites containing CNTs fillers has become an area of interest due to aspirations to produce a material with superior mechanical, electrical and thermal properties.[100] Much research has been done involving the electrospinning of polymer composites containing CNTs which have been compatibilized through chemical functionalization so as to interact with the polymeric matrix material.[100-102] Das *et al.*[103] showed the preparation of polyvinyl alcohol (PVA)/graphene nanofibres via electrospinning in which the graphene was noncovalently functionalized using pyrrolidone compounds to allow for its dispersion in the PVA matrix.[103] However, according to our knowledge, there are no reported instances of nanocomposites of MWNT compatibilized with the matrix material noncovalently through π-π stacking interaction.

The polymer solution is placed in a syringe and is forced through the needle tip by a pump whilst a high electrical potential is applied to the needle tip. A grounded collector plate is placed a certain distance from the needle tip. The potential difference between the grounded collector plate and the electrically charged needle tip creates an electrostatic charge gradient. When the applied voltage overcomes the surface tension of the polymer solution of the droplet at the needle tip, the free charges (usually ions), in the polymer solution move in response to the electric field to form a jet which stretches and splays radially due to radial electrical forces. During this stretching, the polymer solution solvent is evaporated leaving behind extremely thin nanofibres on the collector plate.[1,98]

2.6. Analysis Techniques

A number of analysis techniques were used to characterize and confirm whether the covalent and noncovalent interactions had taken place and to which degree in some cases too. The noncovalent interactions between CNTs and the interacting π-system are difficult to prove directly. However, noncovalent interactions through π-π stacking involving CNTs have been reported in literature[53,104,105] to be observed in NMR as a broadening, weakening or a slight shifting in certain ^{1}H peaks as a result of the electrostatic interaction between the ring currents of the nanotube carbons and the π-system of pyrene molecules.[106]

Since pyrenes have a strong fluorescence, they are easily detected by this method of spectroscopy. When this pyrene π-system is noncovalently attached to the CNT carbon network, this strong fluorescence signal is seen to be quenched due to the energy transfer between the nanotubes and pyrene moieties.[107-109]

Further techniques used for the characterization of noncovalent and covalent functionalization of CNTs are TGA in which the percentage of weight loss over a specific temperature range gives an indication of the degree of functionalization that has occurred since CNTs have distinct thermal properties; Raman spectroscopy which enables the electronic structure of the CNTs to be analysed, and UV/Vis as well as UV/Vis/NIR which can be used to determine the chemical composition of the CNTs as a result of functionalization.[6,52,62,110] FT-IR, NMR and X-ray photoelectron spectroscopy can be used to determine the covalent surface functionalization of CNTs if chemical groups of distinct correlation frequencies are introduced during functionalization.[6,49,52,62]

2.7. References

1. Bayley GM. Synthesis and characterisation of organic-inorganic hybrid block copolymers of polydimethylsiloxane and polystyrene. Doctoral Dissertation. Stellenbosch: University of Stellenbosch. 2007

2. Spitalsky Z, Tasis D, Papagelis K, Galiotis C. Carbon nanotube–polymer composites: Chemistry, processing, mechanical and electrical properties. Progress in Polymer Science. 2010;35(3):357-401.

3. Ramasubramaniam R, Chen J, Liu H. Homogeneous carbon nanotube/polymer composites for electrical applications. Applied Physics Letters. 2003;83:2928.

4. Ajayan P, Stephan O, Colliex C, Trauth D. Aligned carbon nanotube arrays formed by cutting a polymer resin—nanotube composite. Science. 1994;265(5176):1212-4.

5. Awasthi K, Srivastava A, Srivastava O. Synthesis of carbon nanotubes. Journal of Nanoscience and Nanotechnology. 2005;5(10):1616-36.

6. Britz DA, Khlobystov AN. Noncovalent interactions of molecules with single walled carbon nanotubes. Chemical Society Reviews. 2006;35(7):637-59.

7. Che G, Lakshmi B, Martin C, Fisher E, Ruoff RS. Chemical vapor deposition based synthesis of carbon nanotubes and nanofibres using a template method. Chemistry of Materials. 1998;10(1):260-7.

8. Coleman JN, Khan U, Gun'ko YK. Mechanical reinforcement of polymers using carbon nanotubes. Advanced Materials. 2006;18(6):689-706.

9. Fischer JE, Gogotsi Y. Carbon nanotubes: Structure and properties. Carbon Nanomaterials. CRC Press, Boca Raton, USA. 2006:41.

10. Joselevich E. Electronic structure and chemical reactivity of carbon nanotubes: A chemist's view. ChemPhysChem. 2004;5(5):619-24.

11. Kilbride Be, Coleman J, Fraysse J, Fournet P, Cadek M, Drury A, et al. Experimental observation of scaling laws for alternating current and direct current conductivity in polymer-carbon nanotube composite thin films. Journal of Applied Physics. 2002;92(7):4024-30.

12. Odom TW, Huang J, Kim P, Lieber CM. Atomic structure and electronic properties of single-walled carbon nanotubes. Nature. 1998;391(6662):62-4.

13. Qian D, Dickey EC, Andrews R, Rantell T. Load transfer and deformation mechanisms in carbon nanotube-polystyrene composites. Applied Physics Letters. 2000;76:2868.

14. Bellayer S, Gilman JW, Eidelman N, Bourbigot S, Flambard X, Fox DM, et al. Preparation of homogeneously dispersed multiwalled carbon nanotube/polystyrene nanocomposites via melt extrusion using trialkyl imidazolium compatibilizer. Advanced Functional Materials. 2005;15(6):910-6.

15. Hadjiev V, Mitchell C, Arepalli S, Bahr J, Tour J, Krishnamoorti R. Thermal mismatch strains in sidewall functionalized carbon nanotube/polystyrene nanocomposites. The Journal of Chemical Physics. 2005;122:124708.

16. Wu T, Chen E. Preparation and characterization of conductive carbon nanotube–polystyrene nanocomposites using latex technology. Composites Science and Technology. 2008;68(10):2254-9.

17. Iijima S. Helical microtubules of graphitic carbon. Nature. 1991;354(6348):56-8.

18. Petrov PD, Georgiev GL, Müller AHE. Dispersion of multi-walled carbon nanotubes with pyrene-functionalized polymeric micelles in aqueous media. Polymer. 2012;53(24):5502-6.

19. Hirsch A. Functionalization of single-walled carbon nanotubes. Angewandte Chemie International Edition. 2002;41(11):1853-9.

20. Chen RJ, Zhang Y, Wang D, Dai H. Noncovalent sidewall functionalization of single-walled carbon nanotubes for protein immobilization. Journal of the American Chemical Society. 2001;123(16):3838-9.

21. Bose S, Khare RA, Moldenaers P. Assessing the strengths and weaknesses of various types of pre-treatments of carbon nanotubes on the properties of polymer/carbon nanotubes composites: A critical review. Polymer. 2010;51(5):975-93.

22. Terrones M, Hsu WK, Kroto HW, Walton DR. Nanotubes: A revolution in materials science and electronics. In: Fullerenes and Related Structures. Springer; 1999. p. 189-234.

23. Choudhary, V, Gupta, A. Polymer/carbon nanotube nanocomposites.2011.

24. Peigney A, Laurent C, Flahaut E, Bacsa R, Rousset A. Specific surface area of carbon nanotubes and bundles of carbon nanotubes. Carbon. 2001;39(4):507-14.

25. Ebbesen, TW, Ajayan PM. Large-scale synthesis of carbon nanotubes. Nature. 1992;358(6383), 220-222.

26. Yasuda A, Kawase N, Mizutani W. Carbon-nanotube formation mechanism based on in situ TEM observations. The Journal of Physical Chemistry B. 2002;106(51):13294-8.

27. Seraphin S, Zhou D. Single-walled carbon nanotubes produced at high yield by mixed catalysts. Applied Physics Letters. 1994;64(16):2087-9.

28. Saito Y, Okuda M, Koyama T. Carbon nanocapsules and single-wall nanotubes formed by arc evaporation. Surface Review and Letters. 1996;3(01):863-7.

29. Daenen M, De Fouw R, Hamers B, Janssen P, Schouteden K, Veld M. The wondrous world of carbon nanotubes. Eindhoven University of Technology. 2003:1-35.

30. Ishigami M, Cumings J, Zettl A, Chen S. A simple method for the continuous production of carbon nanotubes. Chemical Physics Letters. 2000;319(5):457-9.

31. Meyyappan M. Carbon nanotubes: science and applications. CRC press, 2004.

32. Puretzky A, Geohegan D, Fan X, Pennycook S. Dynamics of single-wall carbon nanotube synthesis by laser vaporization. Applied Physics A. 2000;70(2):153-60.

33. Moss SJ, Ledwith A. Chemistry of the semiconductor industry. Kluwer Academic Print on Demand; 1989.

34. Ohring M. Materials science of thin films. Academic Press; 2001.

35. Liu F, Zhang X, Cheng J, Tu J, Kong F, Huang W, et al. Preparation of short carbon nanotubes by mechanical ball milling and their hydrogen adsorption behavior. Carbon. 2003;41(13):2527-32.

36. Yuan L, Saito K, Pan C, Williams F, Gordon A. Nanotubes from methane flames. Chemical Physics Letters. 2001;340(3):237-41.

37. Schwandt C, Dimitrov AT, Fray DJ. The preparation of nano-structured carbon materials by electrolysis of molten lithium chloride at graphite electrodes. Journal of Electroanalytical Chemistry. 2010;647(2):150-8.

38. Hsu W, Terrones M, Hare J, Terrones H, Kroto H, Walton D. Electrolytic formation of carbon nanostructures. Chemical Physics Letters. 1996;262(1):161-6.

39. Chen GZ, Fan X, Luget A, Shaffer MSP, Fray DJ, Windle AH. Electrolytic conversion of graphite to carbon nanotubes in fused salts. Journal of Electroanalytical Chemistry. 1998;446(1–2):1-6.

40. Cho W, Hamada E, Kondo Y, Takayanagi K. Synthesis of carbon nanotubes from bulk polymer. Applied Physics Letters. 1996;69(2):278-9.

41. Breuer O, Sundararaj U. Big returns from small fibres: A review of polymer/carbon nanotube composites. Polymer Composites. 2004;25(6):630-45.

42. Meng L, Fu C, Lu Q. Advanced technology for functionalization of carbon nanotubes. Progress in Natural Science. 2009;19(7):801-10.

43. Chen Y, Haddon R, Fang S, Rao A, Eklund P, Lee W, et al. Chemical attachment of organic functional groups to single-walled carbon nanotube material. Journal of Materials Research. 1998;13(9):2423-31.

44. Niyogi S, Hamon MA, Hu H, Zhao B, Bhowmik P, Sen R, et al. Chemistry of single-walled carbon nanotubes. Accounts of Chemical Research. 2002;35(12):1105-13.

45. Hong C, You Y, Pan C. Synthesis of water-soluble multiwalled carbon nanotubes with grafted temperature-responsive shells by surface RAFT polymerization. Chemistry of Materials. 2005;17(9):2247-54.

46. Eitan A, Jiang K, Dukes D, Andrews R, Schadler LS. Surface modification of multiwalled carbon nanotubes: Toward the tailoring of the interface in polymer composites. Chemistry of Materials. 2003;15(16):3198-201.

47. Tasis D, Tagmatarchis N, Bianco A, Prato M. Chemistry of carbon nanotubes. Chemical Reviews. 2006;106(3):1105.

48. Hamwi A, Alvergnat H, Bonnamy S, Beguin F. Fluorination of carbon nanotubes. Carbon. 1997;35(6):723-8.

49. Etmimi HM, Tonge MP, Sanderson RD. Synthesis and characterization of polystyrene-graphite nanocomposites via surface RAFT-mediated miniemulsion polymerization. Journal of Polymer Science Part A: Polymer Chemistry. 2011;49(7):1621-32.

50. Sun Y, Fu K, Lin Y, Huang W. Functionalized carbon nanotubes: Properties and applications. Accounts of Chemical Research. 2002;35(12):1096-104.

51. Liu J, Yang W, Tao L, Li D, Boyer C, Davis TP. Thermosensitive graphene nanocomposites formed using pyrene-terminal polymers made by RAFT polymerization. Journal of Polymer Science Part A: Polymer Chemistry. 2010;48(2):425-33.

52. Baskaran D, Mays JW, Bratcher MS. Noncovalent and nonspecific molecular interactions of polymers with multiwalled carbon nanotubes. Chemistry of Materials. 2005;17(13):3389-97.

53. Chen J, Liu H, Weimer WA, Halls MD, Waldeck DH, Walker GC. Noncovalent engineering of carbon nanotube surfaces by rigid, functional conjugated polymers. Journal of the American Chemical Society. 2002;124(31):9034-5.

54. Star A, Liu Y, Grant K, Ridvan L, Stoddart JF, Steuerman DW, et al. Noncovalent side-wall functionalization of single-walled carbon nanotubes. Macromolecules. 2003;36(3):553-60.

55. Dieckmann GR, Dalton AB, Johnson PA, Razal J, Chen J, Giordano GM, et al. Controlled assembly of carbon nanotubes by designed amphiphilic peptide helices. Journal of the American Chemical Society. 2003;125(7):1770-7.

56. Smets G, Hart R. Block and graft copolymers. In: Fortschritte Der Hochpolymeren-Forschung. Springer; 1960. p. 173-220.

57. Feng C, Li Y, Yang D, Hu J, Zhang X, Huang X. Well-defined graft copolymers: From controlled synthesis to multipurpose applications. Chemical Society Reviews. 2011;40(3):1282-95.

58. Li Z, Zhang K, Ma J, Cheng C, Wooley KL. Facile syntheses of cylindrical molecular brushes by a sequential RAFT and ROMP “grafting-through” methodology. Journal of Polymer Science Part A: Polymer Chemistry. 2009;47(20):5557-63.

59. Grubbs RB, Hawker CJ, Dao J, Fréchet JM. A tandem approach to graft and dendritic graft copolymers based on “Living” free radical polymerizations. Angewandte Chemie International Edition in English. 1997;36(3):270-2.

60. Xia J, Matyjaszewski K. Controlled/“living” radical polymerization. Atom transfer radical polymerization using multidentate amine ligands. Macromolecules. 1997;30(25):7697-700.

61. Beers KL, Gaynor SG, Matyjaszewski K, Sheiko SS, Möller M. The synthesis of densely grafted copolymers by atom transfer radical polymerization. Macromolecules. 1998;31:9413-5.

62. Xu G, Wu W, Wang Y, Pang W, Zhu Q, Wang P, et al. Constructing polymer brushes on multiwalled carbon nanotubes by in situ reversible addition fragmentation chain transfer polymerization. Polymer. 2006;47(16):5909-18.

63. Samakande A, Sanderson RD, Hartmann PC. Rheological properties of RAFT-mediated poly (styrene-< i> co</i>-butyl acrylate)–clay nanocomposites [P (S-< i> co</i>-BA)-PCNs]: Emphasis on the effect of structural parameters on thermo-mechanical and melt flow behaviors. Polymer. 2009;50(1):42-9.

64. Feng W, Zhu S, Ishihara K, Brash JL. Adsorption of fibrinogen and lysozyme on silicon grafted with poly (2-methacryloyloxyethyl phosphorylcholine) via surface-initiated atom transfer radical polymerization. Langmuir. 2005;21(13):5980-7.

65. Wang G, Huang S, Wang Y, Liu L, Qiu J, Li Y. Synthesis of water-soluble single-walled carbon nanotubes by RAFT polymerization. Polymer. 2007;48(3):728-33.

66. Ejaz M, Ohno K, Tsujii Y, Fukuda T. Controlled grafting of a well-defined glycopolymer on a solid surface by surface-initiated atom transfer radical polymerization. Macromolecules. 2000;33(8):2870-4.

67. Zhang M, Müller AH. Cylindrical polymer brushes. Journal of Polymer Science Part A: Polymer Chemistry. 2005;43(16):3461-81.

68. Wang W, Neoh K, Kang E. Surface functionalization of Fe3O4 magnetic nanoparticles via RAFT-mediated graft polymerization. Macromolecular Rapid Communications. 2006;27(19):1665-9.

69. Wang J, Matyjaszewski K. Controlled/" living" radical polymerization. Atom transfer radical polymerization in the presence of transition-metal complexes. Journal of the American Chemical Society. 1995;117(20):5614-5.

70. Chiefari J, Chong Y, Ercole F, Krstina J, Jeffery J, Le TP, et al. Living free-radical polymerization by reversible addition-fragmentation chain transfer: The RAFT process. Macromolecules. 1998;31(16):5559.

71. Hawker CJ, Bosman AW, Harth E. New polymer synthesis by nitroxide mediated living radical polymerizations. Chemical Reviews. 2001;101(12):3661-88.

72. Shanmugharaj A, Bae J, Nayak RR, Ryu SH. Preparation of poly (styrene-co-acrylonitrile)-grafted multiwalled carbon nanotubes via surface-initiated atom transfer radical polymerization. Journal of Polymer Science Part A: Polymer Chemistry. 2007;45(3):460-70.

73. Pollino JM, Weck M. Non-covalent side-chain polymers: Design principles, functionalization strategies, and perspectives. Chemical Society Reviews. 2005;34(3):193-207.

74. Matyjaszewski K, Xia J. Atom transfer radical polymerization. Chemical Reviews. 2001;101(9):2921-90.

75. Fürstner A. Olefin metathesis and beyond. Angewandte Chemie International Edition. 2000;39(17):3012-43.

76. Lai JT, Filla D, Shea R. Functional polymers from novel carboxyl-terminated trithiocarbonates as highly efficient RAFT agents. Macromolecules. 2002;35(18):6754-6.

77. Baram J, Shirman E, Ben-Shitrit N, Ustinov A, Weissman H, Pinkas I, et al. Control over self-assembly through reversible charging of the aromatic building blocks in photofunctional supramolecular fibres. Journal of the American Chemical Society. 2008;130(45):14966-7.

78. Carroll JB, Waddon AJ, Nakade H, Rotello VM. ``Plug and play''polymers. thermal and X-ray characterizations of noncovalently grafted polyhedral oligomeric silsesquioxane (POSS)-polystyrene nanocomposites. Macromolecules. 2003;36:6289-91.

79. Bazzi HS, Sleiman HF. Adenine-containing block copolymers via ring-opening metathesis polymerization: Synthesis and self-assembly into rod morphologies. Macromolecules. 2002;35:9617-20.

80. Ren S, Chen D, Jiang M. Noncovalently connected micelles based on a β-cyclodextrin-containing polymer and adamantane end-capped poly (ε-caprolactone) via host–guest interactions. Journal of Polymer Science Part A: Polymer Chemistry. 2009;47(17):4267-78.

81. Baati R, Ihiawakrim D, Mafouana RR, Ersen O, Dietlin C, Duportail G. Hexahistidine-Tagged Single-Walled carbon nanotubes (His6-tagSWNTs): A multifunctional hard template for hierarchical directed Self-Assembly and nanocomposite construction. Advanced Functional Materials. 2012.

82. Szwarc M. Living polymers. Their discovery, characterization, and properties. Journal of Polymer Science Part A: Polymer Chemistry. 1998;36(1):IX-XV.

83. Braunecker WA, Matyjaszewski K. Controlled/living radical polymerization: Features, developments, and perspectives. Progress in Polymer Science. 2007;32(1):93-146.

84. Pound G, Eksteen Z, Pfukwa R, McKenzie JM, Lange RF, Klumperman B. Unexpected reactions associated with the xanthate-mediated polymerization of N-vinylpyrrolidone. Journal of Polymer Science Part A: Polymer Chemistry. 2008;46(19):6575-93.

85. Moad G, Rizzardo E, Thang SH. Living radical polymerization by the RAFT process. Australian Journal of Chemistry. 2005;58(6):379-410.

86. Matyjaszewski K. 8 General concepts and history of living radical polymerization. Handbook of Radical Polymerization. 2002:361.

87. Moad G, Solomon DH. The chemistry of radical polymerization. Elsevier Science Limited; 2006.

88. Rüchardt C. Relations between structure and reactivity in Free-Radical chemistry. Angewandte Chemie International Edition in English. 1970;9(11):830-43.

89. Matyjaszewski K, Davis TP.Handbook of radical polymerization. New York: Wiley-Interscience, 2002.

90. Van Herk AM, Monteiro M. 6 Heterogeneous systems. Handbook of Radical Polymerization. 2002:301.

91. Rizzardo E, Solomon DH. On the origins of nitroxide mediated polymerization (NMP) and reversible Addition–Fragmentation chain transfer (RAFT). Australian Journal of Chemistry. 2012.

92. Mayadunne RT, Rizzardo E, Chiefari J, Chong YK, Moad G, Thang SH. Living radical polymerization with reversible addition-fragmentation chain transfer (RAFT polymerization) using dithiocarbamates as chain transfer agents. Macromolecules. 1999;32(21):6977-80.

93. Moad G, Rizzardo E, Thang SH. Toward living radical polymerization. Accounts of Chemical Research. 2008;41(9):1133-42.

94. Corpart P, Charmot D, Zard SZ, Biadatti T, Michelet D. Method for block polymer synthesis by controlled radical polymerisation. U.S. Patent No. 6,153,705. 28 Nov. 2000.

95. Patten TE, Matyjaszewski K. Atom transfer radical polymerization and the synthesis of polymeric materials. Advanced Materials.1998;10(12):901-915.

96. Chong Y, Le TP, Moad G, Rizzardo E, Thang SH. A more versatile route to block copolymers and other polymers of complex architecture by living radical polymerization: The RAFT process. Macromolecules. 1999;32(6):2071-4.

97. Formhals A. Process and apparatus for preparing artificial threads: U.S. Patent No. 1,975,504. 1934.

98. Reneker DH, Chun I. Nanometre diameter fibres of polymer, produced by electrospinning. Nanotechnology. 1996;7(3):216.

99. Ramakrishna S. An introduction to electrospinning and nanofibres. World Scientific; 2005.

100. Yeo LY, Friend JR. Electrospinning carbon nanotube polymer composite nanofibres. Journal of Experimental Nanoscience. 2006;1(2):177-209.

101. Hou H, Ge JJ, Zeng J, Li Q, Reneker DH, Greiner A, et al. Electrospun polyacrylonitrile nanofibres containing a high concentration of well-aligned multiwall carbon nanotubes. Chemistry of Materials. 2005;17(5):967-73.

102. Bang H, Gopiraman M, Kim B, Kim S, Kim I. Effects of pH on electrospun PVA/acid-treated MWNT composite nanofibres. Colloids and Surfaces A: Physicochemical and Engineering Aspects. 2012;409:112-7.

103. Das S, Wajid AS, Bhattacharia SK, Wilting MD, Rivero IV, Green MJ. Electrospinning of polymer nanofibres loaded with noncovalently functionalized graphene. Journal of Applied Polymer Science. 2012.

104. Zou J, Liu L, Chen H, Khondaker SI, McCullough RD, Huo Q, et al. Dispersion of pristine carbon nanotubes using conjugated block copolymers. Advanced Materials. 2008;20(11):2055-60.

105. Nakashima N, Tomonari Y, Murakami H. Water-soluble single-walled carbon nanotubes via noncovalent sidewall-functionalization with a pyrene-carrying ammonium ion. Chemistry Letters. 2002;31(6):638-9.

106. Haddon R. Magnetism of the carbon allotropes. 1995. 249-255

107. Assali M, Leal MP, Fernández I, Baati R, Mioskowski C, Khiar N. Non-covalent functionalization of carbon nanotubes with glycolipids: Glyconanomaterials with specific lectin-affinity. Soft Matter. 2009;5(5):948-50.

108. Guldi DM, Rahman GA, Jux N, Balbinot D, Hartnagel U, Tagmatarchis N, et al. Functional single-wall carbon nanotube nanohybrids associating SWNTs with water-soluble enzyme model systems. Journal of the American Chemical Society. 2005;127(27):9830-8.

109. Ogoshi T, Takashima Y, Yamaguchi H, Harada A. Chemically-responsive sol-gel transition of supramolecular single-walled carbon nanotubes (SWNTs) hydrogel made by hybrids of SWNTs and cyclodextrins. Journal of the American Chemical Society. 2007;129(16):4878-9.

110. Yan Y, Cui J, Pötschke P, Voit B. Dispersion of pristine single-walled carbon nanotubes using pyrene-capped polystyrene and its application for preparation of polystyrene matrix composites. Carbon. 2010;48(9):2603-2612.

Chapter 3: Preparation of Polystyrene/MWNT nanocomposites via noncovalent versus covalent interactions

3.1. Abstract

The reversible addition fragmentation chain transfer (RAFT) and atom transfer radical polymerization (ATRP) macroinitiators were synthesised via esterification reactions with the appropriate pyrene derivatives. Styrene (S) was polymerized via ATRP and RAFT mediated polymerization using these macroinitiators to synthesise the pyrene-capped polystyrene (PS) chains. Size exclusion chromatography (SEC) was used to characterize the obtained molecular weight. Pristine multi-walled nanotubes (MWNTs) were interacted with these PS chains through π-π stacking. This interaction was characterized using thermal gravimetric analysis (TGA), nuclear magnetic resonance (NMR), ultraviolet-visible-near-infra red spectroscopy (UV/Vis/NIR) and fluorescence spectroscopy. As a means of comparison the same ATRP and RAFT agents were immobilized covalently along an oxidized MWNT surface and styrene was grafted from these active sites to produce the covalently functionalized MWNTs. Suspensions of all the composites in a 20 w/v% PS in chloroform solution were electrospun. The produced fibres were characterized by transmission electron microscopy (TEM) and scanning electron microscopy (SEM). TEM images of the electrospinning solutions and cross-sections through the electrospun fibres showed distinguishable differences between the degree of dispersion of the MWNTs which had been functionalized and those that were unfunctionalized.

3.2. Introduction

The incorporation of carbon nanotubes into composite materials is becoming increasingly popular and common due to its ability to impart desirable thermal, electrical or mechanical properties onto the composite.[1-4] One of the biggest challenges when working with pristine CNTs arises in their lack of solubility in most polymeric matrices. This, as a result, decreases their ability to disperse uniformly in a matrix of a composite. To tackle this problem, the chemical surface functionalization of CNTs through covalent additions to the nanotube carbon–carbon bonds[5-8] has been commonly done to compatibilize the CNTs and allow for their adequate dispersion in solution and in a composite. Several examples of direct surface functionalization of CNTs can be found in literature.[9-15] Etmimi *et al.*[16] describes the covalent functionalization of graphite through the immobilization of the RAFT agent S-1-dodecyl-S'-(isobutyric acid) trithiocarbonate (DIBTC) onto the graphite surface. This was done through

the graphitic surface oxidation followed by an esterification between the graphitic oxide (GO) and the DIBTC to form an active surface from whence styrene was then grafted from. This graphitic composite was found to form a thermally and mechanically more stable composite than the inherent PS polymer.

The covalent functionalization of MWNTs through surface-initiated ATRP polymerization has also been reported. Baskaran *et al.*[17] attached the ATRP initiator HEBrIB onto MWNT surfaces functionalized with surface-bound carboxylic acid groups which were initially treated with thionyl chloride. Styrene (S) and methylmethacrylate (MMA) monomers were then grafted from these points, leading to PS and PMMA covalently grafted from the MWNT surfaces at levels up to 70 wt %.

The major drawback to such a covalent functionalization of the CNTs is realised by the change in the electronic sp^2 hybridization between the carbon atoms in the pristine CNT structure which provides great electrical and transport abilities.[18-20] As a result, noncovalent functionalization through adsorption of various functionalities through use of the delocalized π-electron cloud presented by the sp^2 hybridized carbons of the CNT surface has become a method for CNT functionalization without compromising the desirable intrinsic properties of pristine CNTs.[21] Yan *et al.* describe the formation of a PS nanocomposite through noncovalent interactions.[22] They show that a pyrene-terminated PS compound can successfully be interacted noncovalently with SWNTs through π-π stacking between the pyrene and conjugated carbon surface of the nanotubes. This compound was then dispersed successfully in a PS matrix to form a PS/PyPS/SWNT nanocomposite which was seen to reach a conductivity suitable for anti-static thin film criteria, indicating that the inherent SWNT structure was maintained.

Controlled/living radical polymerization (LRP) allows for the grafting of a variety of monomers from solid supports[23] to synthesise polymers with controlled, well-defined morphologies, topologies, composition, and narrow distribution. RAFT polymerization in particular is a popular method of LRP since it is effective, relatively robust and versatile.[24,25]

Trithiocarbonates such as S,S′-bis(α,α′-dimethyl-α′′-acetic acid)-trithiocarbonate and S-1-Dodecyl-S′-(α,α′-dimethyl-α′′-acetic acid)trithiocarbonate (DIBTC) were shown by Lai *et al.* to provide excellent control over the bulk or solution polymerization of styrene and other monomers due to the extraordinary chain-transfer efficiency afforded by the tertiary carbon

atom attached to the labile sulphur atom as well as the presence of a radical-stabilizing carboxyl group.[26]

The surface-initiated RAFT (SI-RAFT) polymerization from CNTs and other solid surfaces has been reported by several sources.[13,14,16,27,28] The use of several different RAFT agents has been reported for this use. Pei *et al.*[14]describe the immobilization of the RAFT agent 4-(4-Cyanopentanoic Acid) Dithiobenzoate on the MWNTs surface which had previously undergone surface-oxidation. From there RAFT polymerization was done to synthesise the final nanocomposite.

The RAFT agent immobilization on the solid surface for use in SI-RAFT polymerization can be achieved either through immobilization through the Z- or the R-group of the RAFT agent. The Z-group approach is done through the attachment of the RAFT agent via the stabilizing Z-group (see scheme 2.5), allowing the leaving and reinitiating R-group to maintain intact.[29] The R-group approach is done in this project where the hydroxyl groups of the oxidized MWNT surface is esterified with the carboxylic acid (R-group) moiety of the RAFT agent to immobilize the RAFT agent on the MWNT surface. The styrene monomers are then grafted from the MWNT surface by SI-RAFT polymerization using miniemulsion. Miniemulsion is a simple and facile method of incorporating nanofillers into polymeric matrices of differing polarities. Lu *et al.* demonstrated the successful in situ modification of pristine SWNTs via miniemulsion polymerization since such a system includes the oil and aqueous phases which facilitate the problems encountered by differences in monomer and filler solubilities.[30]

Another popular choice of LRP techniques for the synthesis of styrenes and (meth)acrylates is ATRP[7,31-33] since it enables polymers of controlled molecular weight and architectures to be synthesised which have low polydispersity. It also is tolerant to many monomer functionalities which introduce the option of incorporating these functionalities into the polymer chain. The use of the initiator for ATRP determines the end-group found in the polymer chain. Therefore, this can be utilised to tailor the polymer chains and create complex, well-defined polymers.

Several groups have shown the immobilization of a bromo-functional ATRP initiator on carbon nanotubes and the subsequent successful grafting of styrene from these active sites.[17,34-36] In these cases, an ATRP initiator is chosen with a functionality which can chemically bind to the oxidized surface of the CNTs through esterification. As such, the ATRP initiator HEBrIB was chosen for this research since it contains a hydroxyl group

capable of esterification with the carboxylic acid groups on the oxidized MWNT surface, an activating carbonyl group on the α-carbon, as well as bromine as the halide which can rapidly migrate between the propagating chain and the transition metal complex leading to controlled chain growth.[32]

For the preparation of the noncovalently compatibilized MWNT/PS nanocomposite, the PS was synthesised via both ATRP and RAFT polymerizations using a pyrene-functionalized RAFT agent or ATRP macroinitiator to introduce the pyrene functionality into the PS chain ends which are then expected to interact with the MWNT surface through π-π stacking. The RAFT agent and ATRP initiator chosen for this were the same as those used for the SI-RAFT and SI-ATRP polymerizations of styrene in the grafting from the MWNT surface for the synthesis of the covalent nanocomposite. This was done to minimize the variables such that the final nanocomposites could be compared with regards to the effect that covalent and the noncovalent bonding have on the dispersibility of the MWNTs in solution or in a composite. The electrospinning of 20 w/v% PS in $CHCl_3$ solutions containing the various nanocomposites was done to determine the effect of MWNT content and functionalization on fibre production. To our knowledge, no reports exist involving the electrospinning of MWNTs nanocomposite nanofibres where noncovalent compatibilization has been used to disperse the MWNTs within the solution and the matrix.

3.3. Experimental

3.3.1. Chemicals

1-dodecanethiol (97%, Aldrich), tricapryl methyl ammonium chloride (Aliquot 336) (Acros), carbon disulfide (99.9%, Aldrich), acetone (Sigma-Aldrich), chloroform (Sigma-Aldrich,≥99%), hydrochloric acid (HCl) (Merck, 32%), sodium hydroxide 50% solution (Sigma-Aldrich, 50%), and carbon disulfide (CS_2) (KMIX, 99%) were used as is for the synthesis of DIBTC. After which more DIBTC was purchased due to time constraints (Aldrich, 98%) to synthesise the pyrene-functional DIBTC using thionyl chloride ($SOCl_2$) (Merck, ≥99%), Pyridine (SAARCHEM, 99.5%) and Pyrenemethanol (Aldrich, 98%). 2,2'-Azobis(isobutyronitrile) (AIBN) (Aldrich, 98%) which was purified by recrystallization from methanol and styrene (Aldrich, 99%) which was removed of inhibitors using an alumina column were used to synthesise the pyrene-functional polystyrene (PS) via RAFT polymerization. Short-length MWNT (times nano, >95%) were used as received. Sodium

Nitrate ($NaNO_3$) (NT Laboratory Supplies, 99%), potassium permanganate ($KMnO_4$) (Scienceworld, 99%), sulphuric acid (H_2SO_4) (Merck, 95-97%) (Merck, 99%), and hydrogen peroxide (H_2O_2) (Merck, 50%) were used for the oxidation of the MWNTS. 1,3-dicyclohexyl carbodiimide (DCC) (Aldrich, 99%), 4-dimethylamino pyridine (DMAP) (Aldrich, 98%), Sodium dodecylbenzene sulfonate (SDBS) (Fluka, 99%) and Hexadecane (HD) (Sigma-Aldrich, 99%) were used without further purification in the covalent functionalization of the MWNTs. Potassium hydride (KH) (Aldrich, 35 wt% in mineral oil) was used for the cleavage of PS from the covalent MWNT-PS-DIBTC compound for SEC analysis purposes.
Hydroxyethyl-2-bromoisobutyrate (HEBrIB) (Aldrich, 95%) and 1-pyrenebutyric acid (Aldrich, 97%) were purchased and used as is for the synthesis of the pyrene-functional HEBrIB ATRP macroinitiator. N,N,N′,N″,N″-Pentamethyldiethylenetriamine (PMDETA) (Aldrich, 99%) and Copper Chloride (Aldrich, 97%) were used as is for the ATRP polymerization of styrene using the macroinitiator of HEBrIB-Py. Copper bromide (CuBr) (Aldrich, 98%) was used as catalysts for the grafting of styrene from the HEBrIB-immobilized MWNT surface. High molecular weight polystyrene (Aldrich, average $\overline{M_w}$ ~350 000, average $\overline{M_n}$~170 000) was used as matrix material for the composite nanofibres. All solvents used were distilled prior to use.

3.3.2. Analytical techniques

A variety of techniques were used to analyse the various compounds synthesised. Nuclear magnetic resonance (NMR) was done using a Varian VXR-Unity 300 MHz instrument set at 20°C. Solvents used to analyse samples with NMR were deuterated chloroform ($CDCl_3$) or deuterated dimethyl sulfoxide (DMSO-d_6). Both ^{13}C and ^{1}H NMR were done.

Fourier transformed-infrared (FT-IR) was done using a Thermo scientific Nicolet iS10 Smart iTR instrument, and Omnic software. The absorption was measured in attenuated total reflectance (ATR) mode with a resolution of 4, an average number of scans of 32 and over the wavenumber range of 450-4 500cm^{-1}.

Dilute solutions were prepared in chloroform and analysed using fluorescence spectroscopy using a Perkin Elmer Luminescence Spectrometer LS50B instrument and Hellma quartz SUPRASIL® cuvettes with a 10 mm path length. The excitation and emission decay spectra were measured between the wavelengths of 250-650 nm, with 4.0-3.0 nm slit size for excitation and emission mode respectively and a scan speed of 250 nm/min. The emission

peak for the excitation mode was set at 390 nm and the excitation peak was set at 396 nm for the emission mode. The results were analysed using FL WinLab software.

Ultraviolet-visible spectroscopy (UV/Vis) and ultraviolet-visible/near-infra-red (UV/Vis/NIR) spectroscopy results were recorded in Perkin Elmer UV/Vis Spectroscopy Cell quartz cuvettes using an analytik jena Specord 210 plus instrument set on absorbance between 200-600 nm wavelength range for the UV/Vis results and 400-1 000 nm for the UV/Vis/NIR results with a slit size of 1 nm in both cases. Depending on the sample, a reference of THF, DCM or chloroform was used. WinASPECT PLUS software was used to analyse the data.

Size exclusion chromatography (SEC) was done using a Breeze chromatographic system in which a Waters 1515 isocratic HPLC pump, a Waters 717plus auto-sampler and a Waters 600E system controller were operated by Breeze Version 3.30 SPA software. A Waters in-line degasser and a Waters 2414 differential refractometer were operated at 30^{o}C whilst in series with a Waters 2487 dual wavelength absorbance UV/Vis detector set to 254 nm and 365 nm. THF was used as the eluent (HPLC grade, stabilized with 0.125% BHT) with a flow rate of 1 ml/min. An injection volume of 100 µL was used to introduce the sample into Two PLgel (Polymer Laboratories) 5 µm Mixed-C (300 × 7.5 mm) columns and a pre-column (PLgel 5 µm Guard, 50x7.5 mm) which were kept at 30°C. PS standards ranging from 580 g/mol to 2×10^6 g/mol were used as calibration standards in a 5 mg/ml concentration. Samples were dissolved in THF (HPLC grade, stabilized with 0.125% BHT) in a 5 mg/ml concentration and filtered through 0.45 µm nylon filters. All reported results are equivalent to polystyrene molecular weights.

Thermogravimetric analysis (TGA) was done using a Perkin Elmer TGA 7. Samples of approximately 10 mg were analysed under nitrogen atmosphere with a nitrogen gas flow rate of 20 ml/min at a temperature cycle starting at ambient room temperature to 600°C with a 20°C/min heating rate.

An FEI TECNAI G^2 instrument with an accelerating voltage of 200 kV was used to obtain bright-field transmission electron microscopy (TEM) images of the nanotube composite morphologies. The samples analysed were all diluted with chloroform and dropped onto carbon-coated copper grids. After the chloroform was evaporated off, the grid was placed in the TEM instrument and analysed. Electrospun fibres were cut to size and embedded in Spurr's resin. A Reichert Ultracut S ultramicrotome instrument was used to cut 100 nm

ultrathin sections which were collected on 200-mesh copper grids and viewed in the TEM instrument.

SEM was used to determine the fibre morphology and topology of the electrospun nanocomposite fibres. A Leo 1430VP SEM instrument was used with a Centaurus detector with a 133 eV resolution at 5.9 keV and a 10 mm^2 detector area. SEM tubs with double-sided carbon tape were used to mount the fibre samples which were then coated in gold twice to produce a conductive surface from which electrons could scatter to produce a signal and thus an image of the surface. A magnification between $90 \times -3 \times 10^5 \times$ was used to produce the images with a working distance of ~21 mm and a voltage of 7 kV.

3.3.3. Covalent attachment of RAFT mediated PS with pristine MWNTs via "grafting-from"

The RAFT agent DIBTC was covalently attached to oxidized MWNTs through an esterification procedure, after which styrene was grafted from these active sites through miniemulsion polymerization.

3.3.3.1. Oxidation of pristine MWNTs

The preparation of the oxidized MWNTs (MWNT-COOH) was performed based on the preparation of graphitic oxide as presented by Hummers and Offeman.[37] The MWNTs (2 g) and Sodium Nitrate (1 g) were mixed into concentrated sulphuric acid (46 mL). The solution was cooled to 0°C using an ice-bath. Potassium permanganate (6 g) was added whilst stirring vigorously. The temperature was maintained below 20°C through use of the ice bath. After addition of the potassium permanganate, the temperature of the suspension was raised to ~35°C where it was maintained for 30 min. Next, DDI water (92 mL) was slowly stirred into the suspension which caused violent effervescence and gas release along with an increase in reaction temperature. After 15 minutes, warm DDI water (280 mL) treated with 3% hydrogen peroxide was added. This suspension was then centrifuged at 5 000 rpm for 10 min to collect the oxidized nanotubes in the deposit. These were then washed with DDI water and placed in dialysis tubing in a jar of fresh DDI water and left to stir overnight to neutralize the acidic MWNTs. The pH of the surrounding DDI water was tested and replaced until the pH of the DDI water in the jar maintained a neutral pH.

3.3.3.2. Synthesis of S-1-dodecyl-S'-(isobutyric acid) trithiocarbonate (DIBTC) RAFT agent

DIBTC was synthesised according to a procedure from Lai *et al.*[26] 1-dodecanethiol (8.0g, 0.040 mol), acetone (20.1 g, ~6x molar excess), and Aliquot 336 (0.65 g, 0.0016 mol) were mixed in a jacketed reactor cooled in an ice bath under nitrogen atmosphere. A 50% sodium hydroxide (NaOH) solution (3.5 g, 0.042 mol) was added drop wise over 20 minutes. The reaction mixture was stirred for a further 15 minutes before adding a solution of carbon disulphide (3.1 g, 0.040 mol) in acetone (4.0 g, 0.069 mol) over 20 minutes at which point the solution was seen to turn bright yellow. 10 minutes later, chloroform (7.0 g, 0.06 mol) was added to the reaction mixture in one portion, followed by the drop wise addition of a 50% solution NaOH (16.0 g, 0.2 mol) over 30 minutes.

The reaction mixture was stirred overnight under reflux. Afterwards, DDI water (~60 mL) was added to the mixture and poured into a large beaker, where it was stirred at high revolutions. The mixture was then acidified with HCl (33%; 10.0 mL) and stirred for an hour to help evaporate off any acetone. The thick yellow precipitate was then collected via filtration using a Buchner funnel and dissolved in isopropanol (~500 mL). The un-dissolved solid was identified as S,S'-bis(1-dodecyl) trithiocarbonate. The isopropanol filtrate was then concentrated to dryness, and recrystallized from cold hexane to yield the yellow crystals of S-1-dodecyl-S'-(isobutyric acid) trithiocarbonate which were then oven dried overnight; ^{1}H NMR: (300 MHz, ($CDCl_3$) δ (ppm): 0.89 (t, 3H) (CH_3–CH_2–); 1.27–1.71, (m, 20H) (CH_3–CH_2–CH_2–); 1.72, s, 6H (CH_3–); 3.29 (t, 2H) (–CH_2–S); 12.02, (s, 1H) (–*OH*). ^{13}C NMR: (75 MHz, ($CDCl_3$) δ (ppm): 220.69 (*C*=*S*); 177.65 (*C*=*O*); 55.39 (*C*); 36.85 (*C*–*S*); 25.02 (CH_3–); 22.46-31.69 (CH_3–CH_2–CH_2–); 13.89 (CH_3–CH_2–).

3.3.3.3. Immobilization of the RAFT agent DIBTC on the MWNT-COOH surface

The procedure for the RAFT immobilization on the MWNT-COOH surface as well as the subsequent styrene polymerization of this was based on a similar procedure by Etmimi[16] in which the RAFT agent was immobilized onto a graphitic oxide surface. Here the MWNT-COOH (0.2 g) were stirred in DMF (100 mL) for 15 min then sonicated for a further 15 min to allow for adequate dispersion. The sonicator amplitude was set to 90% with a pulse rate of 3 sec on, and 2 sec off. DIBTC (0.5 g) was added to the suspension, which was subsequently stirred for 5 min. Next, DMAP (0.1 g) and DCC (0.5 g) were added, after which the suspension was stirred at room temperature for 24 h whilst under reflux. Afterwards, the solvent was removed under reduced pressure and the resultant solid was washed with DCM to remove any unattached RAFT agent until the washings were free of the DIBTC as

determined by UV analysis. The final product was then dried at 40°C overnight under vacuum. A yield of 54% of MWNT-DIBTC was obtained.

3.3.3.4. Synthesis of the MWNT-PS-DIBTC nanocomposite via RAFT mediated miniemulsion polymerization

MWNT-DIBTC (0.030 g) was stirred in DDI water (~50 g) for 15 min after which it was sonicated for another 15 min using a Vibracell VCX 750 ultrasonicator. AIBN (0.0083 g), styrene (3.01 g) and HD (0.10 g) were added to the suspension which was then stirred for 15 min followed by 15 min of sonication. An aqueous solution of SDBS (0.060 g SDBS in 10 g DDI water) was added to the oil phase. The mixture was then stirred for 1 h followed by ultrasonication of 80% amplitude, pulse rate of 3 sec on, and 2 sec off and a cut-off temperature of the miniemulsion of 40°C so as to avoid polymerization during this stage. The miniemulsion was then transferred to a round bottom flask which was immersed in an oil bath while the contents were purged using nitrogen gas for 15 min before the oil bath temperature was increased to 75°C so as to initiate polymerization. After 10 h under nitrogen atmosphere, the reaction mixture was cooled to room temperature to stop the reaction, followed by precipitation into methanol and vacuum drying overnight to recover the MWNT-PS-DIBTC (0.667 g). Any excess homopolystyrene was removed by the successive dissolution in tetrahydrofuran (THF), ultracentrifugation and removal of the black deposit.

3.3.4. Noncovalent interaction of the pyrene-functional PS (DIBTC-PS-Py) synthesised via RAFT with pristine MWNTs

The noncovalently grafted pristine MWNTs with DIBTC-PS-Py were synthesised via a number of steps as described below. Two PS block lengths were synthesised with the difference between them being that the first had a targeted styrene chain length of 5 000 g/mol, where the second compound targeted a styrene chain length of 15 000 g/mol. The full reaction scheme is shown in scheme 3.1.

3.3.4.1. Synthesis of DIBTC with an acid chloride functionality (DIBTC-Cl)

Acid chloride functionality was added to DIBTC according to the procedure followed by Donkers.[38] DIBTC (5.5 mmol) was dissolved in anhydrous dichloromethane (DCM) (10 mL) under argon atmosphere in an oven dried 3-neck round-bottom flask. The flask was cooled in liquid nitrogen until the mixture solidified. Thionyl chloride (27.5 mmol) was added drop-wise to the solution at the same time, allowing the mixture to reach room temperature while stirring. As the mixture became warmer the development of HCl and SO_2 gas was observed.

Once the flask reached room temperature, the flask was placed into a 30°C preheated oil bath for 3 h. After completion, the solvent and excess thionyl chloride was removed under vacuum overnight. The product of DIBTC-Cl was used immediately for the next reaction without purification so as to avoid any unwanted side reaction.

3.3.4.2. Synthesis of DIBTC-Pyrene (DIBTC-Py)

The pyrene-functional DIBTC RAFT macroinitiator was synthesised through the esterification between the pyrenemethanol hydroxyl group and the acid chloride moiety of the DIBTC-Cl. Pyrenemethanol (2.62 mmol) and pyridine (2.6 mmol) were dissolved in anhydrous THF (20 mL). DIBTC-Cl (2.62 mmol) dissolved in THF (5 mL) was then added drop wise to the mixture while being stirred. After letting the reaction run overnight at room temperature, the solvent was evaporated off. The product was redissolved in THF and extracted three times with brine and three times with water. The organic layer containing the DIBTC-Py was dried over Na_2SO_4 and subsequently vacuum dried to remove the solvent. A yield of 66.44% was obtained.^{1}H NMR: (300 MHz, ($CDCl_3$) δ (ppm): 0.99 (t, 3H) (*CH*$_3$–CH_2–); 1.25-1.85 (m, 20H) (CH_3–*CH*$_2$–CH_2–); 1.55 (m, 6H) (*CH*$_3$–); 5.39 (s, 2H) (O–*CH*$_2$–C). ^{13}C NMR: (75 MHz, ($CDCl_3$) δ (ppm): 221.25 (*C*=*S*); 172.53 (*C*=*O*); 51.89 (*C*); 36.96 (*C*–*S*); 25.85 (*CH*$_3$–); 22.25-31.48 (CH_3–*CH*$_2$–CH_2–); 13.68 (*CH*$_3$–CH_2–).

3.3.4.3. Synthesis of DIBTC-Polystyrene-Pyrene (DIBTC-PS-Py)

Two versions of the pyrene functional PS compounds were synthesised using the RAFT macroinitiator of DIBTC-Py, one with a targeted styrene chain length of 5 000 g/mol and the other of a longer targeted styrene chain length of 15 000 g/mol. The experimental procedures were done in a similar manner, excepting the amount of styrene added with the quantities used indicated in Table 3.1.

AIBN, RAFT macroinitiator DIBTC-Py, styrene monomer and free DIBTC were placed in a round bottom flask and dissolved in toluene. The solution was degassed by purging with argon for 45 minutes, after which the solution was kept under argon atmosphere whilst being placed in an oil bath at 70°C for 72 h. Upon completion, the reaction was terminated through the addition of methanol and further precipitation into methanol. The solid polymer was then filtered and dried in vacuum at room temperature overnight. The final product was purified by column chromatography using silica as the stationary phase and 20:80 ratio of cyclohexane: toluene for the mobile phase.

PS chain length	AIBN	DIBTC-Py	Styrene	Free DIBTC	Toluene	Yield
5 000 g/mol	0.077 mmol	0.193 mmol	9.27 mmol	0.07 mmol	10 mL	0.6695 g
15 000 g/mol	0.077 mmol	0.193 mmol	27.8 mmol	0.07 mmol	10 mL	0.5141 g

Table 3. 1: Quantities used for different target chain lengths of styrene for RAFT polymerization.

3.3.4.4. Noncovalent interaction of the pyrene-functional PS (DIBTC-PS-Py) with pristine MWNTs

Again two compounds were synthesized in which the 5 000 g/mol and the 15 000 g/mol styrene chain length compounds were interacted non-covalently with the pristine MWNTs in the same manner.

The procedure followed was a modified version presented by Yan *et al.*[22] Pristine MWNTs (20 mg) were dispersed in $CHCl_3$ (100 mL) and mixed with DIBTC-PS-Py (125 mg) in $CHCl_3$ (100 mL). The flask was then placed in a water bath and the solution was subsequently ultrasonicated at 35 kHz for 1 h with the water bath temperature maintained at 20°C. Afterwards, the solution containing the suspended MWNTs was centrifuged at 15 000 rpm for 1 h. Upon completion, the supernate containing the free, unbound DIBTC-PS-Py was decanted. The black deposit was redispersed in $CHCl_3$ through ultrasonicating for 5 min. This was then centrifuged again until the supernate was free of DIBTC-PS-Py as detected using UV spectroscopy. Fresh $CHCl_3$ was added to the final deposit which was then filtered to isolate the solid MWNT/PyPS and vacuum dried at 85°C for 3 h. A yield of 4.7 mg of black powdered MWNT/PyPS of styrene chain lengths 5 000 g/mol and 19.3 mg of the 15 000 g/mol chain length variety were obtained.

3.3.5. Covalent attachment of ATRP mediated PS with pristine MWNTs via "grafting-from"

The ATRP agent HEBrIB was covalently attached to oxidized MWNTs through an esterification procedure, after which styrene was grafted from these active sites through ATRP polymerization.

3.3.5.1. Immobilization of HEBrIB onto the pristine MWNTs

The procedure for this reaction as well as the subsequent polymerization was followed as described by Baskaran *et al.*[17] MWNTs (0.2 g) and thionyl chloride (50 mL) were refluxed at 70°C for 24 h. The excess solvent was removed under vacuum and the resultant MWNT-COCl was washed with anhydrous THF and dried under vacuum. HEBrIB (2.3 mL) in

toluene (5 mL) was added to the flask containing the MWNT-COCl and the contents stirred under nitrogen atmosphere for 24 h in an oil bath set at 100°C. Afterwards, the solvent was completely removed under vacuum, and the tubes were filtered and washed several times with ethanol (250 mL). Finally the MWNT-HEBrIB was vacuum dried at 40°C for 10h. A yield of 96.5% was obtained.

3.3.5.2. Synthesis of the MWNT-HEBrIB-PS nanocomposite via ATRP mediated polymerization

MWNT-HEBrIB (20.5 mg) was placed into a Schlenk-flask equipped with a stirrer bar and sealed with a rubber septum. Styrene (1 mL) and a solution of CuBr (0.875 mg) and PMDETA (2.11 mg) in toluene was added to the Schlenk-flask using a syringe under nitrogen atmosphere. The solution was then degassed four times (20 min, 15 min, 10 min and 5 min) using the freeze-pump-thaw method. The flask was then sealed off under vacuum and placed into an oil bath at 100°C to stir for 72 h. After this time, the solution was quench-cooled in liquid nitrogen. The flask was opened and the contents diluted with THF (30 mL) and stirred for a few hours to dissolve the solid polymer. The supernatant THF was filtered, and the product was washed with THF several times. The MWNT-HEBrIB-PS was then dried at 40°C under vacuum for 24 h. A very low yield of 6.0 mg was obtained.

3.3.6. Noncovalent interaction of the pyrene-functional PS (HEBrIB-PS-Py) synthesised via ATRP with pristine MWNTs

The ATRP version of the noncovalently grafted MWNTs with HEBrIB-Py-PS was synthesised via a number of steps as described below in a similar manner to the RAFT version. Two compounds were synthesised with the difference in targeted PS chain length of 5 000 g/mol and of 15 000 g/mol.

3.3.6.1. Synthesis of pyrenebutyric acid with an acid chloride functionality (Py-Cl)

Acid chloride functionality was added to pyrenebutyric acid according to the procedure followed by Donkers.[38] Pyrenebutyric acid (0.2 g) was dissolved in anhydrous dichloromethane (DCM) (1.5 mL) under argon atmosphere in an oven dried 3-neck round-bottom flask. The flask was cooled in liquid nitrogen until the mixture solidified. Thionyl chloride (0.4139 g) was added drop-wise to the solution at the same time, allowing the mixture to reach room temperature while stirring. Once the flask reached room temperature, the flask was placed into a 30°C preheated oil bath for 3 h. After completion, the solvent and excess thionyl chloride was removed under vacuum overnight. The product of Py-Cl was

used immediately for the next reaction without purification so as to avoid any unwanted side reaction.

3.3.6.2. Synthesis of HEBrIB-Pyrene (HEBrIB-Py)

The pyrene-functional HEBrIB ATRP macroinitiator was synthesised through the esterification between the HEBrIB hydroxyl group and the acid chloride moiety of the Py-Cl. HEBrIB (0.0699 g) and pyridine (0.0261 g) were dissolved in anhydrous THF (3 mL). Py-Cl (0.107 g) dissolved in THF (1 mL) was then added drop wise to the mixture while being stirred. After letting the reaction run overnight at room temperature, the solvent was then evaporated off. The product was re-dissolved in THF and extracted three times with brine and three times with water. The organic layer containing the HEBrIB-Py was dried over Na_2SO_4 and subsequently vacuum dried to remove the solvent. A yield of 65.79% was obtained. ^{1}H NMR: (300 MHz, (DMSO-d_6) δ (ppm): 1.75 (m, 2H) (–CH_2–*CH_2*–CH_2–); 1.82 (s, 6H) (*CH_3*–); 2.01 (t, 2H) (–CH_2–*CH_2*–C); 2.61 (t, 2H) (–C–*CH_2*–CH_2–); 4.36 (m, 4H) (–O–*CH_2*–CH_2–); 7.93-8.41 (m, 11H) (*pyrene*).^{13}C NMR: (75 MHz, (DMSO-d_6) δ (ppm): 26.88 (–CH_2–*CH_2*–CH_2–); 32.04 (–CH_2–*CH_2*–C–); 33.46 (*CH_3*–); 55.86 (*C*); 61.41 (–CH_2–*CH_2*–O–); 63.62 (–O–*CH_2*–CH_2–); 123.43-136.37 (*pyrene*); 172.62 (*C=O*); 174.40 (*C=O*).

3.3.6.3. Synthesis of HEBrIB-pyrene-polystyrene (HEBrIB-Py-PS)

Two versions of the HEBrIB-pyrene functional PS compounds were synthesised using the ATRP macroinitiator of HEBrIB-Py, one with a targeted styrene chain length of 5 000 g/mol and the other of a longer targeted styrene chain length of 15 000 g/mol. The experimental procedures were done in a similar manner excepting the amount of styrene added. The quantities used are given below in Table 3.2.

HEBrIB-Py, PMDETA, styrene and Toluene were added to an oven dried Schlenk-flask (flask 1) sealed with a rubber septum. CuCl was added to a second Schlenk-flask (flask 2) together with a stirrer bar. Both flasks were made inert through the freeze-pump-thaw method for a span of first 20 minutes of pumping, followed by 15 min, 10 min and finally 5 min spans. The CuCl flask was filled with Argon gas during the thawed stages. After this, the contents of flask 1 were injected into flask 2 using a degassed syringe. The solution was then placed in an oil bath preheated to 100°C and stirred for 72 h. After completion, the solvent was partially removed and the remnants were precipitated into methanol, filtered and vacuum dried at 50°C overnight.

PS chain length	HEBrIB-Py	PMDETA	Styrene	Toluene	CuCl	Yield
5 000 g/mol	0.0526 mmol	0.104 mmol	0.3 mL	0.25 mL	0.0526 mmol	12.1 mg
15 000 g/mol	0.0858 mmol	0.172 mmol	1.3 mL	0.40 mL	0.0858 mmol	33.8 mg

Table 3.2: Quantities used for different styrene chain lengths for ATRP polymerization.

3.3.6.4. Noncovalent interaction of the pyrene-functional PS (HEBrIB-Py-PS) synthesised via ATRP polymerization with pristine MWNTs

Again two compounds were synthesized in which the 5 000 g/mol and the 15 000 g/mol styrene chain length compounds were interacted noncovalently with the pristine MWNTs in the same manner.

The procedure followed was the same as that described for the RAFT version earlier. Pristine MWNTs (20 mg) were dispersed in $CHCl_3$ (100 mL) by mixing with HEBrIB-Py-PS (125 mg) in $CHCl_3$ (100 mL). The beaker was then placed in a water bath and the solution was subsequently ultrasonicated at 35 kHz for 1 h with the water bath temperature maintained at 20°C. Afterwards, the solution containing the suspended MWNTs was centrifuged at 15 000 rpm for 1 h. Upon completion, the supernate containing the free, unbound HEBrIB-Py-PS was decanted. The black deposit was re-dispersed in $CHCl_3$ via ultrasonicating for 5 min. This was then centrifuged again until the supernate was free of HEBrIB-Py-PS as detected using UV spectroscopy. Fresh $CHCl_3$ was added to the final deposit which was then filtered to isolate the solid MWNT/PyPS and vacuum dried at 85°C for 3 h. A yield of 17.4 mg of black powdered MWNT/PyPS of styrene chain lengths 5 000 g/mol were obtained. Since it was not necessary to fully characterize the longer chain length version of the HEBrIB MWNT/PyPS, this product was left uncentrifuged and in solution, and therefore a yield was not recorded.

3.3.7. Nanocomposite preparation

A similar preparation described by Yan *et al.*[22] was used to prepare the nanocomposites. A 20w/v% PS in chloroform stock solution was mixed with a 2 wt% ratio of functionalized MWNT by stirring vigorously for 30 minutes followed by ultrasonication for 15 min at room temperature. The composites prepared are indicated in table 3.3.

PS synthesis mechanism	Targeted PS chain length (g/mol)	Type of functionalized MWNTs	Actual PS chain length (g/mol)
-	-	pristine	-
DIBTC	5 000	PyPS/MWNT	1 858
DIBTC	15 000	PyPS/MWNT	6 455
DIBTC	-	Covalent MWNT-DIBTC-PS	-
HEBrIB	-	Covalent MWNT-PS-HEBrIB	-
HEBrIB	5 000	PyPS/MWNT	12 890
HEBrIB	15 000	PyPS/MWNT	32 493

Table 3.3: PS/PyPS/MWNT composite formulations.

3.3.8. Electrospinning

To synthesise fibres, a voltage of 10 kV was applied between the spinneret and the collector plate which were a distance of 10 cm apart. A Kent scientific pump (Genie plus model) was used to create a continuous flow rate of 0.203 ml/min. High molecular weight PS (average $\overline{M_w}$ ~350 000 and $\overline{M_n}$ ~170 000) was used as the matrix material for the composites in a 20 w/v% ratio in chloroform, while the filler composition was either 2, 4 or 6 wt%.

3.4. Results and Discussion

3.4.1. Immobilization of the RAFT agent DIBTC on the oxidized MWNT surface

Upon oxidizing the pristine MWNTs, both hydroxyl and carboxyl groups are found along the oxidized MWNT surface.[39] The RAFT agent, DIBTC has a carboxyl functionality which is able to react with the hydroxyl groups of the MWNT-COOH through esterification in the presence of the nucleophilic catalyst DMAP and the coupling reagent DCC.[16] The unattached DIBTC was removed from the product by washing the solid with DCM until the washings were free of any DIBTC as determined by UV/Vis (Figure 3.1). The thiocarbonyl (C=S) moiety in DIBTC has a known maximum absorption around 300-310 nm corresponding to the strong π-π* electronic transition, enabling UV/Vis analysis to be an effective tool to detect the presence of DIBTC.[40]

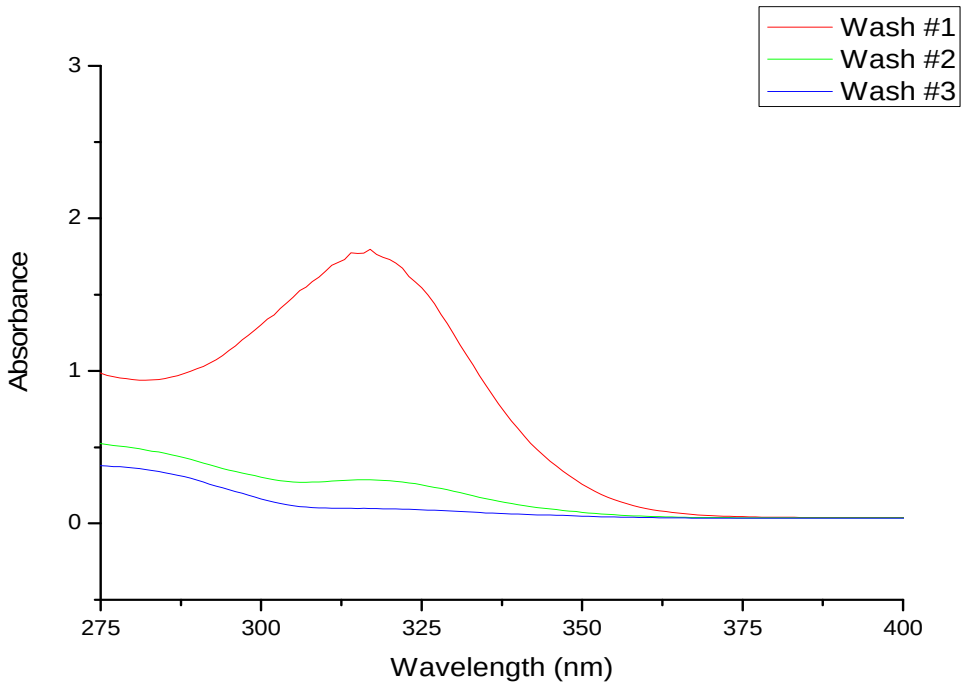

Figure 3.1: UV/Vis spectrum showing the removal of free DIBTC from MWNT-DIBTC by successive washes with DCM

The attachment of DIBTC onto the oxidized MWNT was analysed using FT-IR. The FT-IR absorbance measurements were done in the attenuated total reflectance (ATR) mode. The absorbance spectrum of DIBTC shows the characteristic stretching vibrations of the C-S, C=S, C=O and alkane functionalities at 813 cm^{-1}, 1069 cm^{-1}, 1712 cm^{-1}, and at 2917 cm^{-1} and 2846 cm^{-1} for the C-H stretch of the alkanes. Upon immobilization of the DIBTC onto the MWNT surface, these stretching vibrations were transferred to the spectrum of the MWNT-DIBTC with only very slight alterations in frequencies seen (figure 3.2). The presence of these vibrations in the FT-IR spectrum, together with the removal of unattached DIBTC through washing with DCM as proved by the UV spectrum (figure 3.1), leads to the deduction that the DIBTC peaks seen in the FT-IR spectrum of MWNT-DIBTC are as a result of the successful immobilization of DIBTC onto the MWNT surface.

Figure 3.3 shows the TGA results of pristine MWNTs (**a**), DIBTC (**c**) and MWNT-DIBTC (**d**) which clearly show the immobilization of the DIBTC RAFT agent onto MWNTs since the DIBTC decomposition temperature at 121.90°C is imparted on the decomposition curve of MWNT-DIBTC which is seen to lose 45.21% of its original weight.

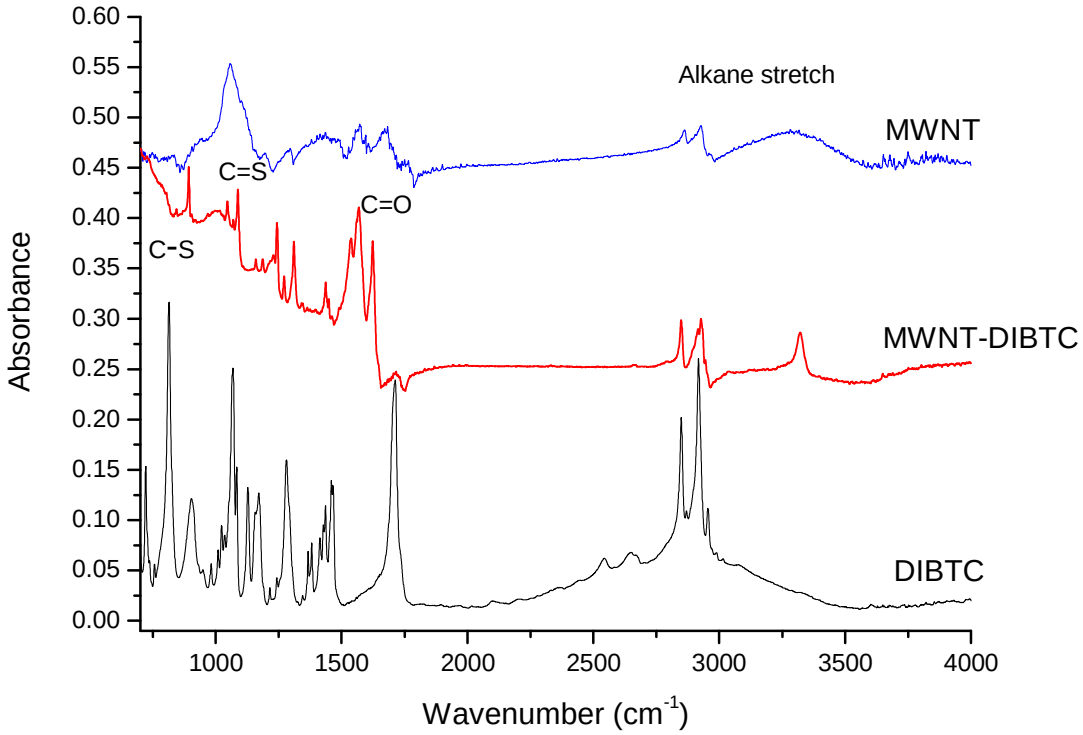

Figure 3.2: FT-IR spectrum of the covalently attached MWNT-DIBTC as proved by specific stretching vibrations.

3.4.2. Grafting of PS from MWNT-DIBTC for the covalent MWNT-PS-DIBTC via RAFT-mediated miniemulsion polymerization

Styrene was grafted from the MWNT-DIBTC via RAFT mediated miniemulsion polymerization. This technique is a simple and effective method for the formation of MWNT-PS-DIBTC. Here the filler material (MWNT-DIBTC) is incorporated into the polystyrene matrix via dispersion of the filler and styrene monomer in water. The filler particles are contained in the styrene monomer droplets[16] which form in the water through the application of a high-shear force introduced by ultrasonication. This dispersion is stabilized by the surfactant (SDBS) and the hydrophobe (HD oil), allowing the styrene to polymerize along the MWNT-DIBTC active sites through RAFT-mediated polymerization.[41,42] The success of this polymerization was determined using FT-IR and TGA. The FT-IR spectrum (see figure A.1 in appendix A), however, did not give conclusive proof of the grafting of styrene from the DIBTC active sites along the MWNT surface. TGA was done to determine the percentage weight compositions of the intermediate products from MWNT to MWNT-PS-DIBTC (see figure 3.3). At 600°C, the pristine MWNTs (**a**) are seen to maintain almost 100% of their original weight. MWNT-COOH (**b**) only shows a 27.08% weight loss, and MWNT-DIBTC (**d**) a 45.21% weight loss, whereas MWNT-PS-DIBTC (**e**) has lost 94.75% of its original

weight at this temperature showing that functionalization has taken place. The TGA curve of the pristine DIBTC RAFT agent is seen to have a relatively low decomposition temperature of 121.90°C (**c**). This is projected into the TGA curve **d** which represents the MWNT-DIBTC which has a decomposition temperature of 114.50°C, which is significantly lower than the decomposition temperature of **b** (MWNT-COOH) at 173.80°C. This decrease in decomposition temperature can be attributed to the loss of the RAFT agent at 114.50°C thus confirming the positive immobilization of DIBTC on the MWNT surface. Furthermore, a second loss peak is seen for **d** at 188.32°C which is postulated to represent the decomposition of the –COOH groups along the MWNTs which have a decomposition temperature of 173.80°C. The difference in weight loss values at 600°C between curves **b** and **d** gives an indication of the weight % of DIBTC that has been successfully immobilized along the surface. This was calculated to be 18.4%. After the RAFT mediated miniemulsion polymerization of MWNT-DIBTC with styrene was completed and any free PS homopolymer had been removed, TGA was done of the product (**e**). Curve **e** showed two main loss zones. Below ~150°C can be attributed to the decomposition of the unreacted MWNT-COOH groups since the first region takes a similar shape to that of curve **b** below ~120°C. The second region of loss of curve **e** between 390°C-480°C represents the decomposition of the PS and DIBTC.

At 485°C, almost all the MWNT-PS-DIBTC has been lost (94.16%), whereas at the same temperature, 0.52% of MWNTs has been lost and 42.52 weight % of the MWNT-DIBTC has decomposed. As a result it can be concluded that the amount of functionalization has occurred through the immobilization of DIBTC onto the MWNT surface is 45.21% from which the styrene was then grafted to give MWNT-PS-DIBTC.

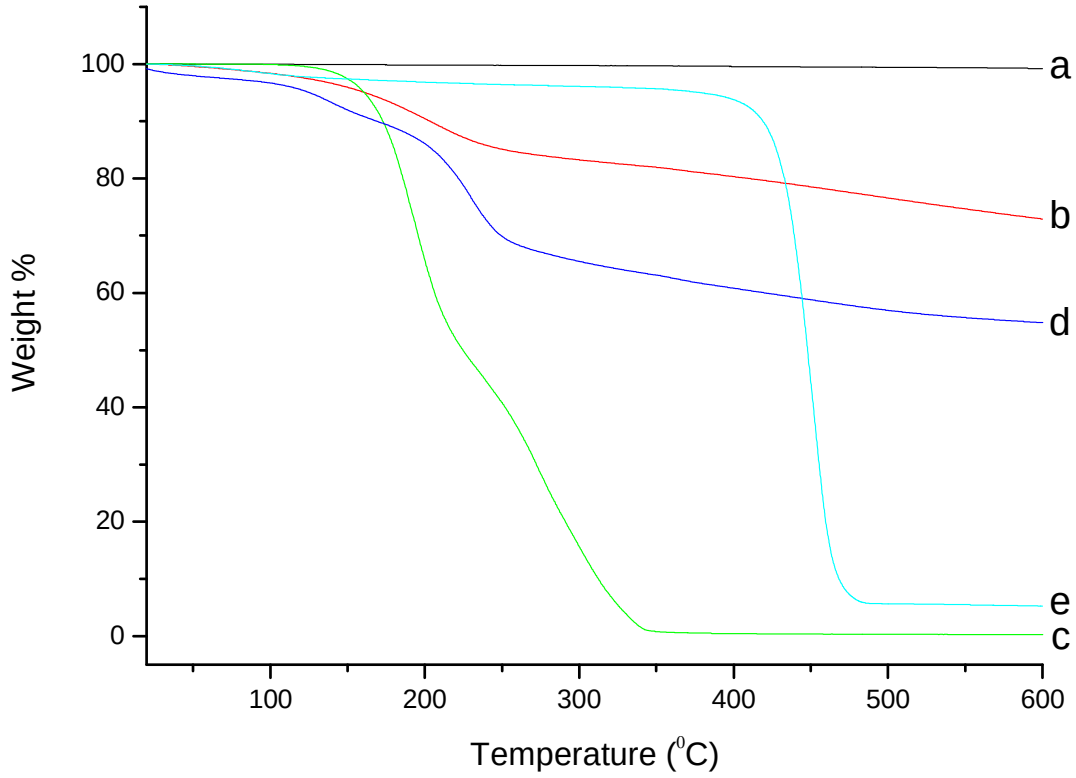

Figure 3.3: TGA curves of (a) pristine MWNTs, (b) MWNT-COOH, (c) DIBTC, (d) MWNT-DIBTC and (e) MWNT-PS-DIBTC.

3.4.3. Synthesis of DIBTC-Pyrene RAFT macroinitiator

The synthesis of DIBTC-Py was achieved through a two-step reaction where, in the first part the carboxylic acid at the end of the DIBTC is treated with thionyl chloride to replace the hydroxyl of the carboxylic acid with a chloride through nucleophilic substitution, such that an acyl chloride functionality is produced (**1** in scheme 3.1). This was done according to the procedure described by Donkers.[38] The acid chloride functionality was introduced since the previous attempts at esterifying the DIBTC without the chloride group and the pyrenemethanol were unsuccessful as determined by NMR. The synthesis of esters from carboxylic acids and alcohols often result in low yields due to the reversibility of this reaction since the hydroxyl group is a poor leaving group. The use of acyl chlorides instead of carboxylic acids however, makes this reaction fast and irreversible as they are well known to be extremely reactive compounds due to the superior leaving ability possessed by the chloride ion compared to the hydroxide.[43] **1** was synthesized and confirmed by ^{13}C NMR in deuterated chloroform ($CDCl_3$). The carboxylic acid carbon has a chemical shift of 177.65 ppm, which is shifted upfield to 175.29 ppm due to the disappearance of the hydroxyl group upon functionalization which induces a higher chemical shift for that carbon than the chloride

does due to the proton exchange that the hydroxyl group undergoes. The alpha carbon is deshielded upon functionalization since the hydroxyl is more electronegative than the chloride group, which results in a chemical shift downfield from the original 55.39 ppm to 67.16 m.

1 was esterified with 1-pyrenemethanol (**2**) through nucleophilic substitution at the carbonyl group. This was confirmed using NMR (figure 3.4). The ^{1}H NMR spectrum of **1** is indicated in insert (ii) of figure 3.4. The peak labelled "g" correlates to the 6 protons belonging to the methyl groups of **1** which are expected to move downfield due to deshielding induced by the removal of the chloride upon esterification. The ^{1}H NMR of **2** is shown in insert (i) of figure 3.4. Here the peak labelled "h" represents the –CH_2– protons as indicated on the skeletal structure. These protons are expected to move slightly downfield upon esterification due to the exchange of the shielding hydroxyl group with the ester group. This confirmed that the

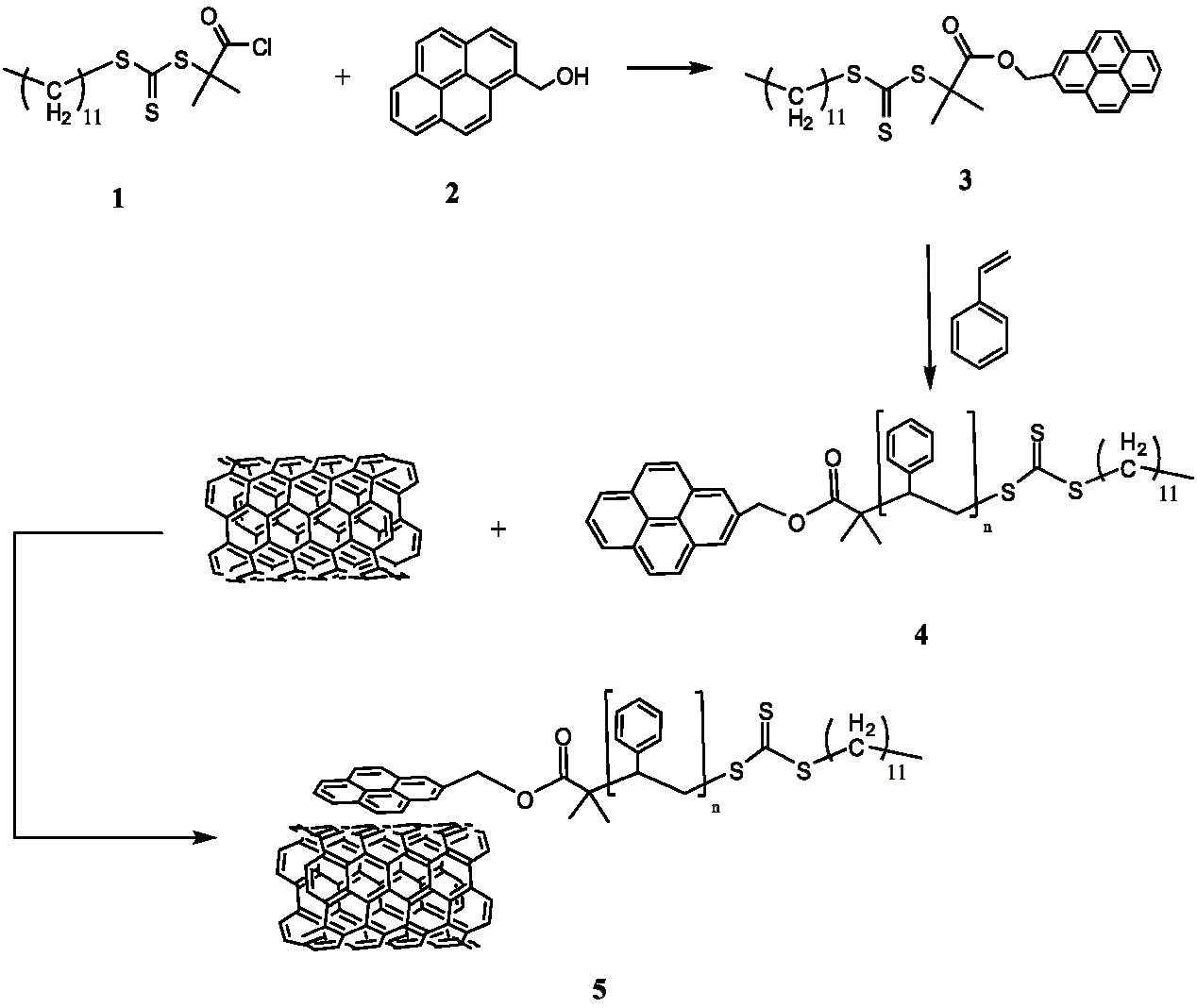

Scheme 3.1: Synthesis scheme of noncovalent MWNT/PyPS via pyrene-functional DIBTC.

RAFT macroinitiator DIBTC-Py (**3**) had been successfully synthesized with a yield of 60.58%. The ^{1}H NMR spectrum of **3** was also used to determine the degree of functionalization that occurred. Upon integrating the peak labelled "h" to another belonging to the aliphatic DIBTC chain a 51.5% degree of functionalization was established. Purification of this product by column chromatography (silica stationary phase and 20:80 cyclohexane:toluene mobile phase) was therefore done to obtain the pure RAFT macroinitiator for the polymerization of styrene.

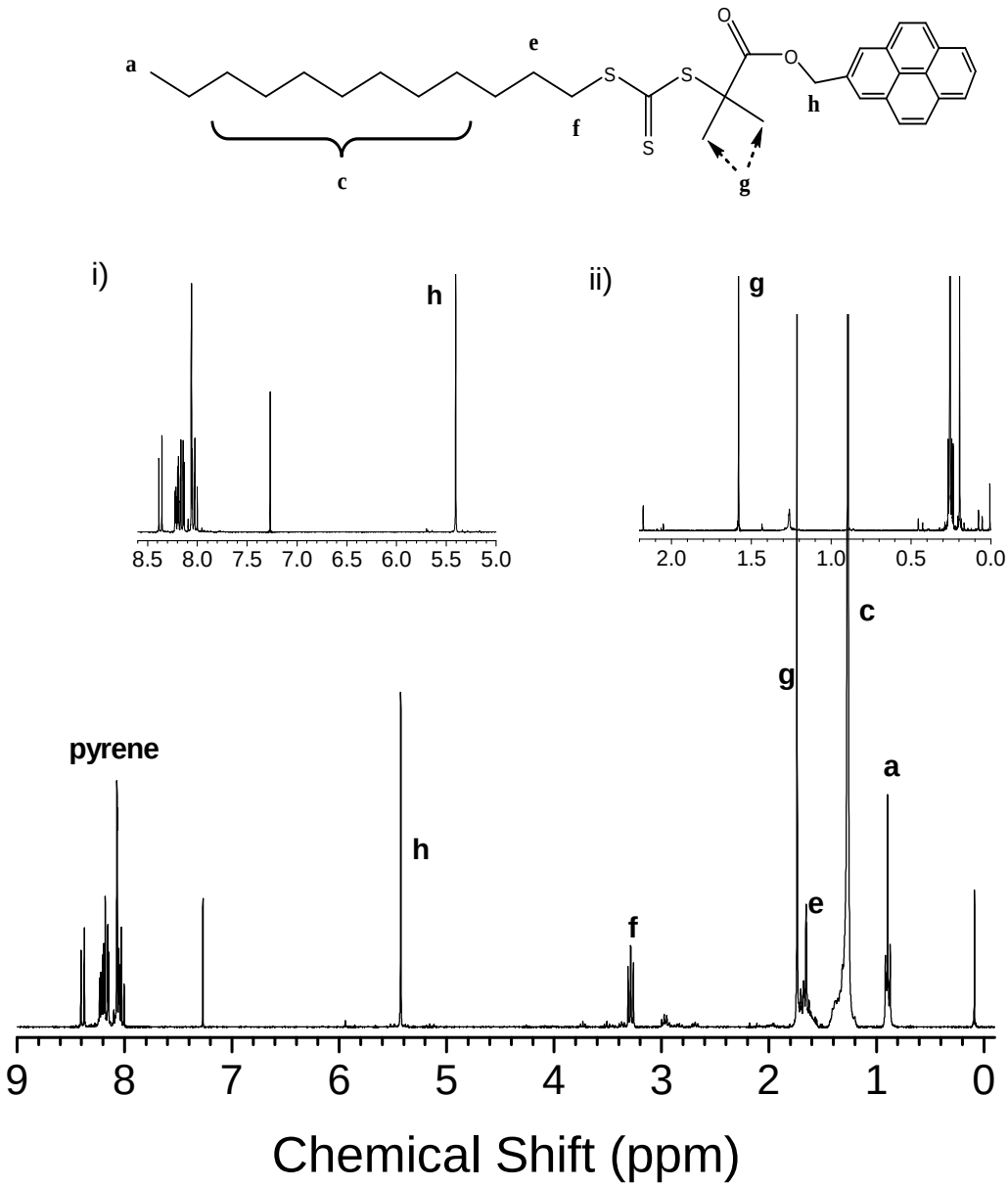

Figure 3.4: ^{1}H NMR spectrum for DIBTC-Py where the peak labeled "h" corresponds to the two protons shown in the skeletal structure and shift from 5.41 ppm in the ^{1}H NMR spectrum of (i)pyrenemethanol to 5.44 ppm. The peak labeled "g" indicates the shift in the 6 methyl protons from 1.58ppm in the ^{1}H NMR spectrum of (ii)DIBTC-Cl to 1.74 ppm.

3.4.4. RAFT-mediated polymerization of styrene using the RAFT macroinitiator DIBTC-Py

A general procedure for RAFT-mediated polymerization of styrene was followed for the synthesis of the pyrene-terminated PS (see scheme 3.1). The NMR spectra for both the 5 000 g/mol and the 15 000 g/mol DIBTC-PS-Py (figure B.1 in appendix B) (**4**) products shows the successful incorporation of the typical aliphatic and aromatic peaks of **3** as described in figure 3.4, as well as the presence of a broad peak around 7.10 ppm belonging to the PS protons. The peak belonging to the 6 methyl protons (labelled "g" in figure 3.4) has shifted from 1.74-1.27 ppm upon polymerization in both the 5 000 g/mol and 15 000 g/mol spectra. Therefore effective polymerization has occurred with the incorporation of the pyrene functional groups.

UV/Vis spectroscopy was used to confirm that the pyrenemethanol was attached to the DIBTC RAFT agent as well as the end of the PS chains since pyrenes are very well known for their ability to fluoresce and to absorb UV light. Figure 3.5 shows the UV/Vis spectra of pyrenemethanol (**a**), the pyrene-RAFT ester (**c**), the two pyrene-terminated PS chains of different targeted styrene chain lengths (**b** and **d**) and of DIBTC (**e**). It is evident that DIBTC and pyrenemethanol have been esterified to form the RAFT macroinitiator DIBTC-Py (**b)** since the characteristic absorbance peaks of the pyrene are translated into the spectrum of the ester. This indicates that the pyrene has been esterified with the DIBTC to produce the RAFT macroinitiator. Similarly, it is shown that the PS chains carry the pyrene-end functionality (**c** and **d**). This coupled with the NMR result make a satisfactory case for the positive introduction of the pyrene functionality onto the PS chains.
The radical azo-initiator used in the polymerization, AIBN, decomposes thermally upon placement of the reaction flask in the 70°C oil bath to release tertiary radicals which initiate the polymerization of the styrene monomers. This growing PS chain containing the radical is then able to add to the trithiocarbonate RAFT agent to create an unstable intermediate carbon-centred radical which consequently fragments to reform the C=S double bond of the trithiocarbonate and releases either the radical containing R group of the RAFT agent or the original incoming radical species which reinitiate the reaction. Termination of these propagating chains is diffusion dependent, therefore shorter chains have a higher probability of terminating than longer chains do which will keep propagating. This creates a lower than anticipated molecular weight as determined by the refractive index (RI) detector in SEC (figure 3.6) as well as a respective degree of conversion of the two compounds which was found to be 42.4% for the short chain PS and 54.8% for the longer PS chain version. The PS

chain lengths which were targeted were 5 000 g/mol and 15 000 g/mol, however the $\overline{M_n}$ of the two respective pyrene-end-functional PS chains was found to be 1.86×10^3 g/mol and 6.46×10^3 g/mol with a polydispersity of 1.14 and 1.24 correspondingly.

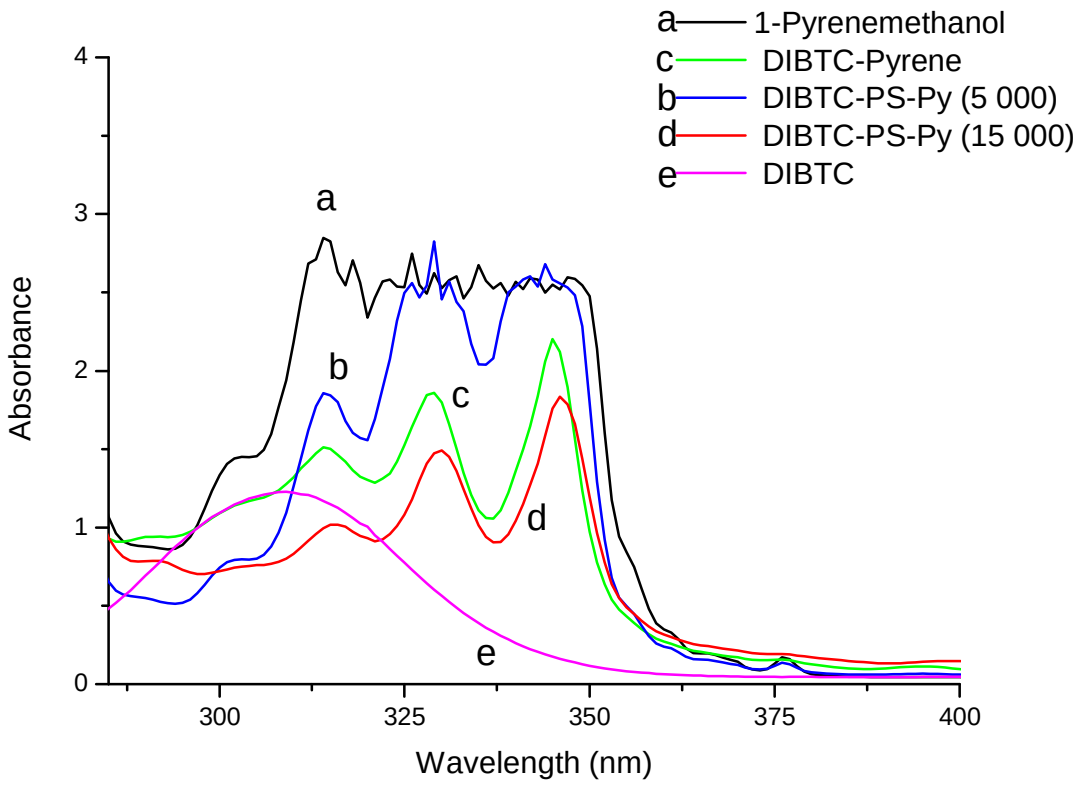

Figure 3.5: UV spectrum of dispersions of (a) 1-pyrenemethanol, (b) DIBTC-Pyrene RAFT macroinitiator, (c) DIBTC-PS-Py of 5 000 g/mol targeted styrene chain length and (d) DIBTC-PS-Py of 15 000 g/mol chain length in chloroform.

The pyrene functionality attached to the PS chains is highly active at a UV wavelength of 365 nm and only slightly at 254 nm, whereas styrene absorbs at 254 nm but not at 365 nm, therefore the use of a dual wavelength UV detector coupled to the RI detector in SEC enables the pyrene attachment to the PS chains to be determined (figure 3.6). It is clear that the first peak of the RI response in both figures is active at both 254 nm and 365 nm, indicating the presence of pyrene and styrene. The second peak around 22 minutes in the shorter version, however, does not show a response at 365 nm and only at 254 nm, thus indicating the presence of some styrene homopolymer. The shoulder seen in the RI response in both graphs is also seen to be active at both 365 nm and at 254 nm. This was determined to be the detection of the unreacted macroinitiator which did not take part in the polymerization. The same reason explains the peaks seen in the DIBTC-PS-Py 15 000 g/mol SEC response (right image in figure 3.6).

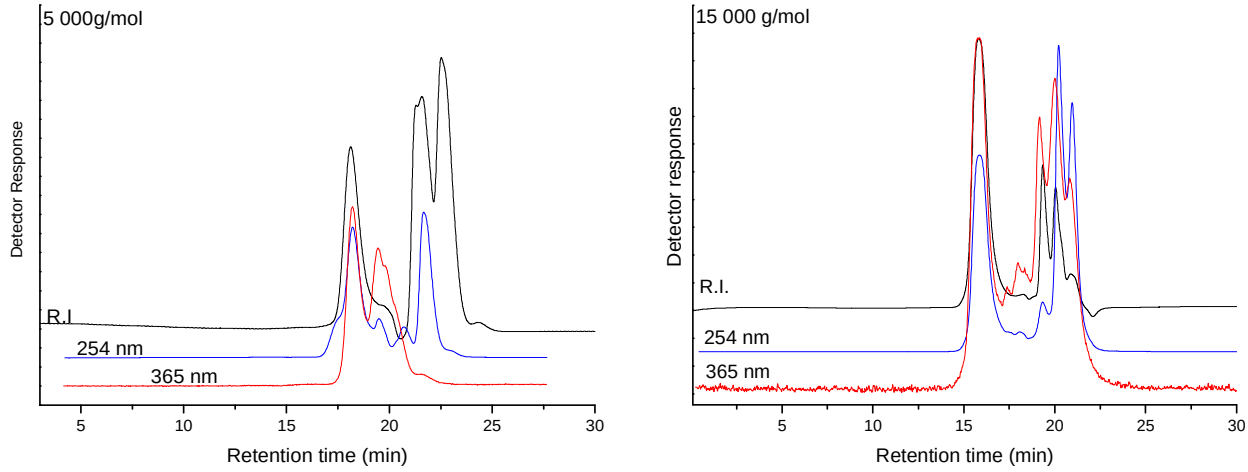

Figure 3.6: SEC with RI and UV detector at 254 nm and 365 nm results for DIBTC-PS-Py of target chain length 5 000 g/mol (left) and 15 000 g/mol chain length (right).

3.4.5. Noncovalent interaction of the pyrene-functional PS (DIBTC-PS-Py) with pristine MWNTs

The pyrene-end-functional PS chains were immobilized along the MWNT surface (see **5** in scheme 3.1) such that the π-orbitals of the conjugated pyrene aromatic rings interacted through noncovalent dispersive forces with the π-orbitals of the conjugated aromatic rings of the MWNTs to form functionalized MWNTs through π-π stacking without compromising the electrical and mechanical integrity of the MWNTs. Both the 5 000 g/mol and the 15 000 g/mol PS chain lengths were used with the pristine MWNTs according to the procedure reported by Yan *et al.*[22] No large difference was observed due to differences in PS chain lengths. During the procedure, the free DIBTC-Py-PS which was present after interaction with the MWNTs was removed by successive ultra-centrifugation followed by washing with chloroform and redispersion. The removal of the free DIBTC-Py-PS was monitored by UV such that the supernate from the centrifugation contained successively less free PyPS. After drying the resultant MWNT/PyPS hybrid complexes, their redispersion in chloroform was significantly improved compared to the same concentration of pristine MWNTs in the same solvent (see image 3.1). The dispersion also improved drastically in stability. The pristine MWNT can be dispersed in chloroform by ultrasonication but the dispersion lasts only a few hours before the black particles are seen to aggregate at the bottom and settle out of solution. The noncovalent hybrid complex, however, is seen to maintain a stable dispersion for several months.

Image 3.1: Dispersion of (left) pristine MWNTs and (right) noncovalently compatibilized MWNT/PyPS (DIBTC 5 000) in chloroform. The pristine MWNTs are seen to settle out at the bottom of the tube opposed to being dispersed uniformly throughout the solvent.

3.4.5.1. TGA

TGA was done to quantitatively determine the extent of noncovalent DIBCT-PS-Py bonding with the MWNT surface. Figure 3.7 shows the thermal decomposition curves of (**a**) pristine MWNTs, (**b**) DIBTC-PS-Py of targeted styrene chain length of 5 000 g/mol and (**c**) the corresponding MWNT/PyPS hybrid complex on the left, and (**d**) DIBTC-PS-Py of targeted styrene chain length of 15 000 g/mol and (**e**) the hybrid complex of MWNT/PyPS (DIBTC 15 000) on the left. At 490°C, the thermograms level off since no weight loss occurred after this point. At this temperature, the pristine MWNTs (**a**) had lost 0.59% of their total weight, whereas the DIBTC-PS-Py (**b**) showed a 94.32% weight loss. The noncovalent MWNT/PyPS hybrid complex (**c**) showed a weight loss of 24.55%. The MWNTs lose only a negligent amount of their total mass upon reaching a temperature of 490°C, which indicates that the weight lost by the hybrid complex is the decomposition of the adsorbed DIBTC-Py-PS, thus indicating their successful adsorption onto the MWNTs via π-π stacking. This type of interaction is confirmed by the levelling out of curve **c** just before 500°C, meaning that after the loss of the DIBTC-PS-Py, only MWNTs are left behind which as seen in curve **a** decompose insignificantly throughout the heating process to 600°C. As such the average amount of DIBTC-Py-PS which has been adsorbed per MWNT can be calculated to be 3.534×10^5 molecules of PyPS per MWNT for the 5 000 g/mol DIBTC MWNT/PyPS and 1.020×10^5 molecules PyPS per MWNT for the 15 000 g/mol version (see appendix C for calculations). The density of the MWNTs is assumed to be 2.14 g/cm^3[3,44] according to the model presented for MWNTs by Lu *et al.* since the exact dimensions and arrangement of the

nanotubes used are not known. The same can be seen from the decomposition curves of thermograms **a**, **d** and **e** of the right-hand-side image of figure 3.7, representing the pristine MWNTs, DIBTC-PS-Py (of 15 000 g/mol chain length) and the resultant hybrid complex MWNT/PyPS (DIBTC 15 000) respectively. Compared to the thermograms of the shorter chain length compounds (left), the curves reach thermal stability at a slightly higher temperature of 540°C, opposed to 490°C. This could be due to the larger number of bonds which must be broken during the decomposition process of the longer chain length of styrene. At 540°C, the MWNT (**a**) are still constant at a % weight loss of 0.59% compared to the % weight lost at 490°C. The DIBTC-PS-Py (15 000) (**d**) showed a % weight loss of 93.83%, whereas the hybrid (**e**) showed a % weight loss of 16.87% at 540°C. As a result, it can be concluded that the overall amount of DIBTC-PS-Py which was adsorbed onto the MWNT surface was higher for the shorter chain length compound than for the longer chain length compound. This is expected since steric hindrance introduced by larger polystyrene chains prevents the pyrene from approaching the MWNT surface and thus forming the π-π stacking interactions required for adsorption.

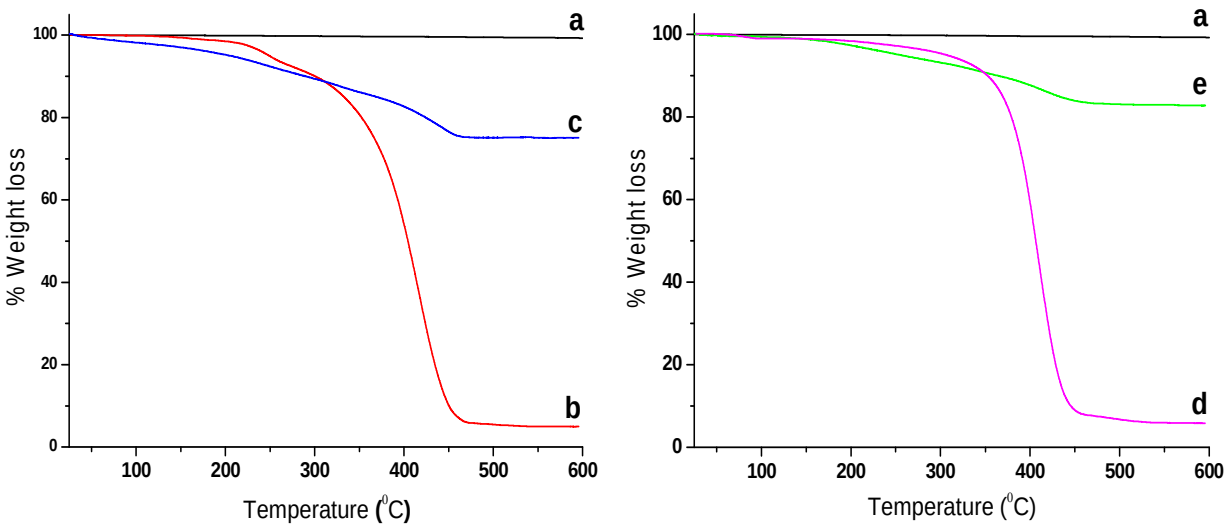

Figure 3.7: TGA decomposition curves of (a) pristine MWNTs, (left) (b) DIBTC-PS-Py 5 000 g/mol, (c) MWNT/PyPS (DIBTC 5 000), (right) (d) DIBTC-PS-Py 15 000 g/mol and (e) MWNT/PyPS (DIBTC 15 000)

3.4.5.2. ^{1}H NMR

Previous studies have reported that π-stacking interactions can cause shifting, broadening or weakening of the proton signals in NMR.[22,45-47] This is because the closer the protons are to the surface of the MWNTs, the broader and weaker the corresponding ^{1}H peak will appear

due to π-π stacking.[48] The pyrene protons in figure 3.8, representing the ^{1}H NMR spectrum of MWNT/PyPS (PS chain length of 5 000 g/mol) (8.01-8.22 ppm) weaken substantially, indicating that the pyrene groups are closely adsorbed to the MWNT surface. These peaks have shifted slightly upfield from 8.09-8.03 ppm, which is attributed to higher shielding of these protons as a result of the ring current created by the pyrene-CNT π-system.[22,49] The ^{1}H spectrum further reveals that the peak intensity of the two protons of the pyrene group at 8.09 ppm in the DIBTC-PS-Py spectrum has an intensity of 0.14 relative to the six methyl protons (labelled "g" in figure 3.4), which decreases drastically to a relative intensity of 0.01 in the MWNT/PyPS spectrum.

According to the ^{1}H NMR spectra of the pristine MWNTs, a single large peak is present at 1.55 ppm. The ^{1}H NMR spectrum of the MWNT/PyPS of 5 000 g/mol chain length shows the same pristine MWNT at 1.55 ppm and the peak labelled "g" in figure 3.4, still at the same chemical shift of 1.27 ppm which it shifted to upon polymerization of styrene using the RAFT macroinitiator. Since both these peaks are present in the MWNT/PyPS and there is no change in the chemical shift of these peaks upon interaction, it can be assumed that the aliphatic chain of the RAFT macroinitiator is not closely associated with the MWNTs and is rather free in solution since the magnetic field of the three methyl protons is not affected by the presence of the nanotube ring-current.

The broadening of these peaks, therefore, can be attributed to the presence of the conductive MWNTs present during application of the magnetic field which cause broadening in all peaks.[48]

The MWNT/PyPS complex of the longer PS chain length of 15 000 g/mol shows similar NMR results (figure B.3 in appendix B) in that the pyrene and PS peaks are not visible at all indicating close absorbance to the MWNT surface. The three methyl protons of the final carbon of the DIBTC aliphatic chain shift upfield by a factor of 0.03 ppm, indicative of noncovalent interaction between the DIBTC-PS-Py and the MWNT surface. The peak labelled "g" in figure 3.4 is also visible at 1.27 ppm but is broadened as well, most likely due to the same phenomena described above for the shorter chain length complex.

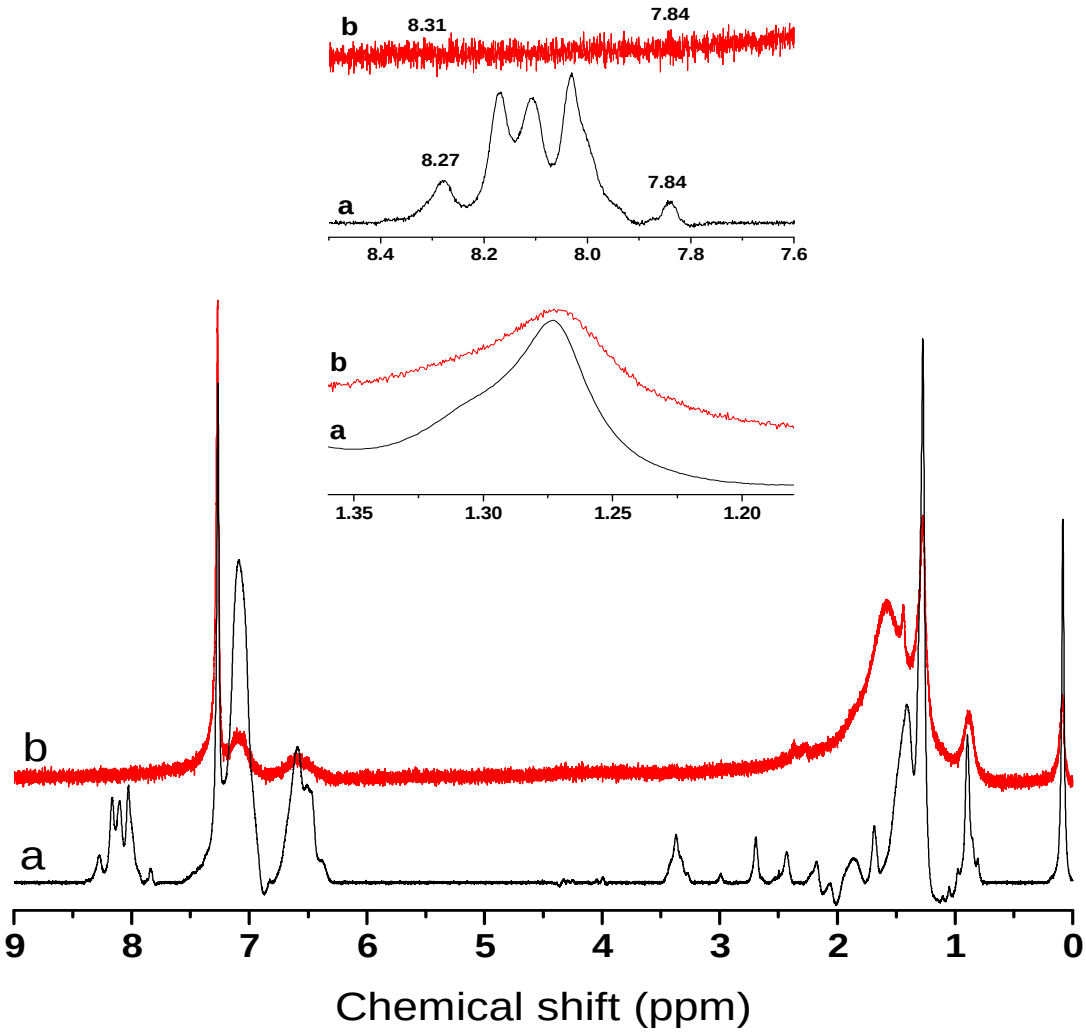

Figure 3.8: ^{1}H NMR spectrum of (a) DIBTC-PS-Py 5 000 g/mol chain length and (b) the corresponding noncovalent MWNT/PyPS hybrid complex.

3.4.5.3. UV/Vis/NIR

The DIBTC-PS-Py compounds of both the 5 000 g/mol and 15 000 g/mol chain lengths absorb strongly within 300-350 nm due to the characteristic pyrene π-π* electronic transitions as seen in figure 3.5. Pristine MWNTs, however, do not show any sharp absorption peaks.[22] Figure 3.9 shows the UV/Vis/NIR spectra of the noncovalently functionalized MWNT/PyPS of short and long chain lengths (**a** and **b**) as well as of the pristine MWNTs (**c**). The noncovalent adsorption of DIBTC-PS-Py onto the MWNTs is expected to result in a spectrum which is not distinctly different from the pristine MWNT spectrum since the MWNT structure should remain intact upon noncovalent functionalization. The electronic transitions for semiconductors are found in the NIR region of the spectrum between 850-1 600 nm for the first transition E_{11}^{S} and 550-850 nm for the second transition E_{22}^{S}.[22,50]

Figure 3.9 shows the first semiconducting subband between 850-900 nm, and the second between 950-1 000 nm. In both the chain length hybrid complexes of MWNT/PyPS, these transitions are clearly observed and the UV/Vis/NIR spectra (**a** and **b** in figure 3.9) are not recognizably different, indicating that the MWNT electronic structure has remained undisturbed.

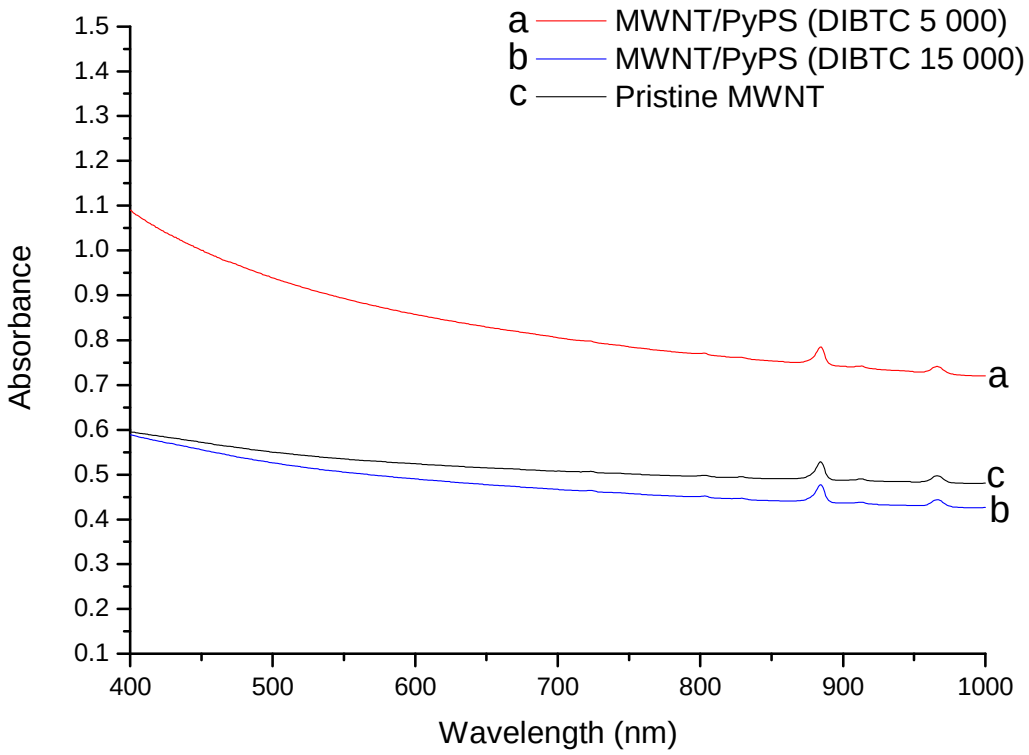

Figure 3.9: UV/Vis/NIR spectrum of the dispersion of (a) MWNT/PyPS of5 000 g/mol chain length, (b) MWNT/PyPS of 15 000 g/mol chain length and (c) pristine MWNTs in $CHCl_3$.

3.4.5.4. Fluorescence

The final confirmation of π-stacking between the pyrene-end functional PS and the MWNT surface was obtained by fluorescence spectroscopy. This form of spectroscopy allows for investigation of the MWNT electronic structure upon coupling with different molecular orbitals through π-π stacking.[21] Both the emission and excitation spectra were recorded for the DIBTC-PS-Py dispersion and the corresponding MWNT/PyPS hybrid complex in chloroform. Both styrene chain lengths of 5 000 g/mol and 15 000 g/mol gave similar results. Figure 3.10 shows the emission decay signal recorded at 396 nm of DIBTC-PS-Py of both chain lengths. It can be seen in the figure that emission is visibly quenched upon noncovalent compatibilization with the MWNTs. The faster rate of emission decay upon noncovalent interaction with the MWNT surface arises due to the rapid and efficient transfer of energy

between the MWNTs and the pyrene-end functional PS, and thus indicates that the π-stacking interactions between the pyrene system and the MWNTs are in fact present. Similarly, in (**iii**) in figure 3.10, the longer chain length MWNT/PyPS hybrid exhibits the same behaviour and the energy transfer is even more evident in this case. Furthermore, upon excitation at 390 nm, the fluorescence spectra of the DIBTC-PS-Py compounds (**a** and **c**) show defined fluorescence which is visibly quenched upon noncovalent interaction with the MWNTs (**b** and **d**) in both cases indicating that the transfer of electrons or energy is efficiently occurring between the pyrene system and the MWNT surface due to π-stacking interactions. These phenomena are reported in literature and are acceptable proof of such interactions.[22,48,51,52]

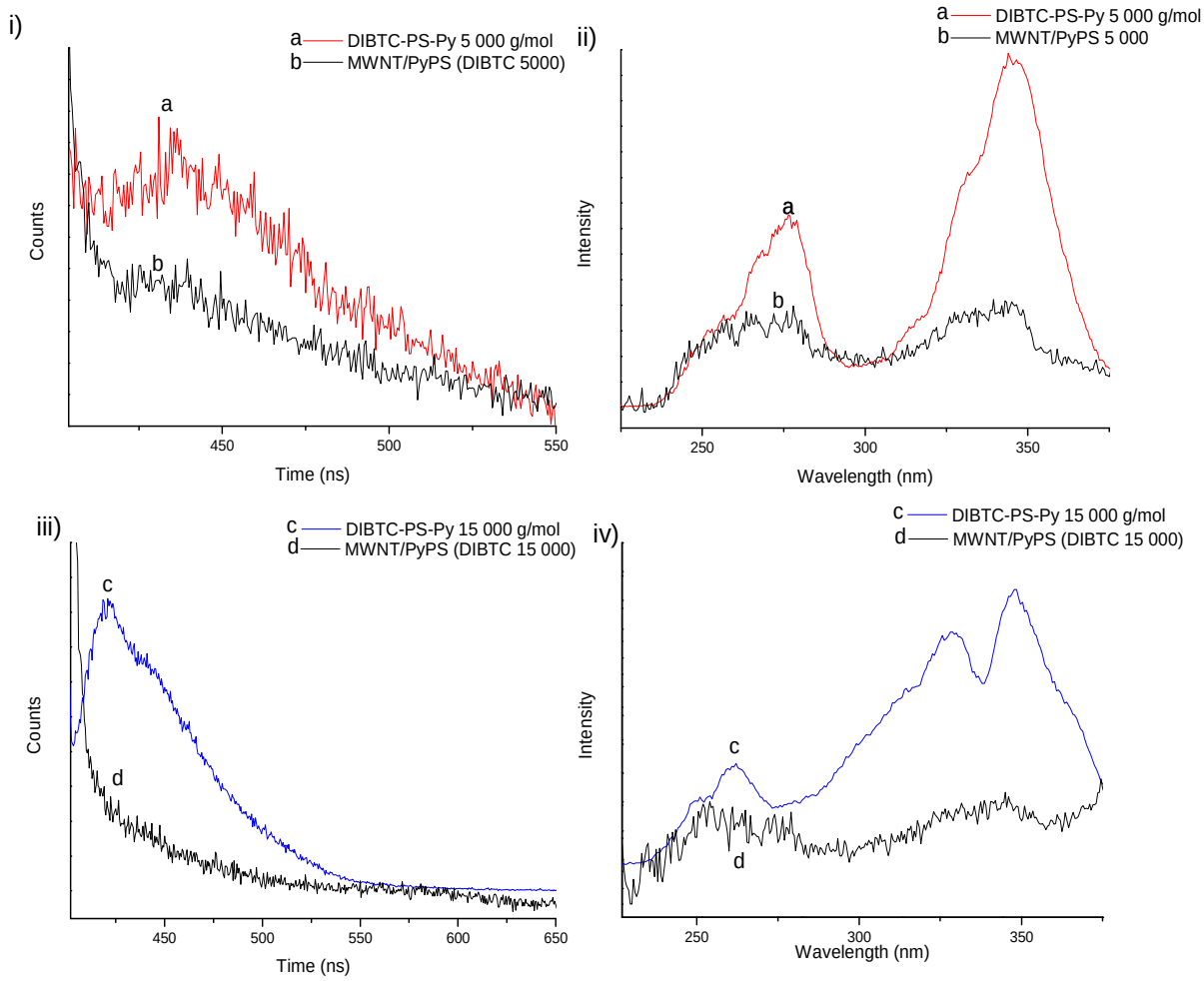

Figure 3.10: (i and iii) Emission decay curves recorded at 396 nm and (ii and iv) the fluorescence spectra excited at 390 nm of a dispersion in chloroform of (a) DIBTC-PS-Py of PS chain length 5 000 g/mol, (b) the corresponding MWNT/PyPS hybrid complex, (c) DIBTC-PS-Py of 15 000 g/mol chain length and (d) the resultant MWNT/PyPS hybrid complex.

3.4.6. TEM results for MWNT functionalization with DIBTC mediated PS

Dispersions of pristine MWNT, MWNT-PS-DIBTC, MWNT/PyPS (DIBTC 5 000 g/mol) and MWNT/PyPS (DIBTC 15 000 g/mol) in chloroform were prepared for TEM analysis.

Using a micropipette, a single drop of the respective dispersion was placed on a copper grid and analysed using TEM. The MWNTs range notably in diameter and length. The diameter of the pristine MWNTs gives an average of 26.04 nm and nanotubes of longer lengths were observed (see figure 3.11, top left image). However, the MWNTs in the compounds which had undergone ultrasonication have shorter lengths in general, showing the negative effect of ultrasonication on the MWNT structure. The average MWNT diameters were determined to be 25.82 nm and 28.24 nm for the 5 000 g/mol and 15 000 g/mol noncovalent MWNT/PyPS produced via RAFT polymerization respectively (bottom left and right respectively). The increased diameter from the shorter to the longer chain length of PS is not believed to be an indication of the longer chain length since the PS chains are not visible on the 100 nm scale. Therefore, this difference in diameter is attributed merely to natural variation in average MWNT diameter as introduced during the actual nanotube synthesis. The same theory holds for the diameter of 24.46 nm of the covalent MWNT-PS-DIBTC (top right in figure 3.11). However, it was interesting to discover that a greater degree of dispersion was observed in the nanotubes in the MWNT/PyPS (DIBTC 15 000 g/mol) TEM images (bottom right in figure 3.11) compared to those of the pristine MWNT images. This is projected to be a result of the noncovalent interactions introduced by the π-π stacking of the pyrene with the MWNT surfaces which break up their bundled aggregates, thus introducing a greater dispersibility in the solvent which was expected to occur upon functionalization. However, it should be noted that in this case the functionalization of the MWNT surface with the PS may result in the observed aggregation during TEM sample preparation.

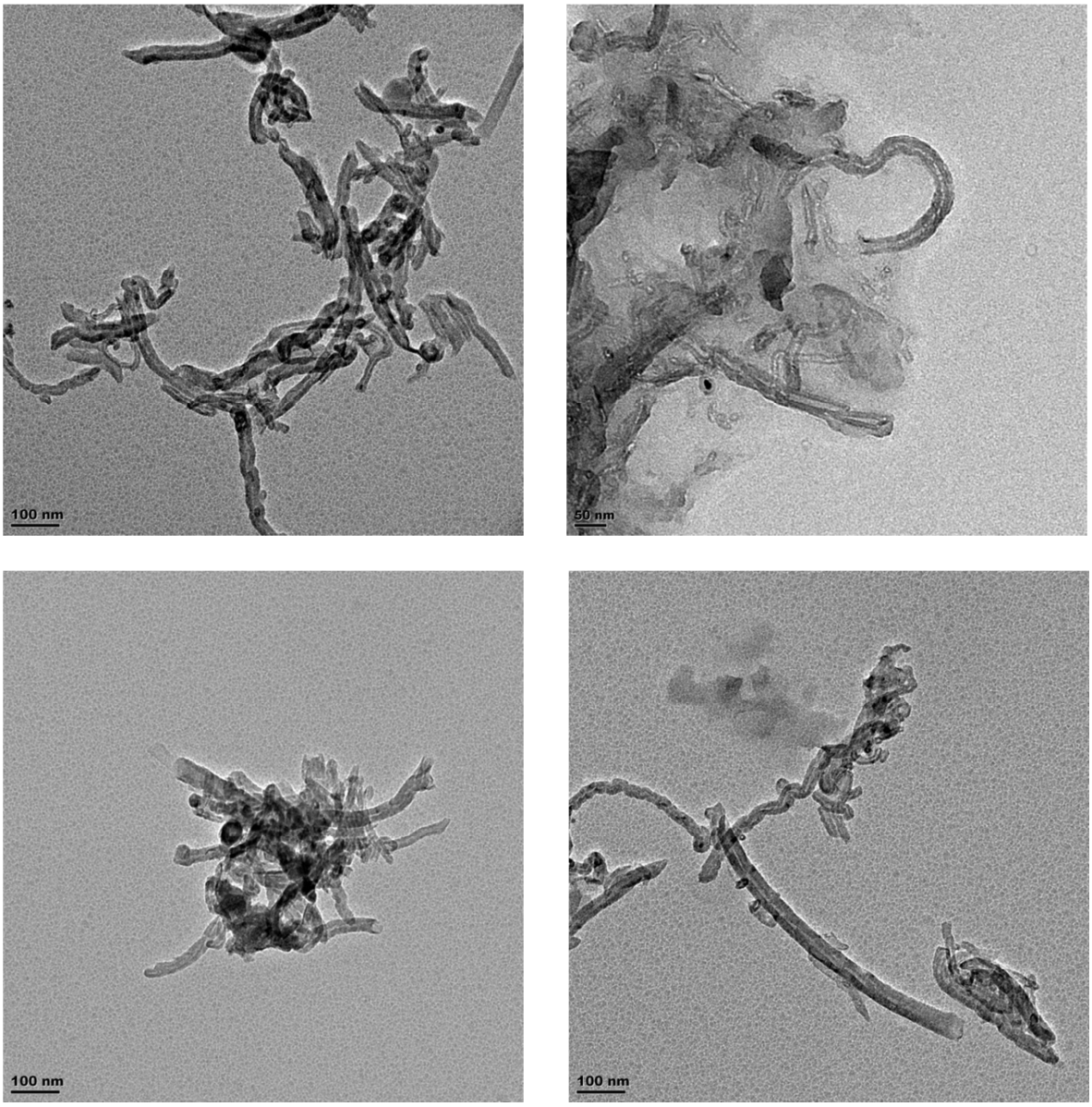

Figure 3.11: TEM images of (top left) pristine MWNTs; (top right) covalent MWNT-PS-DIBTC; (bottom left) noncovalent MWNT/PyPS (DIBTC 5 000 g/mol) and (bottom right) noncovalent MWNT/PyPS (DIBTC 15 000 g/mol).

Furthermore, the synthesised composites were dispersed in a 20 w/v% PS in $CHCl_3$ matrix in a 2, 4 and 6 % weight ratio of MWNTs to the PS content. The PS solutions containing the nanocomposites were then analyses by TEM again. Figure 3.12 shows the results of the interaction of the functionalized MWNT nanocomposites in a 2 wt% ratio with the PS matrix. It is clear that the pristine MWNTs do not disperse in the PS matrix well and instead aggregate in bundles. The functionalized MWNTs are more dispersed in the matrix although the MWNTs are still seen to bundle to a certain degree. The non-covalently functionalized MWNT/PyPS hybrids show the best dispersion of the individual nanotubes in the matrix as is visible in the bottom images of figure 3.12.

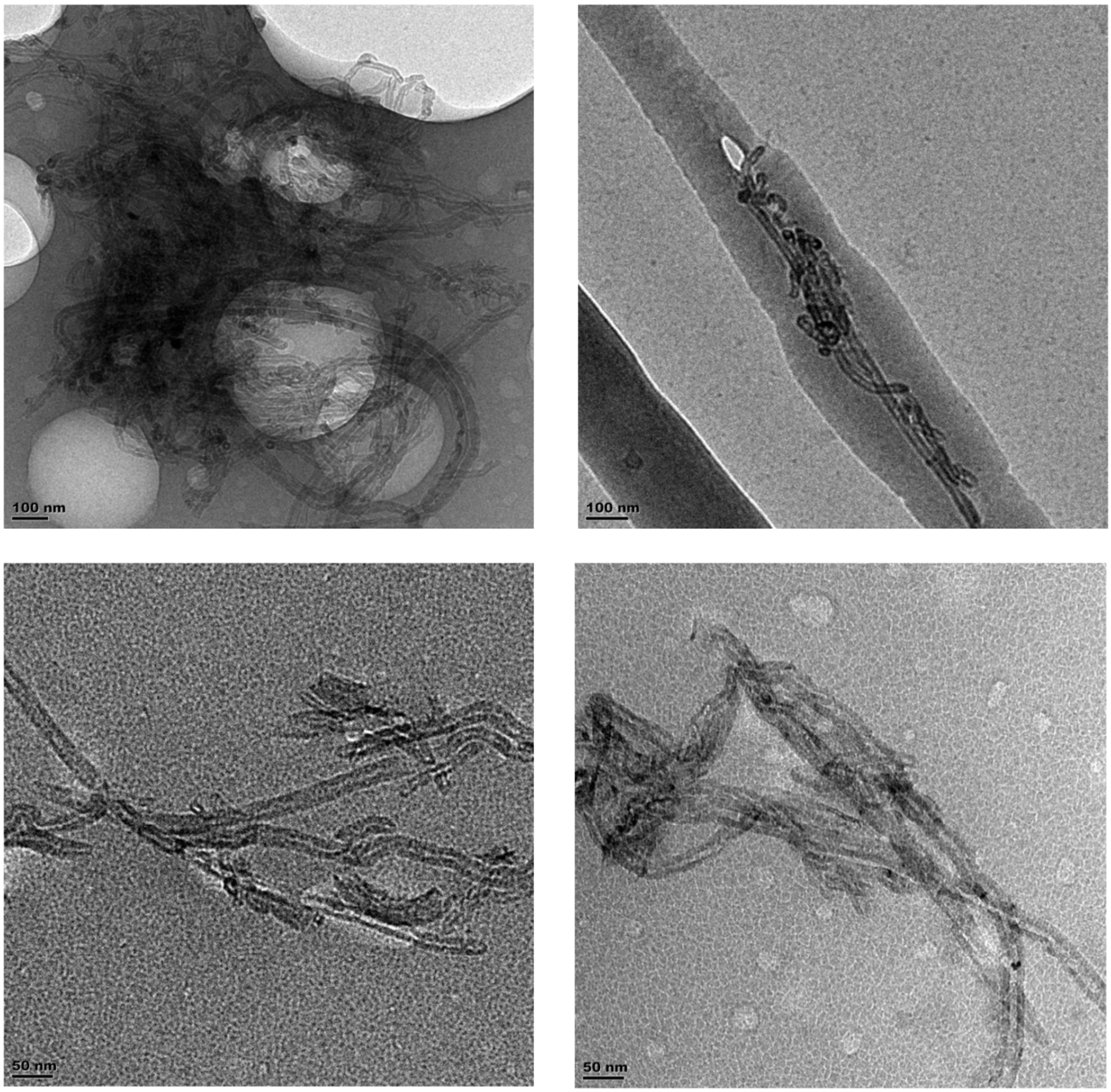

Figure 3.12: TEM images of (top left) pristine MWNTs; (top right) covalent MWNT-PS-DIBTC; (bottom left) noncovalent MWNT/PyPS (DIBTC 5 000 g/mol) and (bottom right) noncovalent MWNT/PyPS (DIBTC 15 000 g/mol) in a 20 w/v% PS in chloroform matrix.

3.4.7. Electrospinning of nanocomposites

3.4.7.1. Low molecular weight PS matrix synthesised via anionic polymerization

PS synthesized via anionic polymerization was analysed via SEC to give a molecular weight of 1.39×10^5 g/mol. Electrospinning of this PS was attempted. A voltage of 15 kV was applied between the spinneret and the collector plate which were separated by 10 cm while the 12.5 w/v% PS in chloroform solution was flowing at 0.03 ml/min. Only beading and no visible fibres were seen to form under these conditions. It was postulated that the molecular

weight of the PS was not high enough to provide sufficient crosslinking points for chain entanglement to occur and for fibres to form. The inclusion of a filler material in a polymer matrix provides an increase probability of chain entanglement to occur. As a result, pristine MWNTs were dispersed in the PS matrix. After sufficient stirring and sonication the solution was electrospun. This also was unsuccessful. To confirm the hypothesis about insufficient crosslinking due to low PS molecular weight, the compatibilized MWNT-DIBTC-PS was dispersed in the PS matrix and was electrospun. This too, however, did not produce fibres. As a result it was confirmed that the PS matrix was not of sufficient molecular weight. Literature reports the need for higher molecular weight PS for use in electrospinning.[56] As a result higher molecular weight PS was purchased which was seen to form fibres during electrospinning.

3.4.7.2. High molecular weight PS matrix

High molecular weight PS was purchased (Aldrich, $\overline{M_w}$ ~350 000 g/mol, $\overline{M_n}$ ~170 000 g/mol) and dissolved in chloroform. The dissolution process was somewhat tedious due to the extremely high molecular weight which required several rounds of ultrasonication and stirring in order to obtain a homogeneous solution and to prevent the presence of gel states in the electrospinning solution. The highly viscous 20 w/v% PS in chloroform solution was then subjected to a 10 kV difference and a higher flow rate of 0.203 ml/min. Visible fibre production was observed. Pristine MWNTs were then included in a 2wt% ratio to the PS and fibres formed successfully. Subsequently the other composites as indicated in table 3.3 were all spun. SEM analysis was done to show the fibre morphology and topology.

3.4.8. SEM results for electrospun DIBTC-mediated PS nanocomposite fibres

Electrospinning PS required a high molecular weight PS in order to obtain fibres without beading. Incorporation of MWNTs increases the probability of chain entanglement which is required to induce fibre formation. According to literature, a percolation threshold of 0.17-0.3 wt% is required in order to obtain a conductive nanocomposite.[122] As a result, a 2 wt% MWNT filler concentration in a 20 w/v% of PS was electrospun. Stable suspensions were observed for the dispersion of the covalent and noncovalent DIBTC functionalized MWNTs in the PS solution. The pristine MWNTs in PS were not dispersed as efficiently as small black particles were still observed in the solution due to the bundled aggregates which were difficult to break up and disperse.

Fibres were obtained by incorporation of pristine MWNTs, as well as both the covalently and noncovalently compatibilzed MWNTs. The fibre morphology was then analysed using SEM (figures 3.13-15) and the fibre diameter distribution was determined (see appendix D.1 and D.2). According to literature, the fibre diameter is expected to decrease with an increase in MWNT content due to an increase in conductivity which increases the repulsive forces within the electrospinning solution and allows for the cohesive forces to be overcome and ultimately produces fibres of a smaller diameter.[53,54] The PS nanocomposite prepared with 2 wt% pristine MWNTs (see appendix E) produced grey fibres but which showed some beading upon SEM anaysis. The nanocomposite containing the 2 wt% covalent MWNT-DIBTC-PS produced acceptable nanofibres (figure 3.13). Figure 3.13 shows that the solvent had not evaporated off sufficiently during fibre formation between the spinneret and the collection plate such that some fibres collapsed upon drying to form flat ribbon-like fibres and "puddles" of nanocomposites. The fibres that did form properly, however, were analysed at a higher magnification to show the relatively smooth, bead free surface. The noncovalently compatibilzed MWNT/PyPS (figure 3.14 and 3.15) show similar results. These showed much better fibre formation under the same electrospinning conditions than the covalent version did. This suggests that in this case, the degree of chain entanglement is in fact higher in the noncovalently comatibilzed MWNT nanocomposite than in the covalently compatibilzed MWNT nanocomposite under the same electrospinning conditions. In addition, the high conductivity of the intact pristine MWNTs most probably leads to better fibre formation.

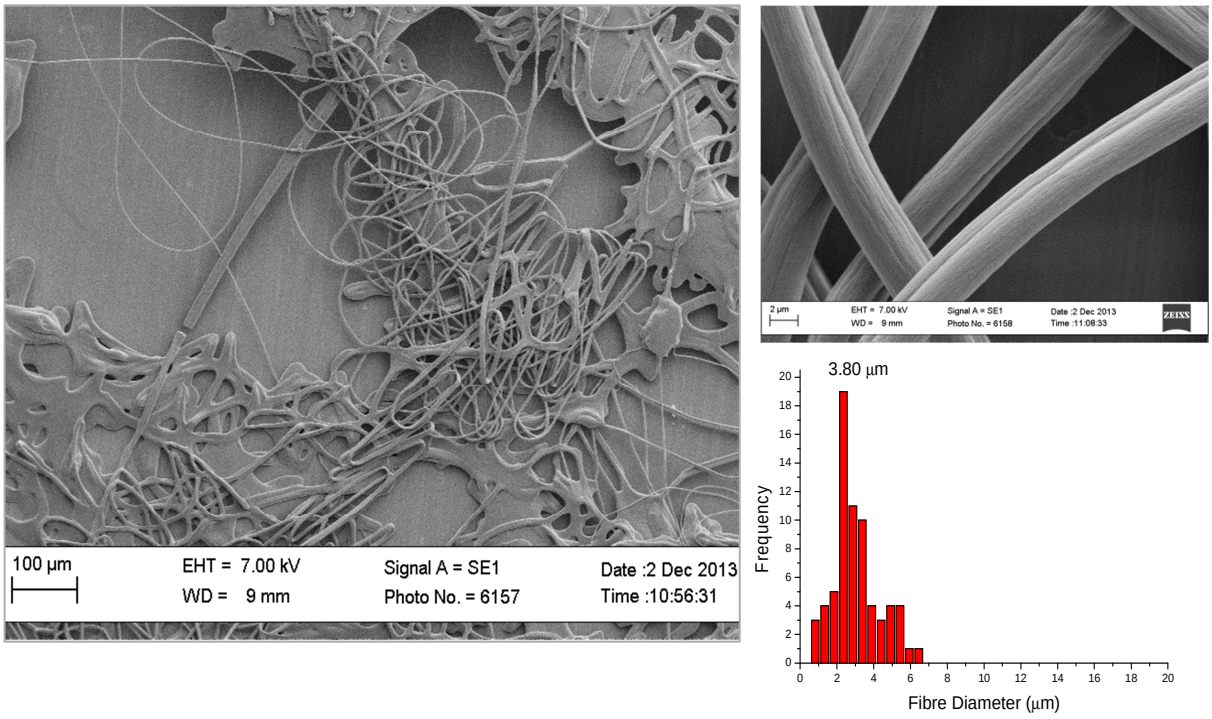

Figure 3.13: SEM images of nanofibres electrospun with 2 wt % covalent MWNT-DIBTC-PS in chloroform. The fibre diameter distribution indicates an average fibre diameter of 3.80 µm.

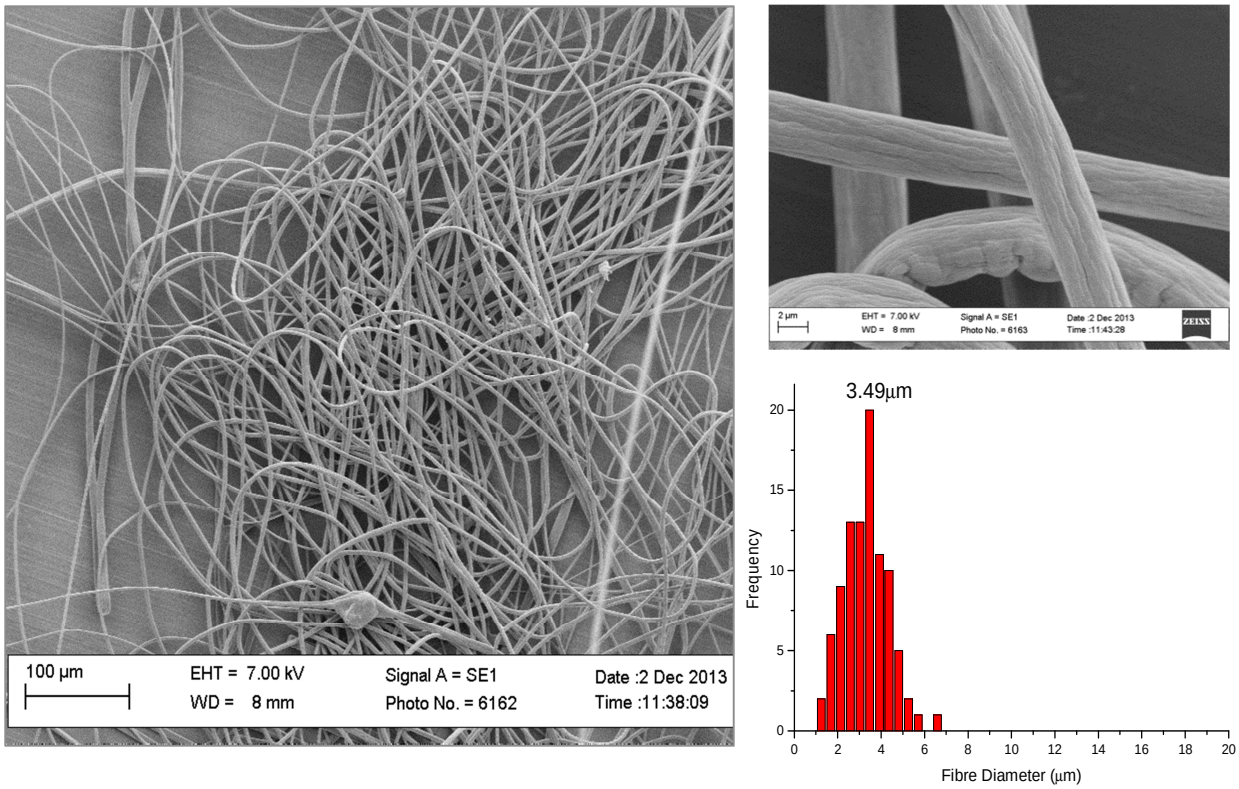

Figure 3.14: SEM images of nanofibres electrospun with 2 wt % noncovalent MWNT/PyPS (DIBTC 5 000 g/mol) in chloroform. The fibre diameter distribution indicates an average fibre diameter of 3.49 µm.

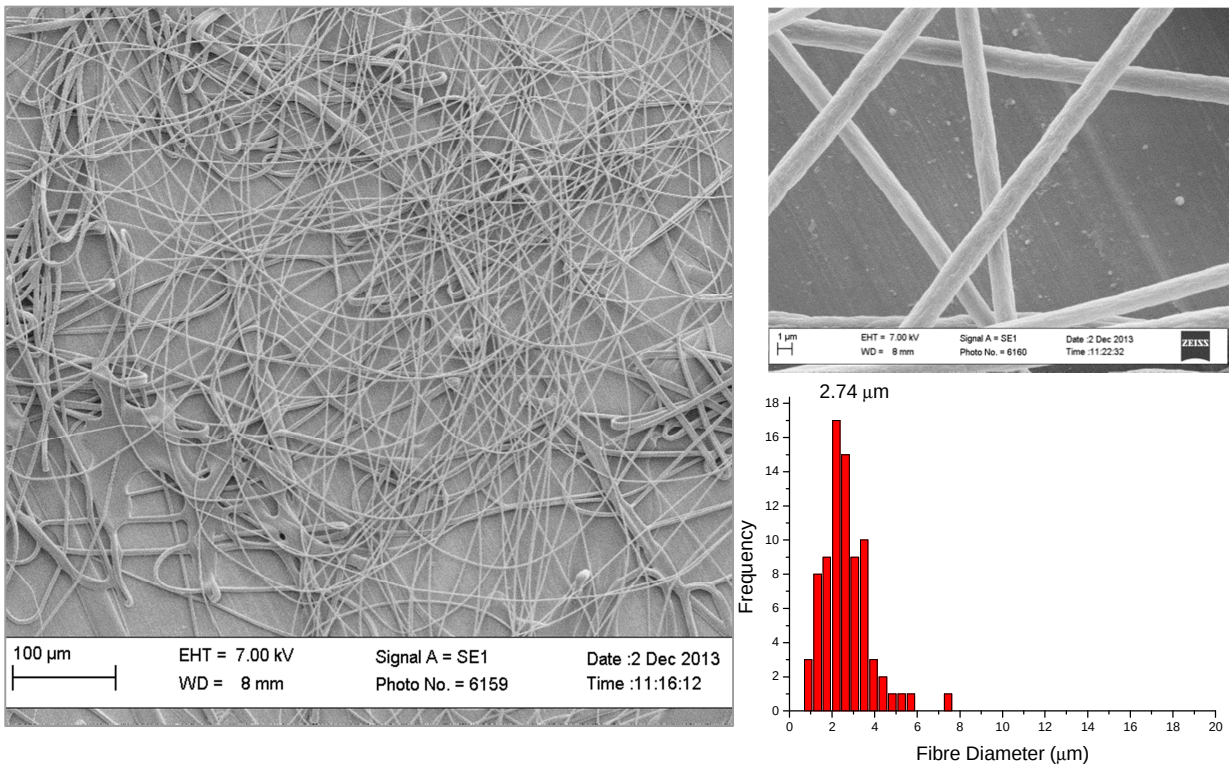

Figure 3. 15: SEM images of nanofibres electrospun with 2 wt % MWNT/PyPS (DIBTC 15 000 g/mol) in 20 w/v% PS in chloroform. The fibre diameter distribution indicates an average fibre diameter of 2.74 µm.

The fibre diameter distributions of the various fibres (see table 3.4) indicate that all the fibres containing the functionalized MWNTs have a smaller fibre diameter compared to the homopolymer. The smallest fibre diameter is seen in the noncovalent MWNT/PyPS (DIBTC 5 000) hybrid of shorter PS chain length. This trend is thought to exist due to a combination of increased chain entanglement brought about by an increased amount of "crosslinking points" as introduced by the MWNTs, and an increased conductivity of the electrospinning solution introduced by the presence of the pristine MWNTs which are dispersed in the PS matrix which leads to a smaller diameter.

Composite type	Lowest	Highest	Standard deviation	Average
PS homopolymer	2.05	28.46	4.33	7.28
pristine MWNTs	1.74	12.75	2.46	4.49
MWNT-DIBTC-PS	1.41	5.98	1.29	3.80
MWNT/PyPS (DIBTC 5 000)	0.88	5.26	0.85	2.74
MWNT/PyPS (DIBTC 15 000)	1.75	4.96	0.86	3.49

Table 3.4: Fibre diameter analysis of various electrospun nanocomposite fibres at 2 wt% filler composition. All values are given in µm.

As a means of comparison of fibre diameter between the different functionalized MWNT nanocomposites, fibres of 4 wt% and 6 wt% MWNTs in PS were also electrospun for all the nanocomposites. Image 3.2 shows that the fibres which were obtained revealed a grey to black colour as a result of the inclusion of the MWNTs into the fibres.

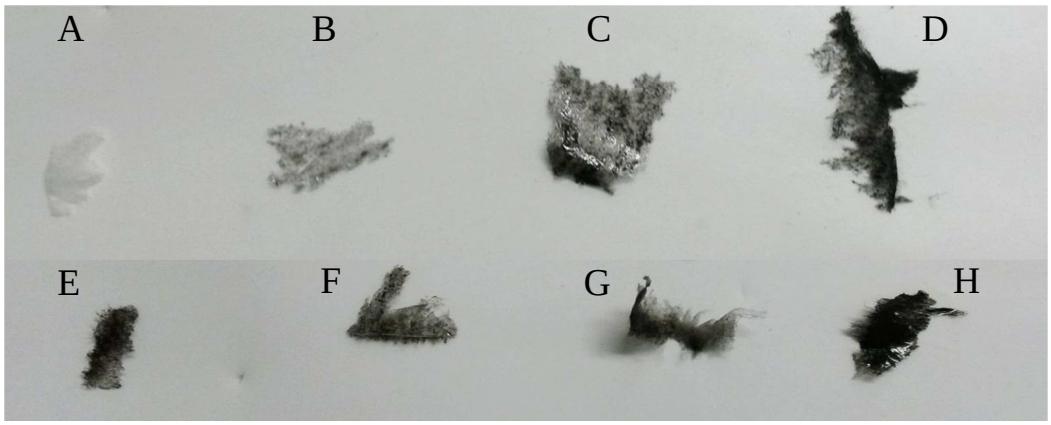

Image 3.2: Photographs of electrospun fibres of (A) PS homopolymer, (B) 2 wt% pristine MWNTs, (C) 4 wt% MWNT-HEBrIB-PS, (D) 4 wt% MWNT-DIBTC-PS, (E) 4 wt% MWNT/PyPS (HEBrIB 15 000), (F) 4 wt% MWNT/PyPS (HEBrIB 5 000), (G) 4 wt% MWNT/PyPS (DIBTC 5 000) and (H) 4 wt% MWNT/PyPS (DIBTC 15 000)

According to the study by Mazinani *et al.*[53] fibre diameter averages were obtained in the nanometer range. In this study, however, larger fibres were produced in all cases which is attributed to not having electrospun under the optimal conditions. However, the trend in fibre diameter behaviour in relation to MWNT content is depicted in these results. The SEM images of the 4 and 6 wt% nanofibres did not differ much in appearance with regard to the 2 wt% nanofibres as shown in figures 3.13-15. However, table 3.5 shows the differences in average fibre diameter between the different nanocomposites. These results are depicted graphically in figure 3.16 and indicate a clear trend in the relationship between fibre diameter and wt% of MWNTs. Upon increasing the weight percentage of MWNT in the nanocomposite, a decrease in average fibre diameter is observed in most nanocomposites. Interestlingly, a difference in diameter between the functionalized and unfunctionalized (or pristine) MWNTs is noted in that the pristine unfunctionalized MWNTs produce electrospun fibres of a substantially larger average fibre diameter than the functionalized MWNT containing fibres. This is as a result of the poor dispersion realised by the pristine MWNTs in the PS matrix and electrospinning solution which creates a larger fibre diameter during electrospinning. Furthermore, both the noncovalently functionalized MWNT/PyPS hybrid nanocomposites formed fibres of a smaller fibre diameter than the covalent MWNT-DIBTC-PS fibres did. This behaviour can be partially attributed to the increased conductivity of the noncovalent MWNT/PyPS hybrid electrospinning solutions which is brought about by the undamaged nanotube surface which is dispersed in the PS matrix more efficiently by the functionalization with the pyrene-end-functional PS via π-π stacking between the pyrene moiety and the nanotube walls. An increased dispersion aids in increasing the conductivity of the electrospinning solution which in turn leads to a smaller average fibre diameter. This decrease in fibre diameter can not be attributed to the greater conductivity of the solution alone, it also indicates that a larger degree of chain entanglement exists for the noncovalent compatibilzed MWNTs which then efectively act as “crosslinking points” which allow for a decrease fibre diameter to be realised. This observation is oppposed to the covalent functionalization in MWNT-DIBTC-PS which is destructive to the nanotube surface since it creates covalent bonds between the RAFT agent and the nanotube surface, thereby breaking the π-electron network created by the conjugated C-C bonds of the nanotube surface and leading to an increase in fibre diameter at 6 wt%. Despite this phenomenon, there is a slight decrease in the 4 wt% covalent MWNT-DIBTC-PS fibres which show a decrease in fibre diameter at this filler loading.

	2 wt%	4 wt%	6 wt%
Pristine MWNTs	4.49	4.66	5.58
MWNT-DIBTC-PS	3.80	3.28	3.65
MWNT/PyPS (DIBTC 5 000)	2.74	2.72	2.44
MWNT/PyPS (DIBTC 15 000)	3.49	3.42	3.35

Table 3.5: Average Fibre diameter (µm) of MWNTs functionalized using DIBTC in a 2, 4 and 6 wt% MWNT to PS ratio.

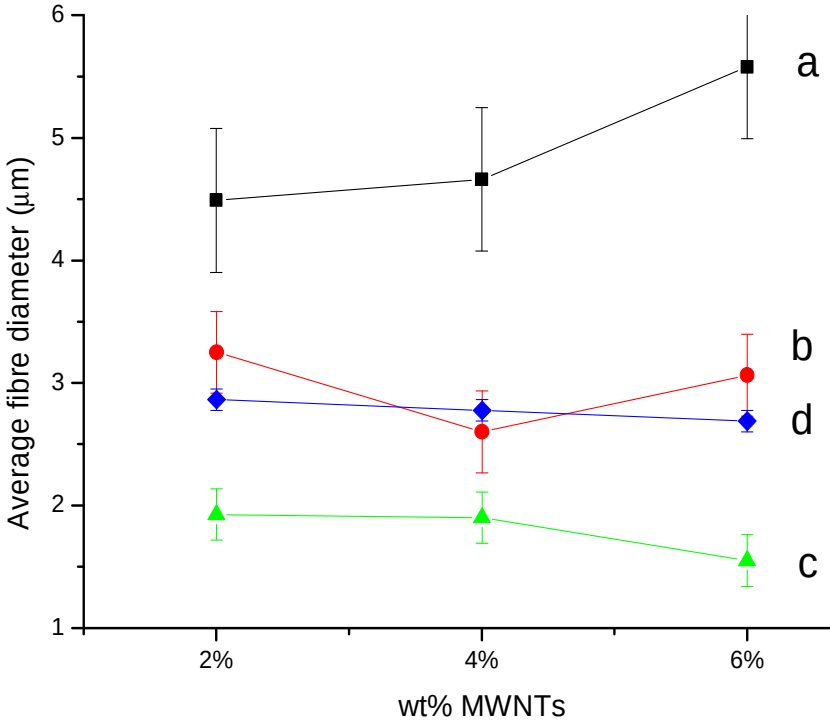

Figure 3.16: Average fibre diameter as a function of wt% MWNT of (a) pristine MWNTs, (b) MWNT-DIBTC-PS, (c) MWNT/PyPS (DIBTC 5 000) and (d) MWNT/PyPS (DIBTC 15 000)

3.4.9. TEM results for electrospun fibres containing MWNT functionalized via ATRP mediated PS

The chloroform solutions containing the nanocomposites in the PS matrix were then electrospun as described earlier. The fibres which were obtained revealed a grey to black colour as a result of the inclusion of the MWNTs into the fibres (see image 3.2).

The electrospun fibres were set in Spurr's resin and cured in an oven in order to obtain TEM images of the electrospun fibres. The resin was microtomed into ultrathin slices and analysed by TEM. Figure 3.17 shows the TEM images of cross-sections through the electrospun fibres containing a 6 wt% MWNT/PyPS (DIBTC 5 000 g/mol) content in a PS matrix (left), and MWNT/PyPS (DIBTC 15 000 g/mol) (right) in PS. To our knowledge, no reports exist discussing the electrospinning of PS nanocomposites containing noncovalently compatibilized MWNTs as shown here. These images indicate that the MWNTs are all located within close vicinity yet outside the electrospun fibres. From image 3.2 it is clear that the obtained electrospun fibres contain MWNTs due to their grey-black nature. Therefore, it is likely that the MWNTs are located on the surface of the nanofibres and are not embedding within the nanofibres themselves. Upon TEM sample preparation these MWNTs seem to then disperse within the liquid resin.

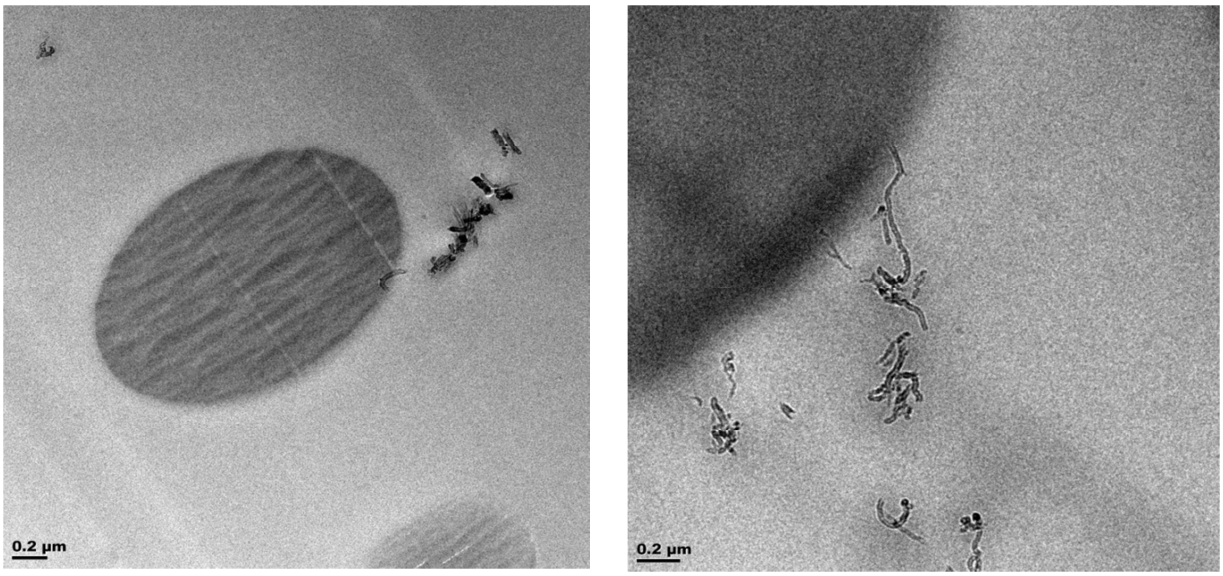

Figure 3.17: TEM images of microtomed sections of electrospun nanofibers containing 6 wt% (left) noncovalent MWNT/PyPS (DIBTC 5 000 g/mol) and (right) noncovalent MWNT/PyPS (DIBTC 15 000 g/mol) in a PS matrix.

3.4.10. Immobilization of the ATRP initiator HEBrIB onto the oxidized MWNT surface and the surface-initiated polymerization of styrene from MWNT-HEBrIB

Pristine MWNTs were refluxed with thionyl chloride to introduce acyl chloride functionality onto the MWNT surface from which the esterification with the hydroxyl end group of HEBrIB could take place. The removal of HEBrIB through washing the nanotubes with ethanol several times was followed by thin layer chromatography (TLC) of the filtrate. The FT-IR spectrum of the MWNT-HEBrIB showed the presence of C-H stretching vibration signal at 2913 cm^{-1} as well as the carbonyl stretching vibration at 1733 cm^{-1} which indicates that the HEBrIB had indeed been attached onto the MWNT surface. However, since HEBrIB does not contain any distinct functional groups that are different to those introduced into the product through the oxidation of the MWNT surface, it was not possible to determine the success of the reaction using FT-IR alone. TGA was therefore done which also enabled the quantitative analysis of HEBrIB attachment onto the MWNT surface (figure 3.18). Pristine MWNTs (**a**) are seen to maintain almost 100 weight % after 600°C.

Upon oxidation and consequent chlorination with $SOCl_2$, the produced MWNT-COCl is seen to exhibit a higher weight loss of 2.30% at 600°C (**b**) therefore suggesting the successful attachment of the acyl functionality along the MWNT surface. The immobilization of the ATRP initiator HEBrIB along these sites on the MWNT surface is confirmed by the TGA curve (**c**) which indicates a 7.5 weight % loss at 600°C. Since the MWNT-HEBrIB was thoroughly washed with THF to remove unattached HEBrIB which was followed using TLC, it can be concluded that the ATRP initiator has been successfully immobilized along the MWNT surface through esterification with the attached –COCl groups. After it was established that the HEBrIB had successfully been immobilized on the MWNT surface, the surface-initiated ATRP-mediated polymerization was completed. The TGA results also demonstrate the positive ATRP mediated polymerization of styrene via the “grafting from” approach (**d**). Any unreacted monomer and soluble homopolymer was removed by washing the MWNT product thoroughly with THF. Hence the formation of the covalent MWNT-HEBrIB-PS can be established due to the larger weight loss of 29.23% at 600°C which occurs as a result of the decomposition of styrene.

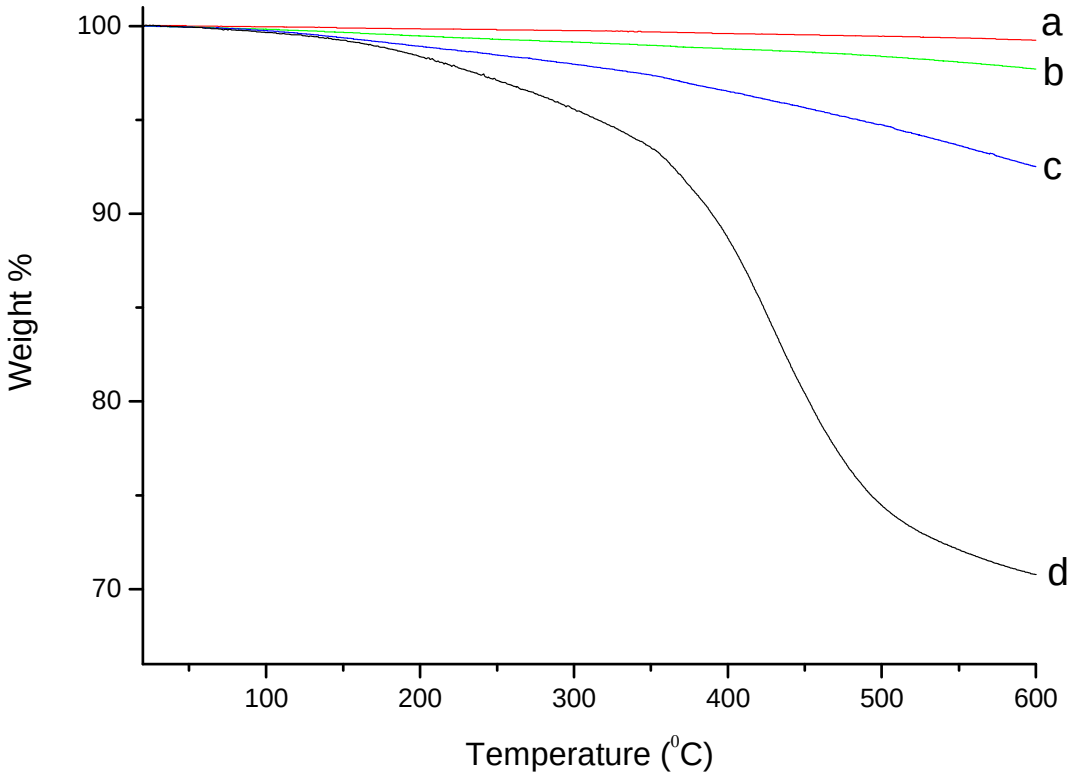

Figure 3.18: TGA curves of (a) pristine MWNTs, (b) MWNT-COCl, (c) MWNT-HEBrIB and (d) MWNT-HEBrIB-PS.

3.4.11. Synthesis of HEBrIB-Pyrene ATRP macroinitiator

Since an the esterification between the RAFT agent DIBTC and 1-pyrenemethanol was more successfully achieved via the introduction of an acyl chloride moiety on the carboxylic acid group of DIBTC, the same procedure was also followed for the esterification between HEBrIB and pyrenebutyric acid. Here, the pyrene functionality, however, contained the carboxylic acid which was first chlorinated (**1** in scheme 3.2) and subsequently esterified with the hydroxyl of HEBrIB via nucleophilic substitution to give the pyrene-functional ATRP initiator HEBrIB-Py (**3**) with a yield of 57.59%.

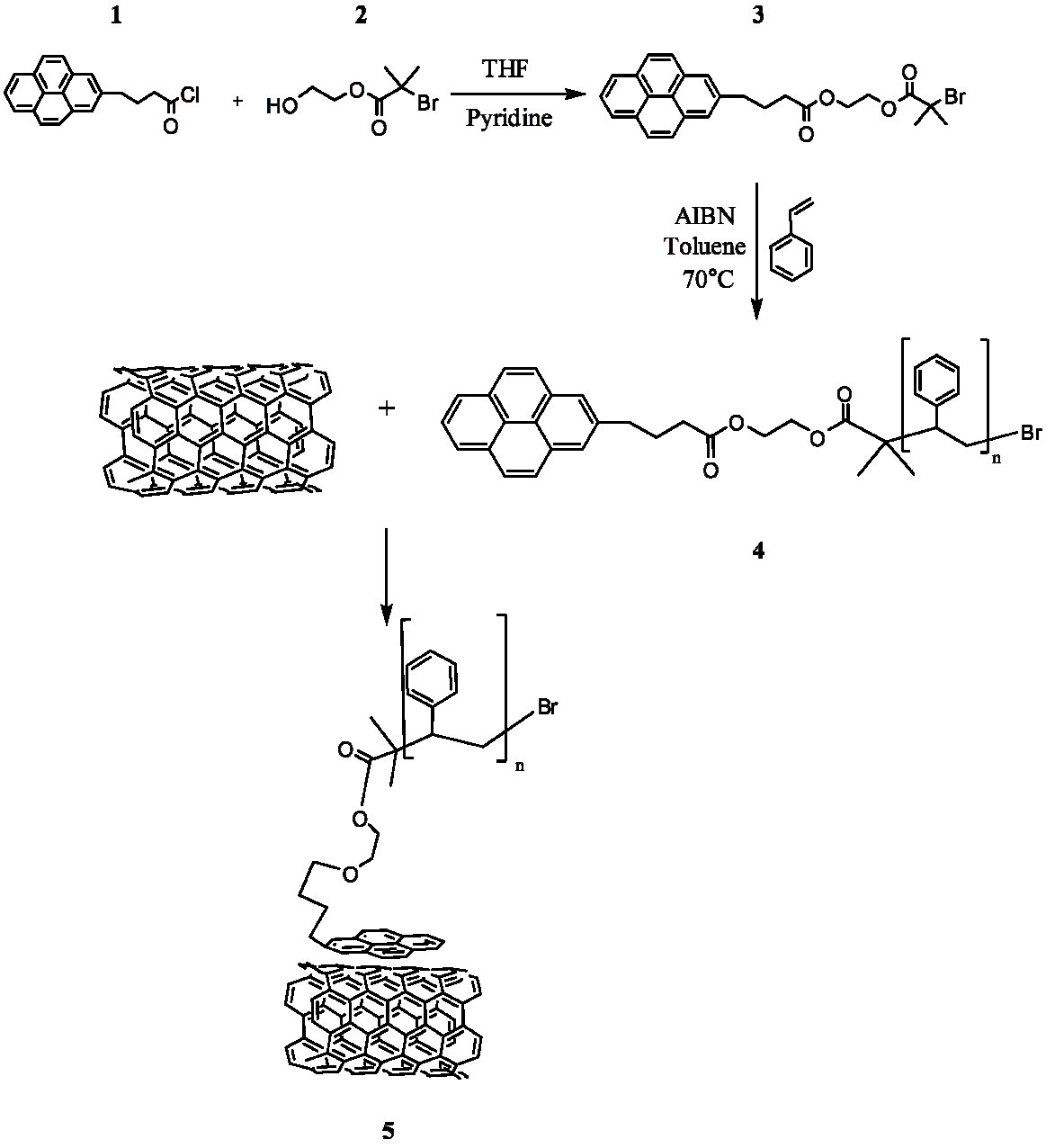

Scheme 3.2: Synthesis of MWNT/PyPS via macroinitiated ATRP of styrene.

^{13}C NMR of the ATRP macroinitiator (**3**) as well as ^{1}H NMR (see appendix B, figure B.4) was done to confirm that the esterification between HEBrIB and pyrenebutyric acid had occurred. Figure 3.19 shows the ^{13}C NMR spectrum of **3**. The peak labelled "a" on the skeletal structure of **3** moved downfield from 58.68 ppm as seen in the ^{13}C NMR spectrum of HEBrIB (see insert (ii)) to 61.41 ppm. This is as a result of the presence of an increased amount of oxygen atoms introduced by esterification which leads to the deshielding of this carbon.

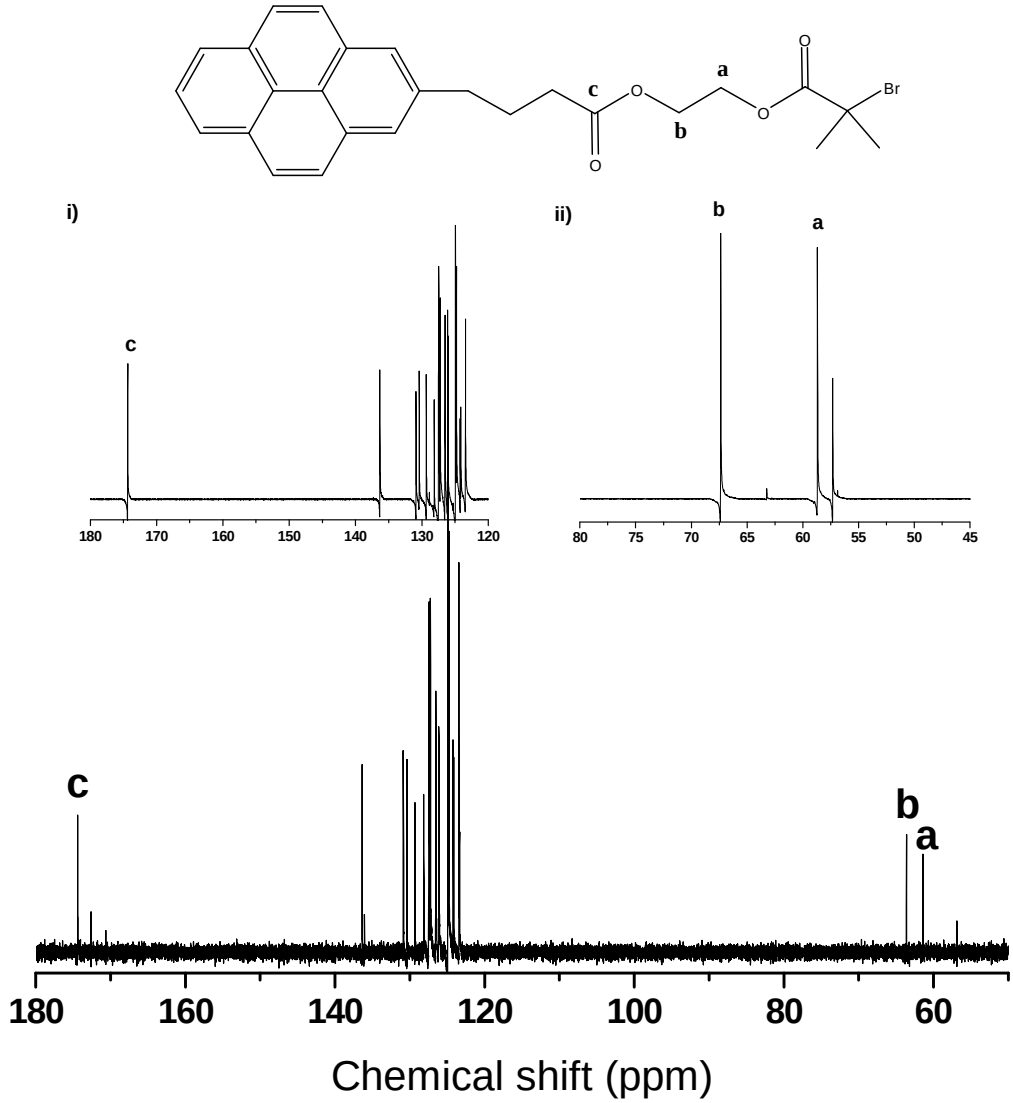

Figure 3.19: ^{13}C NMR spectrum for HEBrIB-Py where the peak "a" corresponds to the carbon shown in the skeletal structure and shifts from 58.68 ppm in (ii) the ^{13}C NMR spectrum of HEBrIB to 61.41 ppm. Peaks "b" and "c" represent the carbons which are most affected by the esterification and shift from 67.36 ppm in (ii) to 63.62 ppm and from 174.36 ppm in (i) the ^{13}C NMR spectrum of pyrenebutyric acid to 174.40 ppm respectively.

Peak "b" however moved upfield from 67.36 ppm in insert (ii) to 63.62 ppm as a result of increased shielding introduced by the closer proximity to the C=O moiety, which leads to the conclusion that esterification has taken place. The slight downfield shift in the peak labelled "c" from 174.36 ppm in the ^{13}C spectrum of pyrenebutyric acid (see insert (i)) to 174.40 ppm confirms that the esterification was successful. The NMR spectrum also indicated the success of this reaction through the relative integration between the proton peaks of the two protons attached to the carbon in the α-position to the pyrene compared to two protons of the aliphatic carbon belonging to the HEBrIB section of **3**. 67.0% functionality was obtained, thus indicating that this reaction equilibrium is favourable towards the product.

3.4.12. ATRP-mediated polymerization of styrene using the ATRP macroinitiator HEBrIB-Py

Styrene was polymerized via ATRP mediated polymerization using HEBrIB-Py (**3**) as the macroinitiator (scheme 3.2). PS chain lengths of 5 000 g/mol and 15 000 g/mol were targeted. The ^{1}H NMR spectra of both chain lengths of HEBrIB-Py-PS (**4**) show similar results, however the shorter chain lengths show a better relative intensity of the PS peaks to those belonging to the macroinitiator than the longer chain length does. The ^{1}H NMR spectrum of the 5 000g /mol version of **4** shows the presence of characteristic aromatic styrene peaks around 7.11 ppm (see figure B.5. in appendix B) as well as the pyrene peaks between 7.84 ppm-8.28 ppm. Confirmation that the PS chains are in fact pyrene-terminated and are not just present separately comes in the change in chemical shift realised by the peak belonging to the 6 methyl protons of the aliphatic part belonging to the HEBrIB component of the macroinitiator. These shift upfield from 1.82 ppm-1.27 ppm as predicted due to the increased shielding of these protons introduced by the aromatic PS rings.

The UV/Vis spectrum of pyrenebutyric acid (see **a** in figure 3.20) has clear absorbance peaks between 260-280 nm and 310-350 nm which are indicative of the π-π* electronic transitions experienced by the electrons of the aromatic network in the pyrene-group. The ^{1}H NMR spectrum of HEBrIB-Py (figure 3.19) suggests the successful esterification between HEBrIB and pyrenebutyric acid. This is further confirmed by the UV/Vis spectrum of HEBrIB-Py (**b**). The characteristic pyrene-peaks are present in HEBrIB-Py as well. The formation of pyrene-end-functionalized PS chains is also proved by the UV/Vis graph (**c**) since the pyrene-peaks are clearly seen in the functional polymer. The 5 000 g/mol and 15 000 g/mol HEBrIB-Py-PS compounds show similar UV/Vis spectra, except that the intensity of absorbance for the

pyrene-group is lower for the 15 000 g/mol HEBrIB-Py-PS (see appendix F) than for the 5 000 g/mol version. This is because of the relative concentration of pyrene groups per mass of sample is lower in the longer chain length version.

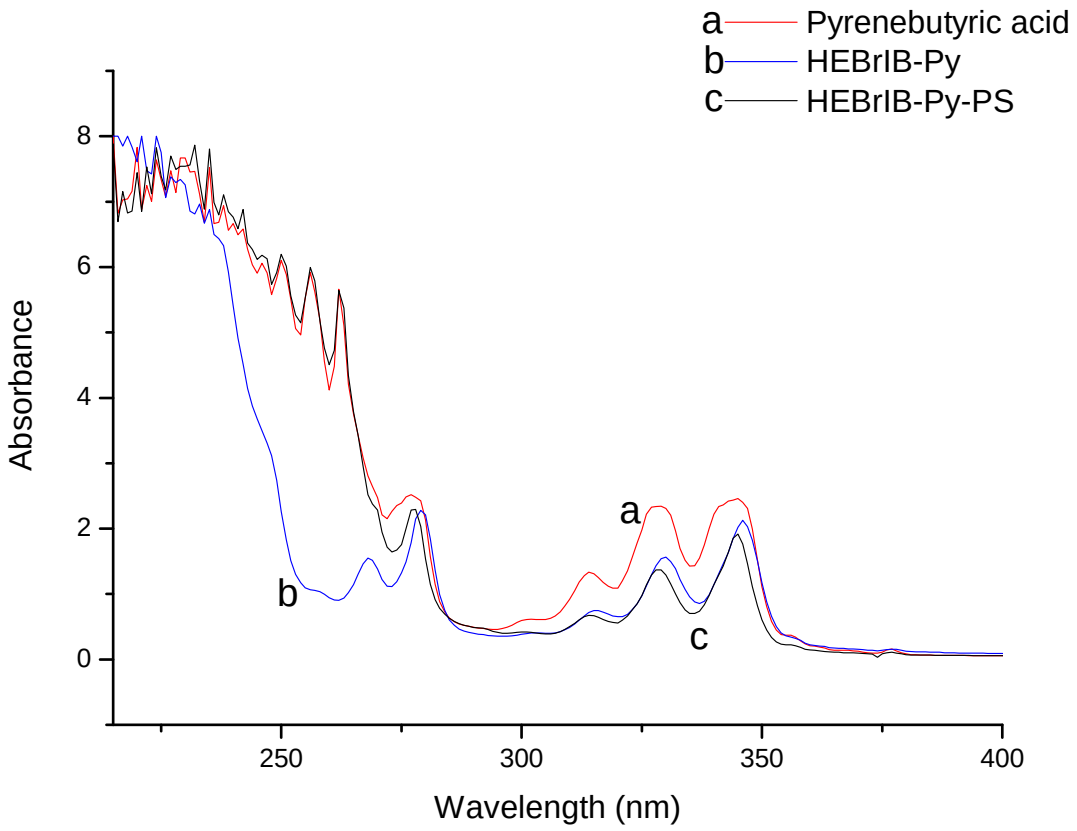

Figure 3.20: UV/Vis spectra of a dispersion of (a) pyrenebutyric acid, (b) HEBrIB-Py ATRP macroinitiator and (c) HEBrIB-Py-PS of 5 000g/mol chain length in chloroform.

SEC was done to determine the molecular weight of the 5 000 g/mol and 15 000 g/mol HEBrIB-Py-PS through the RI detector. The $\overline{M_n}$ of the two compounds were 1.29×10^4 g/mol and 3.25×10^4 g/mol respectively and with a dispersity (Đ) of 1.19 and 1.29 correspondingly. The RI response showed a much higher molecular weight than targeted, which is not unexpected since the reaction time was increased by 42 h in order to ensure sufficient polymer would precipitate in methanol. As discussed previously, the dual wavelength UV detector was used to determine the presence of pyrene and styrene groups according to their absorbance of UV wavelengths of 254 nm or 365 nm. Figure 3.21 demonstrates that around 15 min in both the chain length variations there is a large signal response for all three detectors, which indicates that this elution peak represents the pyrene-

end function PS chains since PS is active at 254 nm and pyrene at 365 nm and both signals are intense in the spectra. The RI peak also reaches its peak intensity thus specifying that the majority of polymer is indeed end-capped by pyrenes. The later peaks in the signal responses after ~18 min can be accredited as the signal response to the eluting unreacted macroinitiator since the pyrene group is active at both 365 nm and 254 nm (although much less intense).

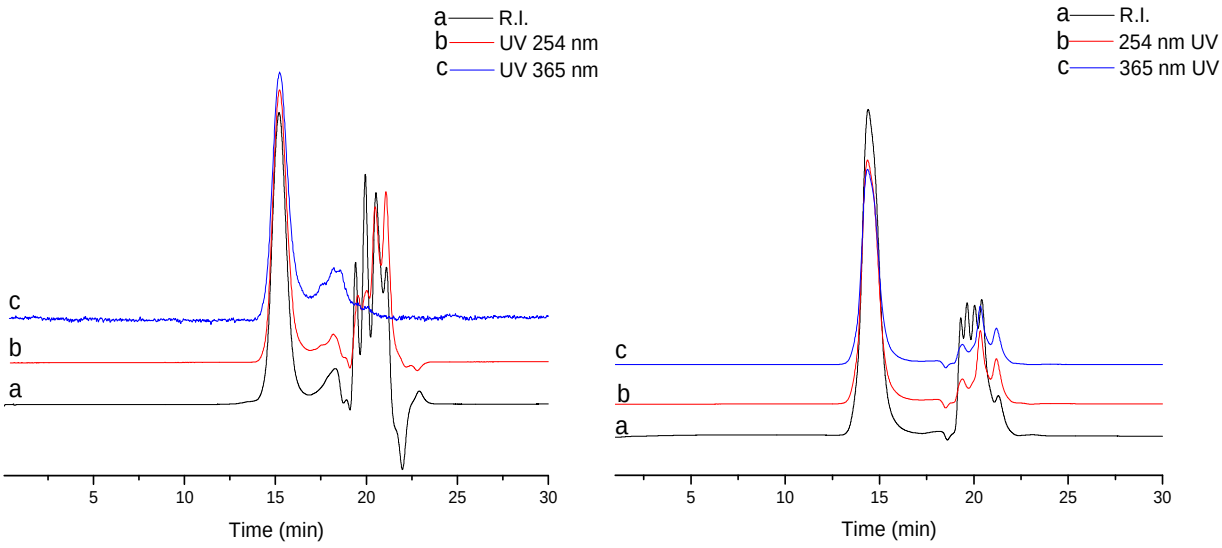

Figure 3.21: SEC results of (left) HEBrIB-Py-PS of 5 000 g/mol target chain length and (right) the 15 000 g/mol version.

3.4.13. Noncovalent interaction of the pyrene-functional PS (HEBrIB-PS-Py) with pristine MWNTs

The same procedure described in section 3.4.5 involving the RAFT polymerized DIBTC-PS-Py with MWNTs was followed for the noncovalent functionalization of the MWNTs with the ATRP polymerized HEBrIB-Py-PS. Again both targeted chain lengths of 5 000 g/mol and 15 000 g/mol were interacted with the pristine MWNTs although no significant differences were observed as a result of the differences in styrene chain lengths. As a result, the same trends in NMR, fluorescence and UV spectra were pursued. Any unattached HEBrIB-Py-PS was removed from the product through repetitive centrifugation, separation and redispersion in chloroform until no pyrene compounds were detected in the centrifuge supernate according to the UV detector response. In the case of the ATRP version of the noncovalent MWNT/PyPS compounds, an increased and more stable dispersion in several solvents such as chloroform and THF was noticed compared to that of pristine MWNTs, which is a good

indication that some functionalization has taken place to improve the dispersibility of the nanotubes.

3.4.13.1. TGA

Figure 3.22 indicates the thermal decomposition curves of (**a**) pristine MWNTs, (**b**) HEBrIB-Py-PS of 5 000 g/mol targeted styrene chain length, and (**c**) the corresponding noncovalent hybrid complex of MWNT/PyPS (HEBrIB 5 000). At 510°C thermal stability is reached in all three complexes. The MWNTs (**a**) have lost 0.59% of their weight at this point, whereas HEBrIB-Py-PS (**b**) has lost 99.61% and the hybrid complex MWNT/PyPS (**c**) has lost 10.07% of its weight. The weight loss observed in **a** is insignificant, therefore the 10.07% weight loss seen for curve **c** is deemed to represent the loss of adsorbed HEBrIB-Py-PS since at this temperature curve **b** levels off similar to curve **a** but has lost weight corresponding to that lost for curve **b**, which at this temperature has maintained only 0.39% of its original weight. This confirms the positive formation of the noncovalent hybrid complex through adsorption of the pyrene-end-functional PS onto the MWNT surface. The average amount of HEBrIB-Py-PS which has been adsorbed per MWNT can be calculated similarly as done in section 3.4.5.1 to be 1.758×10^4 molecules of PyPS per MWNT for the 5 000 g/mol HEBrIB MWNT/PyPS and 6.973×10^3 molecules PyPS per MWNT for the 15 000 g/mol version (see appendix C for calculations).

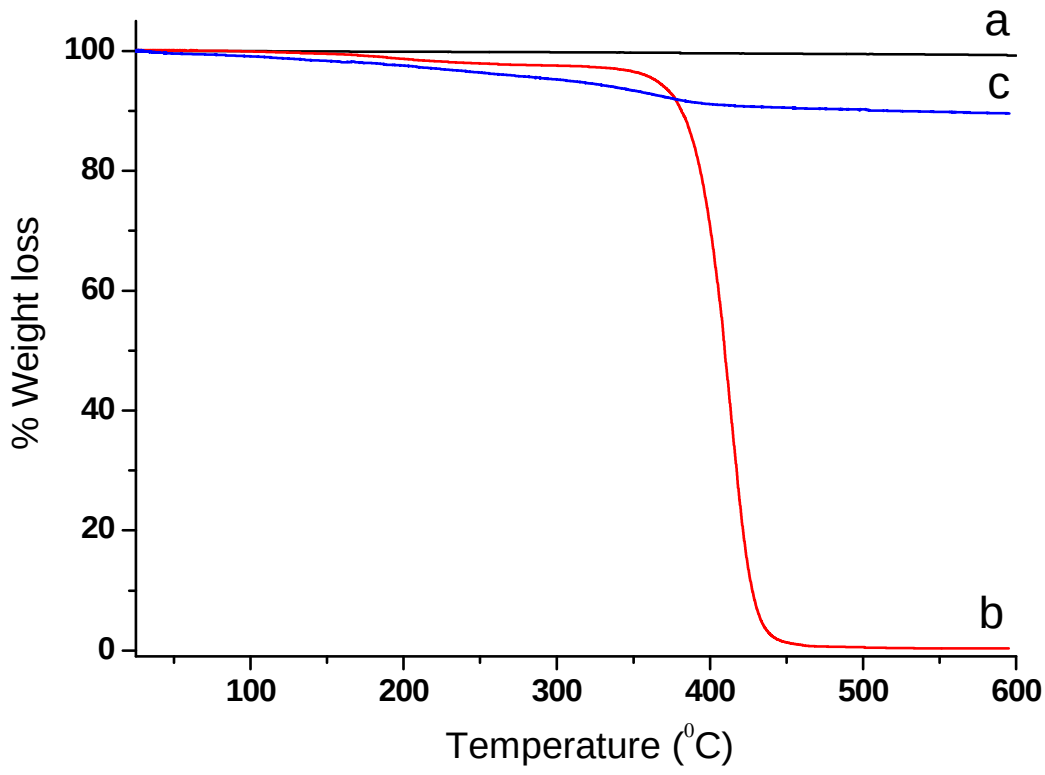

Figure 3.22: TGA thermogram of (a) pristine MWNTs, (b) HEBrIB-Py-PS (5 000) and (c) the resultant MWNT/PyPS hybrid.

3.4.13.2. NMR

Figure 3.23 shows the ^{1}H NMR spectrum of HEBrIB-Py-PS (5 000 g/mol) (**a**) and the corresponding MWNT/PyPS complex (**b**). The pyrene signal is clearly visible between 7.84 ppm-8.27 ppm in **a**, but is almost completely absent in the MWNT/PyPS hybrid spectrum **b**. π-π stacking between pyrenes and MWNT surface occurs during noncovalent compatibilization which results in shifting, broadening and/or weakening of the signal peaks upon interaction. The pyrene signal is almost absent in **b** (8.26 ppm-7.84 ppm). A slight upfield shift in the peaks is also seen, therefore, it is assumed that the π-π stacking interactions have indeed taken place to an extent such that the signal is nearly absent since the pyrene groups are closely adsorbed to the nanotube surface and the electrons are delocalized by the MWNTs conjugated aromatic π-electron network. The general trend in weakening, shifting and broadening of signal peaks is seen from spectra **a** to **b**. The two protons on the α-carbon of the carbonyl of the pyrene component are visible in the ^{1}H NMR spectrum of HEBrIB-Py-PS (**a**) at 2.43 ppm. This peak shifted significantly upfield to 2.37 ppm upon noncovalent interaction of the pyrene moiety with the MWNT surface. This peak also broadened by a factor of 0.05 ppm and weakened significantly, thus indicating its closer proximity to the MWNT ring current. The ^{1}H spectrum further reveals that the peak intensity of these two protons at 1.96 ppm in spectrum **a** have an intensity of 1.47 relative to the six methyl protons seen at 1.27 ppm, which decreased drastically to a relative intensity of 0.46 in the MWNT/PyPS spectrum.

An insert of the six methyl protons of the HEBrIB component is shown in figure 3.23. Here a slight broadening is observed upon functionalization of HEBrIB-Py-PS (**a**) with MWNTs (**b**) by a factor of 0.04, however no change in the chemical shift is observed, thus suggesting that the aliphatic chain is not as closely adsorbed to the MWNTs and the magnetic field of these methyl protons is not affected by the presence of the nanotube ring current and rather just influenced by the general conductivity introduced to the NMR sample by the nanotube presence. This, together with the presence of the methyl proton peak in spectrum **b,** indicates that the MWNTs have been functionalized with HEBrIB-Py-PS via π-π stacking.

The MWNT/PyPS created with the 15 000 g/mol targeted chain length of HEBrIB-Py-PS was not fully characterized since the isolation of the hybrid complex from unattached HEBrIB-Py-PS was extremely time consuming and since the desired noncovalent functionalization was proven to be successful for both the ATRP and RAFT short chain length versions of PS

and the longer chain length version of DIBTC, it was deduced that the same results would be found for the longer chain length ATRP PS.

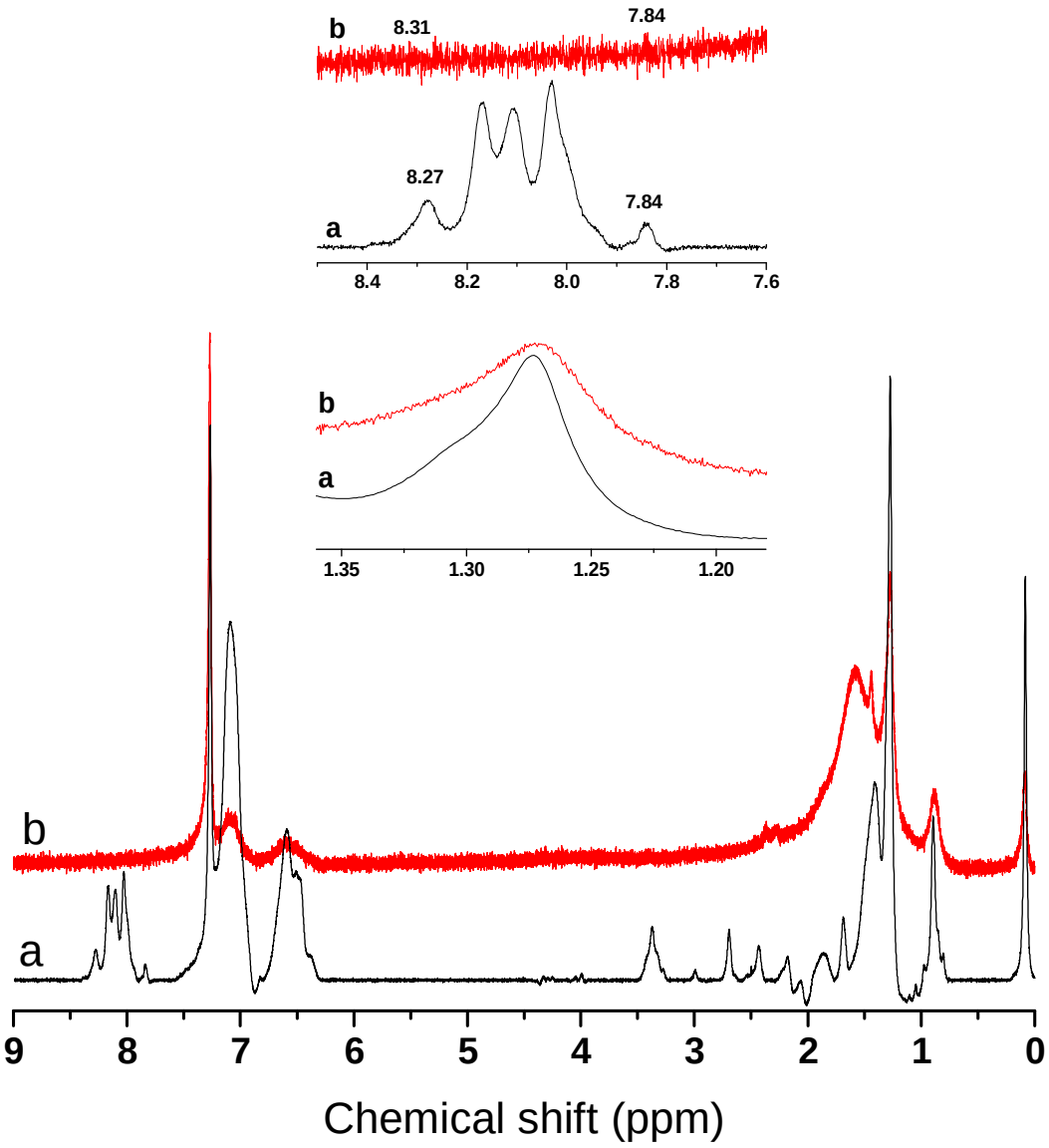

Figure 3.23: ^{1}H NMR spectrum of (a) HEBrIB-Py-PS 5 000 g/mol chain length and (b) the corresponding noncovalent MWNT/PyPS hybrid complex.

3.4.13.3. UV/Vis/NIR

The same principles discussed in section 3.4.5.3 were used in the analysis of the UV/Vis/NIR spectra of the MWNT/PyPS hybrid created using HEBrIB-Py-PS of 5 000 g/mol and 15 000 g/mol chain lengths. Figure 3.24 shows the results. The PyPS component has been confirmed to be present by NMR. The fact that the interaction is indeed noncovalent is proved by the UV/Vis/NIR spectra. This is because MWNTs do not significantly absorb in the UV/Vis/NIR region. The HEBrIB-Py-PS compound does show the characteristic pyrene absorbance peaks (refer to figure 3.20). Thus it can be concluded that the PyPS complex has interacted with the MWNTs in a noncovalent manner such that the MWNT molecular structure is maintained. The presence of the characteristic semiconductor electronic transitions E_{11}^{S} and E_{22}^{S} indicates that the electronic structure has not been altered and as such the interaction between the MWNT surface and the HEBrIB-Py-PS complex is indeed noncovalent.

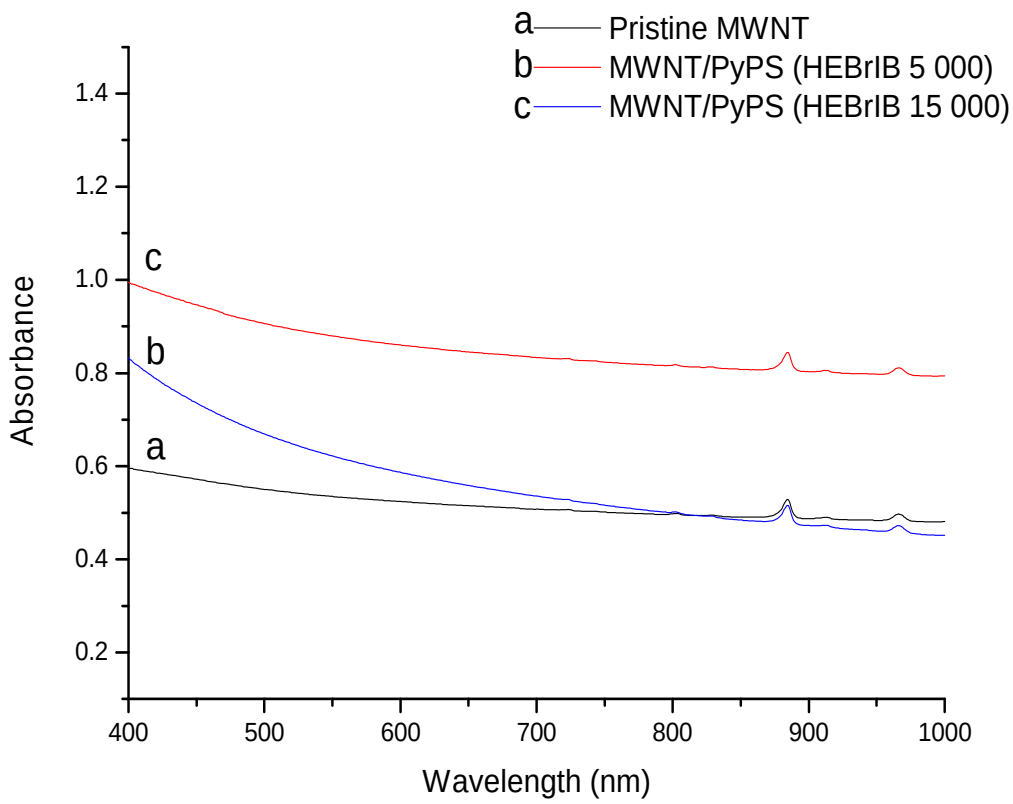

Figure 3.24: UV/Vis/NIR spectra of a dispersion of (a) pristine MWNTs, (b) MWNT/PyPS (HEBrIB 5 000 g/mol) hybrid and (c) MWNT/PyPS (HEBrIB 15 000g/mol) hybrid in chloroform.

3.4.13.4. Fluorescence

The same results were desired for the ATRP version of the MWNT/PyPS hybrid complex as those presented for the RAFT version of MWNT/PyPS in section 3.4.5.4. Figure 3.25 shows the excitation and emission spectra the HEBrIB-Py-PS of both targeted chain lengths of 5 000 g/mol and 15 000 g/mol in comparison to the respective MWNT/PyPS hybrid complex they constitute. Both chain length complexes give similar results. In both cases, the emission decay signal released after excitation at a wavelength of 396 nm is visibly quenched upon formation of the noncovalent hybrid complex. This is because the rate of energy transfer between the HEBrIB-Py-PS is increased due to the interactions through π-π stacking with the MWNT ring current which is present along its surface.

Upon excitation at 390 nm, both **a** and **c** show clear fluorescence (see (ii) and (iv)). This signal is significantly quenched in the corresponding MWNT/PyPS hybrid complexes indicating efficient and rapid transfer of energy between the MWNTs and the pyrene groups of HEBrIB-Py-PS. This leads to the confirmation that the MWNT/PyPS hybrid has formed by the noncovalent π-π stacking interaction between the pyrene-end functionality of the HEBrIB-Py-PS chains and the pristine MWNT surfaces.

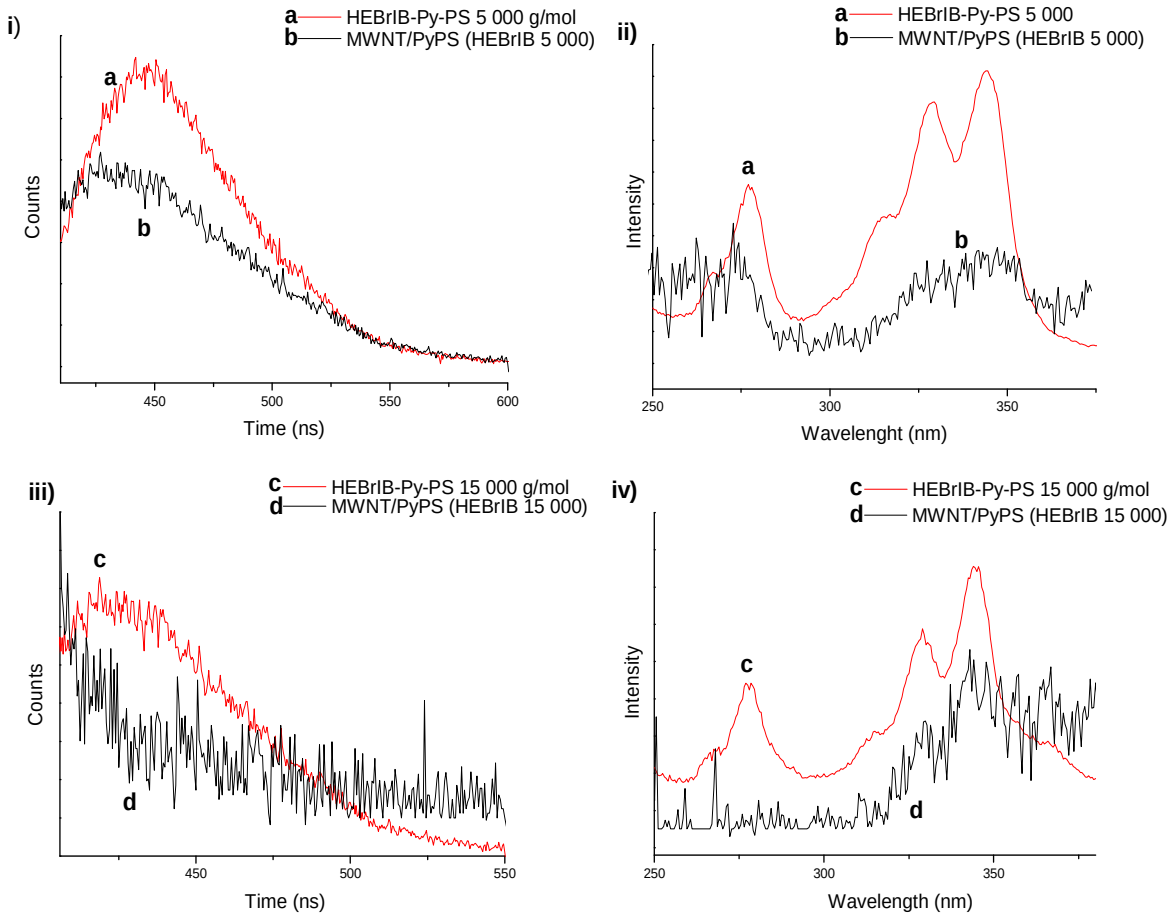

Figure 3.25: (i and iii) Emission decay curves recorded at 396 nm and (ii and iv) the fluorescence spectra excited at 390 nm of a dispersion in chloroform of (a) HEBrIB-Py-PS of PS chain length 5 000 g/mol, (b) the corresponding MWNT/PyPS hybrid complex, (c) HEBrIB-Py-PS of 15 000 g/mol chain length and (d) the resultant MWNT/PyPS hybrid complex.

3.4.14. TEM results for MWNT functionalization with ATRP mediated PS

Dispersions of pristine MWNT, MWNT-HEBrIB-PS, MWNT/PyPS (HEBrIB 5 000 g/mol) and MWNT/PyPS (HEBrIB 15 000 g/mol) were prepared in chloroform for TEM analysis. The same technique for sample preparation was done as described for the RAFT version. The MWNTs as mentioned earlier, ranged in diameter and length which is thought to arise naturally during the actual CNT synthesis. Figure 3.26 shows the dispersion of the functionalized and unfunctionalized MWNTs in chloroform. The pristine MWNTs have longer tubes in general and an average diameter of 26.04 nm (see figure 3.26, top left image). Most of the other samples had undergone ultrasonication in order to break up the MWNT bundles and aggregates and to disperse them successfully in solution so that the functionalization of the nanotube surface could take place effectively which could have potentially damaged and therefore decreased the nanotube diameters. The average diameter of the covalent MWNT-HEBrIB-PS complex (top right in figure 3.26) was 42.59 nm. The noncovalent MWNT/PyPS complexes of 5 000 g/mol and 15 000 g/mol chain lengths were determined to be 26.97 nm and 25.01 nm respectively. The notably larger diameter for the covalent MWNT-HEBrIB-PS is deemed to be a result of random diameter distribution which is introduced during MWNT synthesis. With these TEM images, it is also noted (as it was in figure 3.11) that there is a greater degree of dispersibility in the noncovalent MWNT/PyPS hybrid complexes in solution than in the pristine MWNTs. Therefore, it seems that the noncovalent interactions are indeed effective at breaking apart the MWNT aggregates and prevent their re-bundling in solution.

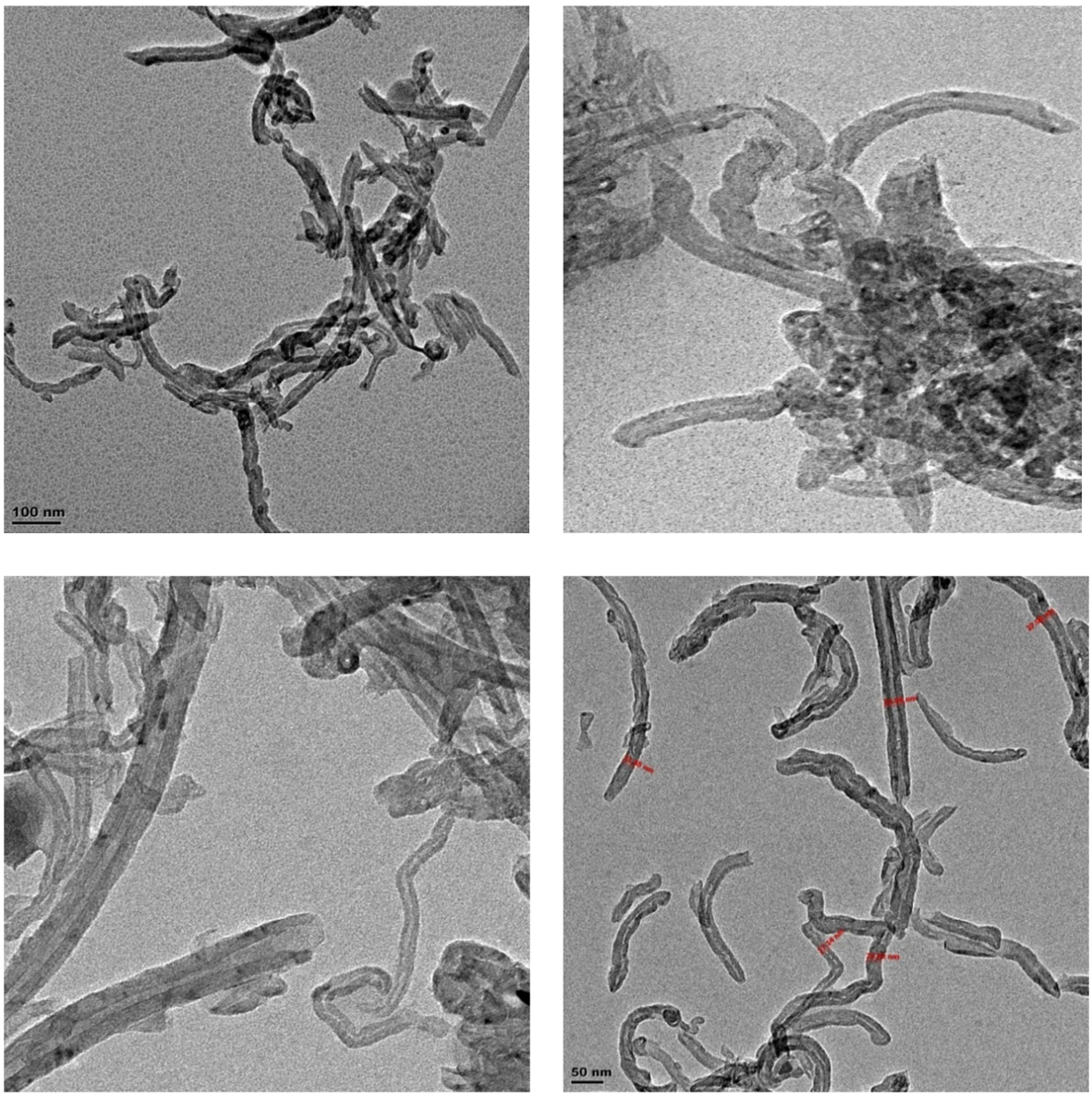

Figure 3.26: TEM images of (top left) pristine MWNTs; (top right) covalent MWNT-HEBrIB-PS; (bottom left) noncovalent MWNT/PyPS (HEBrIB 5 000 g/mol) and (bottom right) noncovalent MWNT/PyPS (HEBrIB 15 000 g/mol).

Nanocomposites of 2 wt%, 4 wt% and 6 wt% of the MWNT composites in a 20 w/v% PS in chloroform stock solution were prepared and analysed using TEM. Figure 3.27 shows that the interaction between the MWNTs and the PS matrix, and it was found in all cases that the functionalized MWNTs were more dispersed in the PS matrix than the pristine unfunctionalized MWNTs are which are seen to form aggregated bundles. The longer chain length noncovalent MWNT/PyPS (HEBrIB 15 000 g/mol) did not produce acceptable images in TEM due to a shortage of product which lead to a very low concentration which made the carbon nanotubes difficult to find in interaction with one another. However, from the other

images it is confirmed that the dispersion of the MWNTs in the PS is indeed greatly improved upon functionalization.

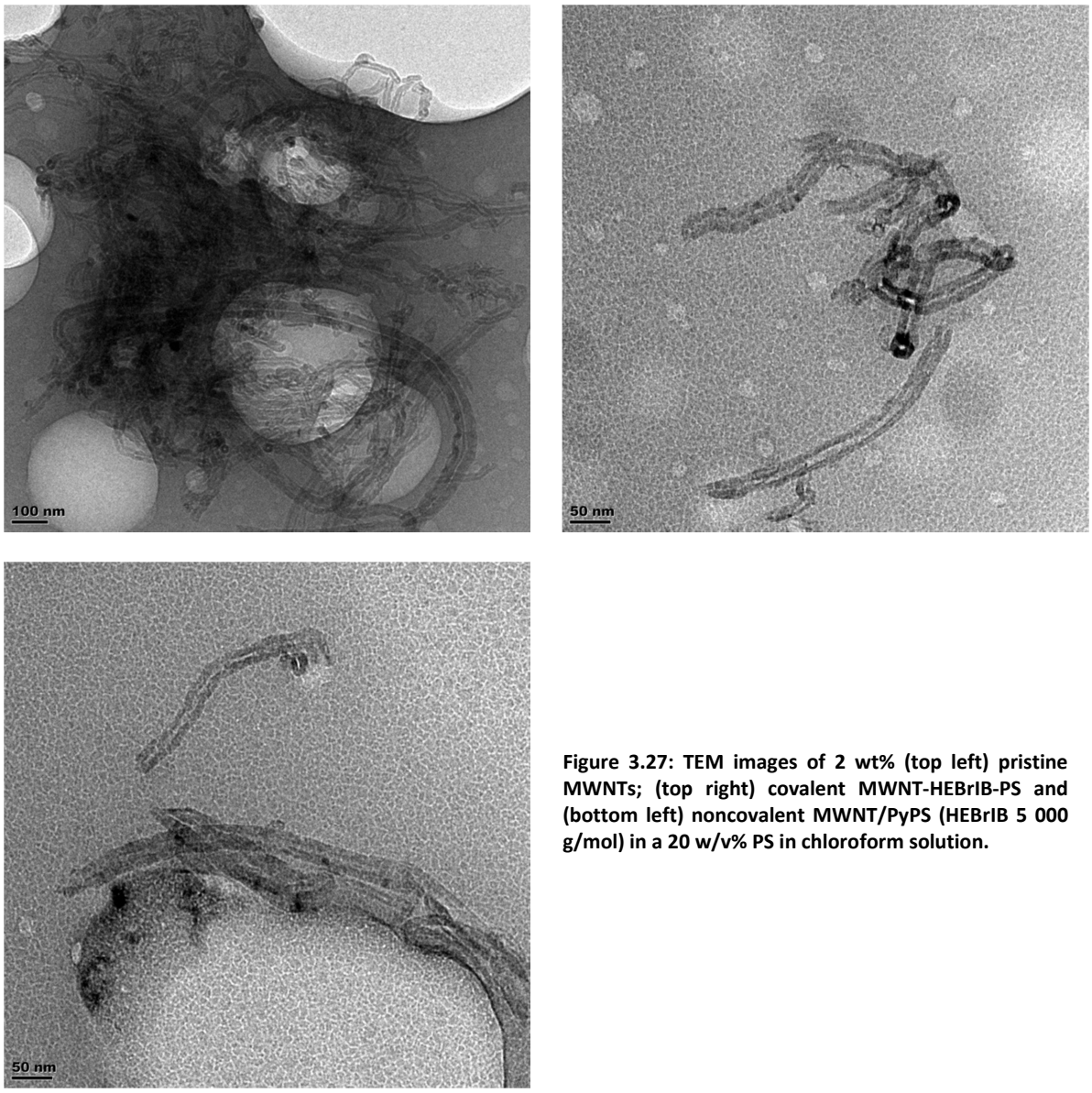

Figure 3.27: TEM images of 2 wt% (top left) pristine MWNTs; (top right) covalent MWNT-HEBrIB-PS and (bottom left) noncovalent MWNT/PyPS (HEBrIB 5 000 g/mol) in a 20 w/v% PS in chloroform solution.

3.4.15. Electrospinning of nanocomposites

Nanofibres of 20 w/v% PS in chloroform containing the various nanocomposites as indicated in table 3.6 were electrospun. Fibre production was observed for all of the different nanocomposites. The fibres were seen to change in colour from clear for those spun without MWNTs to black with MWNTs present (see image 3.2).

3.4.16. SEM results for MWNT functionalization with ATRP mediated PS

Figures 3.28-30 show the SEM images of the covalent MWNT-HEBrIB-PS complex (figure 3.28), and the two noncovalent MWNT/PyPS (HEBrIB) of 5 000 g/mol (figure 3.29) and 15 000 g/mol chain length (figure 3.30). Here again it can be seen that the solvent has not evaporated off completely before reaching the collector plate during electrospinning as indicated by the flat ribbon-like fibres which formed. However, there are many fibres that did form sufficiently and these were investigated at higher magnification. The PS fibres containing the covalently-compatibilized MWNT-HEBrIB-PS (figure 3.28) showed a porous surface which was not observed as clearly in the noncovalent nanocomposites. These images provide evidence that the noncovalent as well as the covalent compatibilized MWNT products can indeed be electrospun into nanofibres under the right electrospinning conditions.

The fibre diameter distribution histograms indicate that a fairly large distribution of fibre diameter exists in the covalent product (figure 3.28). This is seen to follow more of a trend towards one diameter category in the noncovalent MWNT/PyPS hybrids as these fibre diameters are more uniform than in the covalent fibres. This is possibly due to a more uniform distribution of the MWNTs in the electrospinning PS solution which is promoted by the efficient noncovalent functionalization of the MWNTs.

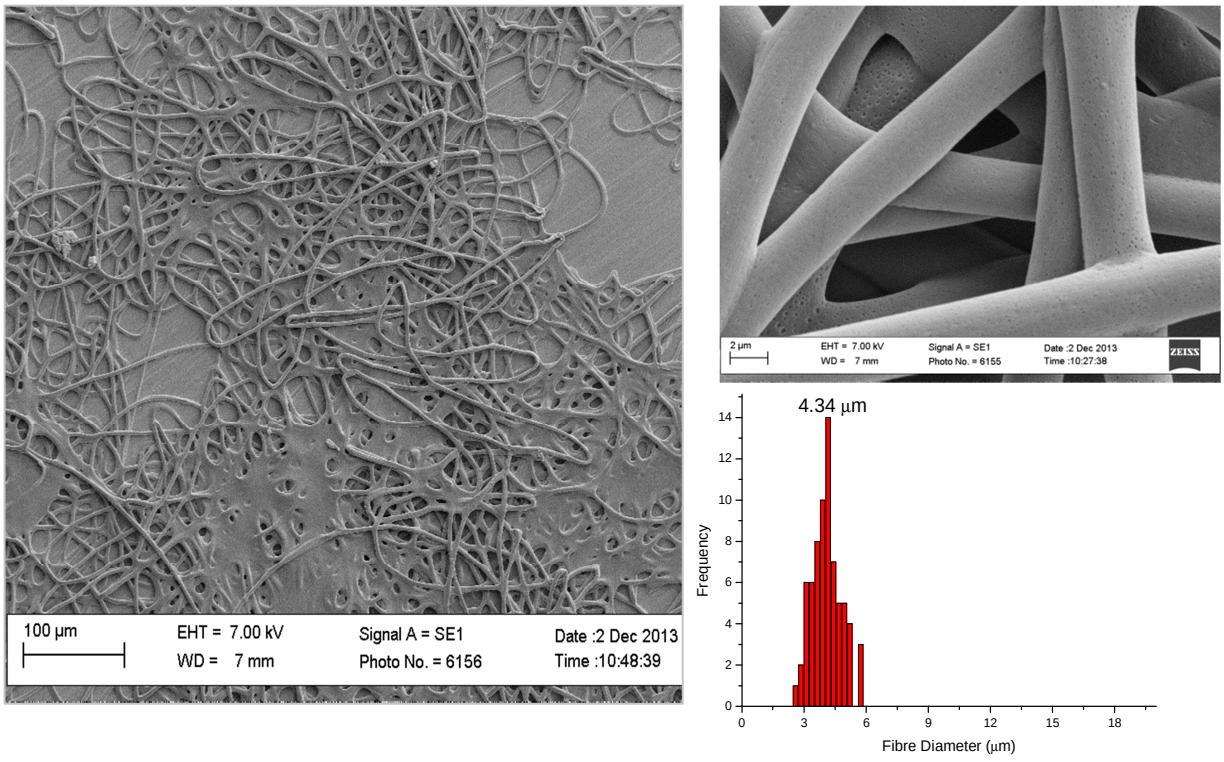

Figure 3.28: SEM images of nanofibres electrospun with 2 wt % covalent MWNT-HEBrIB-PS in 20 w/v% PS in chloroform. The fibre diameter distribution analysis gives an average of 4.34 µm.

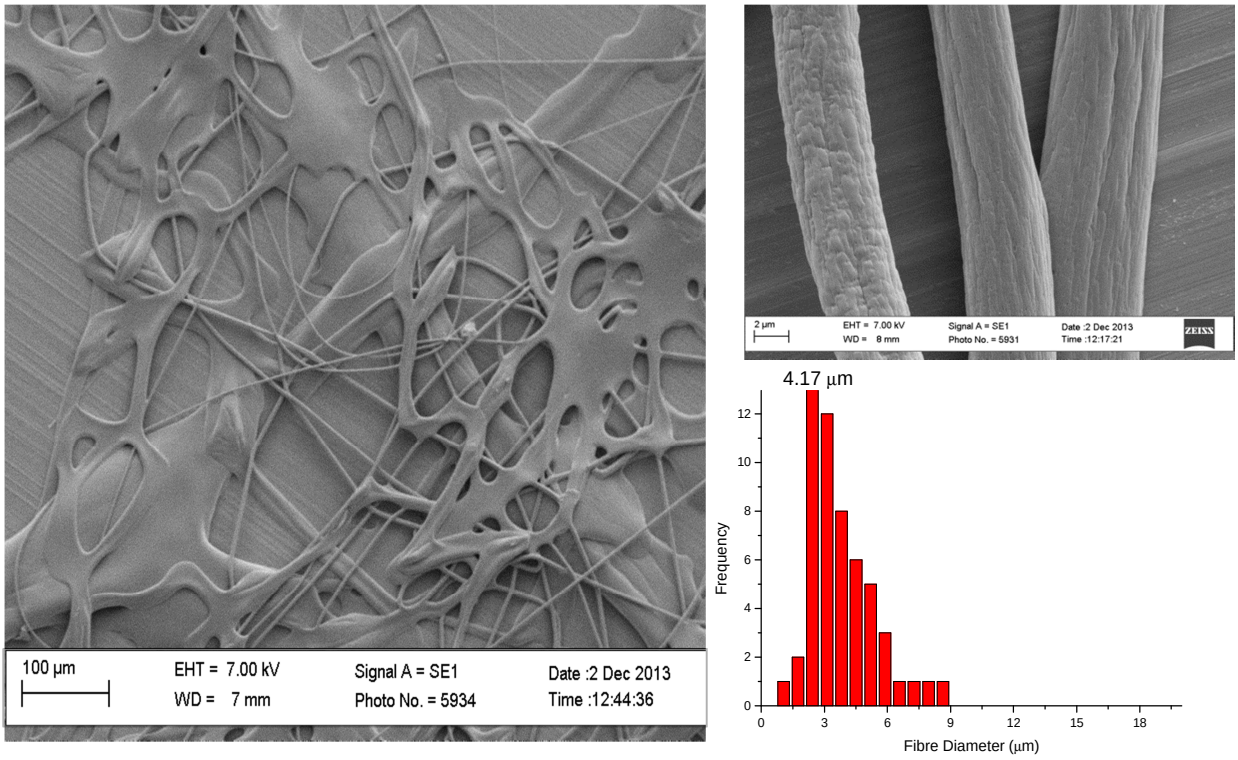

Figure 3.30: SEM images of nanofibres electrospun with 2 wt % noncovalent MWNT/PyPS (HEBrIB 5 000 g/mol) in 20 w/v% PS in chloroform. The fibre diameter distribution analysis gives an average of 4.17µm.

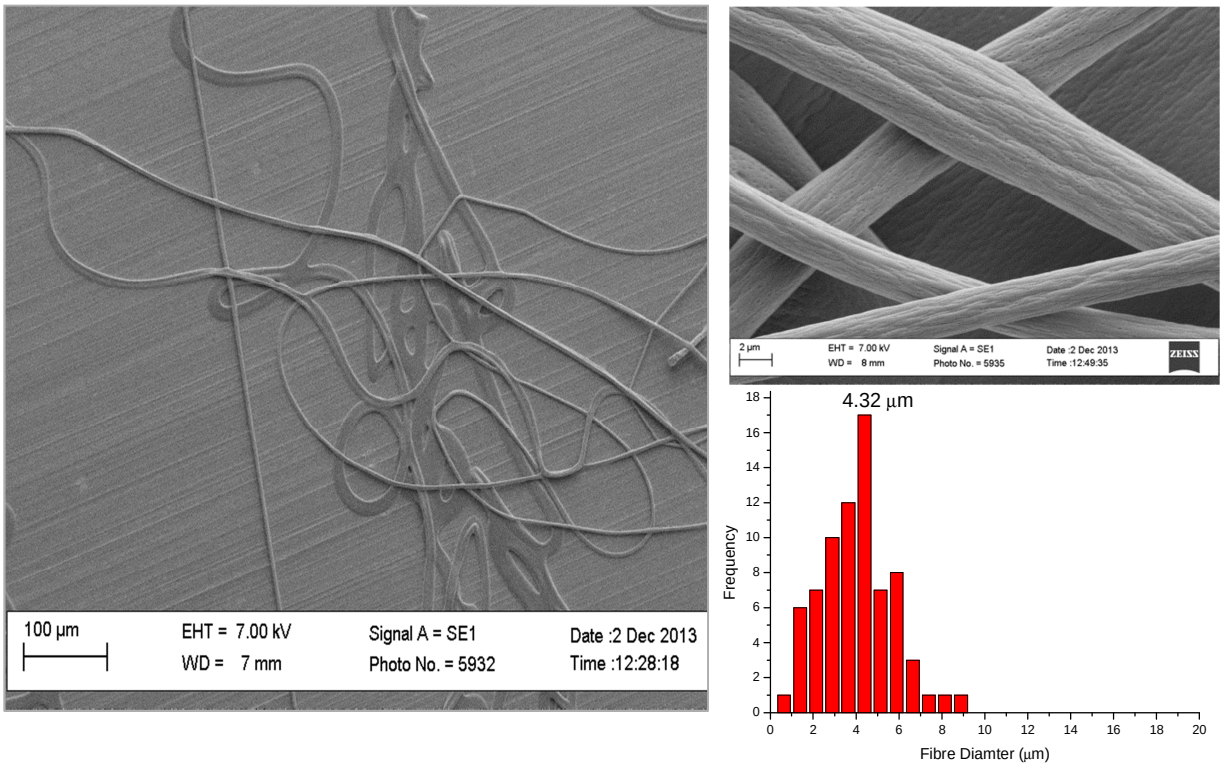

Figure 3. 30: SEM images of nanofibres electrospun with 2 wt % noncovalent MWNT/PyPS (HEBrIB 15 000 g/mol) in 20 w/v% PS in chloroform. The fibre diameter distribution analysis gives an average of 4.32µm.

Table 3.6 shows the results of the fibre diameter analysis using the SEM images. Again, the short chain noncovalent MWNT/PyPS (HEBrIB 5 000 g/mol) hybrid nanofibres produced the

smallest diameter. This is most likely a result of the increased conductivity of the electrospinning solution coupled with an increased chain entanglement which is introduced through an improved MWNT dispersion upon functionalization. Figure 3.31 depicts these results graphically. (See appendix D.2 for more fibre diameter analysis histograms)

Composite type	Lowest	Highest	Average	Standard deviation
PS homopolymer	2.05	15.75	6.95	3.42
pristine MWNTs	1.74	12.75	4.49	2.46
MWNT-HEBrIB-PS	3.59	7.05	4.34	0.88
MWNT/PyPS (HEBrIB 5 000)	1.75	11.40	4.17	1.77
MWNT/PyPS (HEBrIB 15 000)	1.39	8.89	4.32	1.58

Table 3.6: Fibre diameter analysis of various electrospun nanofibres. All values are given in µm.

It is clear from this figure that as the wt% MWNTs in the fibres increases, the fibre diameter decreases. This is attributed to the increased amount of "crosslinking points" provided by the noncovalent functionalized MWNTs which provides a larger extent of chain entanglement and a smaller diameter. An increased conductivity of the electrospinning solution, which is caused by a larger network of MWNTs in the solution also contributes to a smaller fibre diameter since this allows for the cohesive forces in the solution to be overcome. Together with a resultant increase in repulsive forces, a smaller fibre diameter is produced by the fluid jet during electrospinning. This effect is enhanced by an improved dispersibility. This is visibly recognisable in the noncovalent MWNT/PyPS hybrid composites which are well dispersed and most probably have an higher degree of chain entanglement as well as the contribution from the relatively high conductivity compared to the covalent MWNTs due to the unharmed MWNT surface as a result of noncovalent functionalization compared to direct, covalent surface functionalization which degrades the electronic properties of the MWNTs. The increase in fibre diameter for the pristine MWNT fibres at increased MWNT loadings is attributed to a poor degree of dispersion since the MWNTs form bundled aggregates which are not easily broken up and therefore do not disperse properly in the PS matrix and as such form a larger fibre diameter.

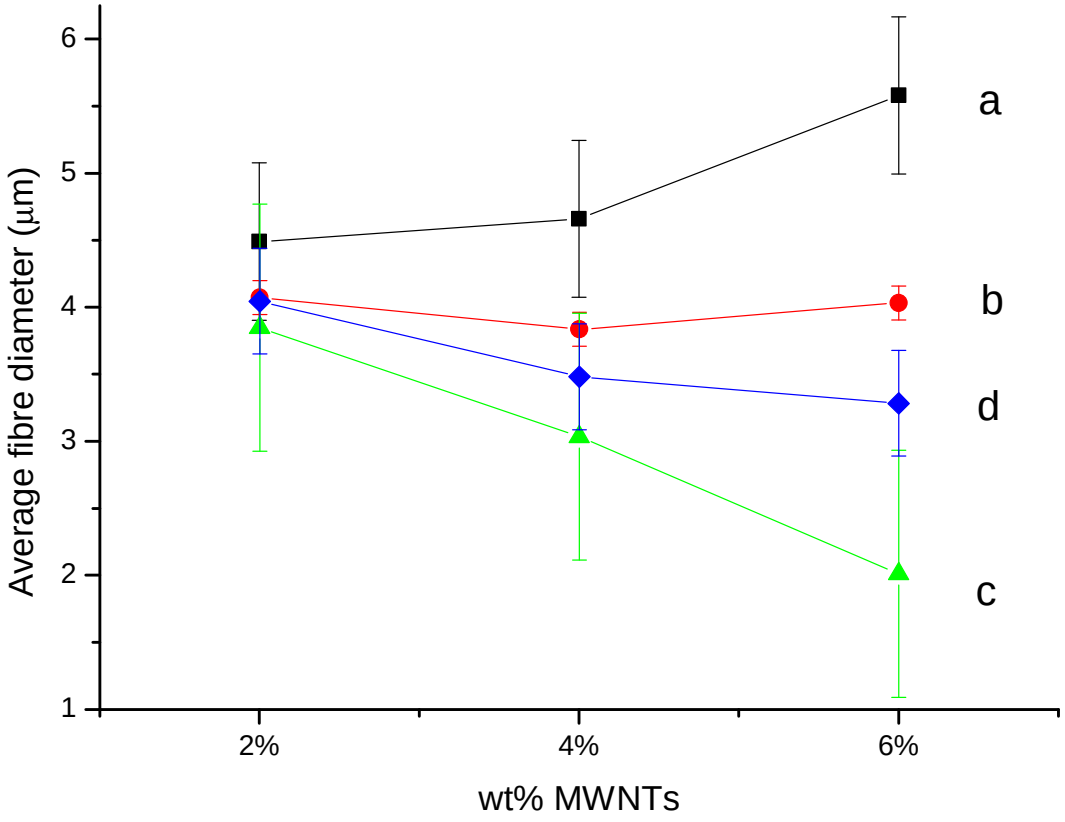

Figure 3.31: Average fibre diameter of (a) pristine MWNTs, (b) MWNT-HEBrIB-PS, (c) MWNT/PyPS (HEBrIB 5 000) and (d) MWNT/PyPS (DIBTC 15 000) containing MWNTs functionalized via HEBrIB as a function of wt% MWNT content.

3.4.17. TEM results for electrospun fibres containing MWNT functionalized via ATRP mediated PS

The fibres spun from the PS in chloroform solutions containing the various nanocomposites produced fibres of grey to black colours, indicating that the MWNTs are present in the fibres. TEM images (as indicated in figure 3.32) were obtained by embedding these fibres in resin. After curing, the resin was microtomed into extremely thin slices and analysed by TEM to give an indication of the fibre morphology. To our knowledge no reports exist of noncovalently functionalized MWNTs being electrospun in PS.[53-55] Figure 3.32 depicts a cross-section through the obtained PS fibres containing a 6 wt% of the covalent MWNT-HEBrIB-PS nanocomposite shows that the dispersion of the individual MWNTs is limited and that the MWNTs are in fact all located along the edges of the covalent MWNT-HEBrIB-PS containing fibres and are only found dispersed within the fibres themselves if the fibres have a smaller diameter, as can be seen in the top left image of figure 3.32. Therefore it

seems that the distribution of the covalently functionalized MWNTs within the PS fibres may be dependent on the fibre diameter.

In both of the noncovalent MWNT/PyPS hybrid containing fibres it was observed that although the MWNTs were well dispersed, they were all located outside the fibres themselves. It is suspected that the noncovalently functionalized MWNTs are initially located along the fibre surface since the obtained fibres show a black colour (see image 3.2) but are in fact dispersed from the surface of the nanofibres into the liquid resin during TEM sample preparation. Therefore, through the setting of this resin the MWNTs seem to disperse throughout the resin around the fibres.

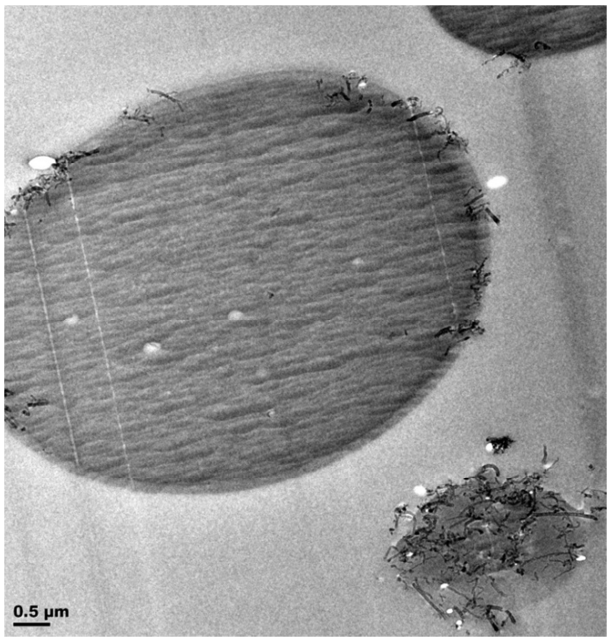

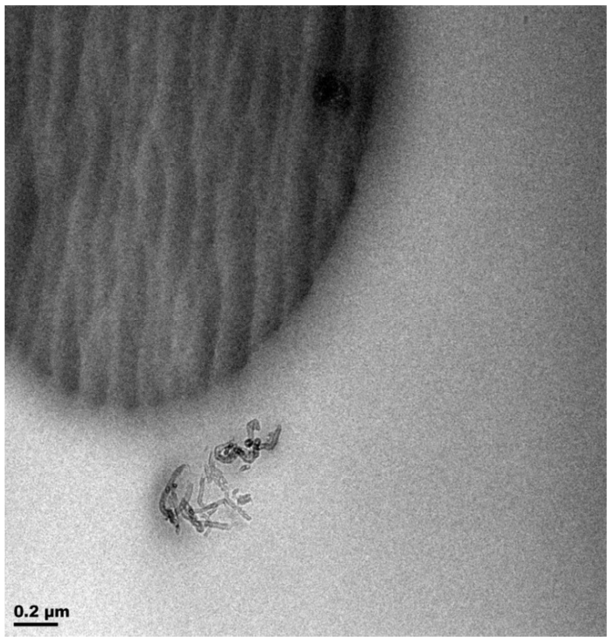

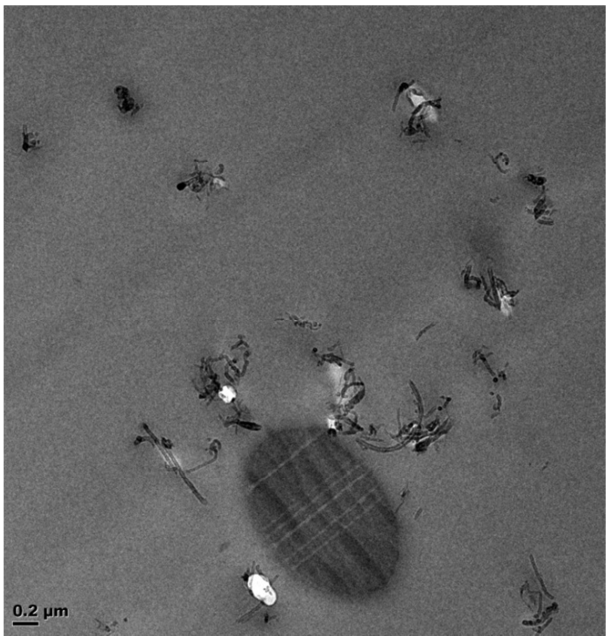

Figure 3.32: TEM images of microtomed sections of 6 wt% electrospun nanofibers containing (top left) covalent MWNT-HEBrIB-PS; (top right) noncovalent MWNT/PyPS (HEBrIB 5 000 g/mol) and (bottom left) noncovalent MWNT/PyPS (HEBrIB 15 000 g/mol) in a PS matrix.

3.5. Summary

The pyrene functional RAFT and ATRP macroinitiators were successfully used to polymerize PS via controlled living radical polymerization. The covalent and noncovalent compatibilization of the pristine MWNTs was proved to be successful according to the NMR, TGA and fluorescence spectra obtained. The imaging techniques employed showed the interaction of the MWNTs with the PS matrix with differences noted between the unfunctionalized, pristine MWNTs and the covalent as well as noncovalently functionalized MWNTs.

3.6. References

1. Petrov PD, Georgiev GL, Müller AHE. Dispersion of multi-walled carbon nanotubes with pyrene-functionalized polymeric micelles in aqueous media. Polymer. 2012;53(24):5502-6.

2. Malhotra SK, Goda K, Sreekala MS. Part one introduction to polymer composites. 2012.

3. Baati R, Ihiawakrim D, Mafouana RR, Ersen O, Dietlin C, Duportail G. Hexahistidine-Tagged Single-Walled carbon nanotubes (His6-tagSWNTs): A multifunctional hard template for hierarchical directed Self-Assembly and nanocomposite construction. Advanced Functional Materials. 2012.

4. Fischer H. Polymer nanocomposites: From fundamental research to specific applications. Materials Science and Engineering: C.2003;23(6–8):763-72.

5. Hong C, You Y, Pan C. Synthesis of water-soluble multiwalled carbon nanotubes with grafted temperature-responsive shells by surface RAFT polymerization. Chemistry of Materials. 2005;17(9):2247-54.

6. Mansky P, Liu Y, Huang E, Russell T, Hawker C. Controlling polymer-surface interactions with random copolymer brushes. Science. 1997;275(5305):1458-60.

7. Matyjaszewski K, Miller PJ, Shukla N, Immaraporn B, Gelman A, Luokala BB, et al. Polymers at interfaces: Using atom transfer radical polymerization in the controlled growth of homopolymers and block copolymers from silicon surfaces in the absence of untethered sacrificial initiator. Macromolecules. 1999;32(26):8716-24.

8. Husseman M, Malmström EE, McNamara M, Mate M, Mecerreyes D, Benoit DG, et al. Controlled synthesis of polymer brushes by “living” free radical polymerization techniques. Macromolecules. 1999;32(5):1424-31.

9. Chen Y, Haddon R, Fang S, Rao A, Eklund P, Lee W, et al. Chemical attachment of organic functional groups to single-walled carbon nanotube material. Journal of Materials Research. 1998;13(9):2423-31

10. Tasis D, Tagmatarchis N, Bianco A, Prato M. Chemistry of carbon nanotubes. Chemical Reviews. 2006;106(3):1105.

11. Hamwi A, Alvergnat H, Bonnamy S, Beguin F. Fluorination of carbon nanotubes. Carbon. 1997;35(6):723-8.

12. Sun Y, Fu K, Lin Y, Huang W. Functionalized carbon nanotubes: Properties and applications. Accounts of Chemical Research. 2002;35(12):1096-104.

13. Cui J, Wang W, You Y, Liu C, Wang P. Functionalization of multiwalled carbon nanotubes by reversible addition fragmentation chain-transfer polymerization. Polymer. 2004;45(26):8717-21.

14. Pei X, Hao J, Liu W. Preparation and characterization of carbon nanotubes-polymer/Ag hybrid nanocomposites via surface RAFT polymerization. The Journal of Physical Chemistry C. 2007;111(7):2947-52.

15. Eitan A, Jiang K, Dukes D, Andrews R, Schadler LS. Surface modification of multiwalled carbon nanotubes: Toward the tailoring of the interface in polymer composites. Chemistry of Materials. 2003;15(16):3198-201.

16. Etmimi HM, Tonge MP, Sanderson RD. Synthesis and characterization of polystyrene-graphite nanocomposites via surface RAFT-mediated miniemulsion polymerization. Journal of Polymer Science Part A: Polymer Chemistry. 2011;49(7):1621-32.

17. Baskaran D, Mays JW, Bratcher MS. Noncovalent and nonspecific molecular interactions of polymers with multiwalled carbon nanotubes. Chemistry of Materials. 2005;17(13):3389-97.

18. Hirsch A. Functionalization of single-walled carbon nanotubes. Angewandte Chemie International Edition. 2002;41(11):1853-9.

19. Atta S, Ikbal M, Boda N, Gauri SS, Singh NP. Photoremovable protecting groups as controlled-release device for sex pheromone. Photochemical & Photobiological Sciences. 2013;12(2):393-403.

20. Gangopadhyay, R, De A.Conducting polymer nanocomposites: A brief overview. Chemistry of Materials.2000;12(3):608-622.

21. Britz DA, Khlobystov AN. Noncovalent interactions of molecules with single walled carbon nanotubes. Chemical Society Reviews. 2006;35(7):637-59.

22. Yan Y, Cui J, Pötschke P, Voit B. Dispersion of pristine single-walled carbon nanotubes using pyrene-capped polystyrene and its application for preparation of polystyrene matrix composites. Carbon. 2010 8;48(9):2603-12.

23. Braunecker WA, Matyjaszewski K. Controlled/living radical polymerization: Features, developments, and perspectives. Progress in Polymer Science. 2007;32(1):93-146.

24. Pollino JM, Weck M. Non-covalent side-chain polymers: Design principles, functionalization strategies, and perspectives. Chemical Society Reviews. 2005;34(3):193-207.

25. Chong Y, Le TP, Moad G, Rizzardo E, Thang SH. A more versatile route to block copolymers and other polymers of complex architecture by living radical polymerization: The RAFT process. Macromolecules. 1999;32(6):2071-4.

26. Lai JT, Filla D, Shea R. Functional polymers from novel carboxyl-terminated trithiocarbonates as highly efficient RAFT agents. Macromolecules. 2002;35(18):6754-6.

27. Wang G, Huang S, Wang Y, Liu L, Qiu J, Li Y. Synthesis of water-soluble single-walled carbon nanotubes by RAFT polymerization. Polymer. 2007;48(3):728-33.

28. Homenick CM, Lawson G, Adronov A. Polymer Grafting of Carbon Nanotubes Using Living Free-Radical Polymerization. Polymer Reviews. 2007;47(2):265-290.

29. Barbey R, Lavanant L, Paripovic D, Schüwer N, Sugnaux C, Tugulu S, et al. Polymer brushes via surface-initiated controlled radical polymerization: Synthesis, characterization, properties, and applications. Chemical Reviews. 2009;109(11):5437-527.

30. Lu HF, Fei B, Xin JH, Wang RH, Li L, Guan WC. Synthesis and lubricating performance of a carbon nanotube seeded miniemulsion. Carbon. 2007;45(5):936-42.

31. Coessens V, Pintauer T, Matyjaszewski K. Functional polymers by atom transfer radical polymerization. Progress in polymer science. 2001;26(3):337-77.

32. Matyjaszewski K, Xia J. Atom transfer radical polymerization. Chemical Reviews. 2001;101(9):2921-90.

33. Beers KL, Gaynor SG, Matyjaszewski K, Sheiko SS, Möller M. The synthesis of densely grafted copolymers by atom transfer radical polymerization. Macromolecules. 1998;31:9413-5.

34. Qin S, Qin D, Ford WT, Resasco DE, Herrera JE. Functionalization of single-walled carbon nanotubes with polystyrene via grafting to and grafting from methods. Macromolecules. 2004;37(3):752-7.

35. Kong H, Gao C, Yan D. Controlled functionalization of multiwalled carbon nanotubes by in situ atom transfer radical polymerization. Journal of the American Chemical Society. 2004;126(2):412-3.

36. Xu G, Wu W, Wang Y, Pang W, Zhu Q, Wang P, et al. Constructing polymer brushes on multiwalled carbon nanotubes by in situ reversible addition fragmentation chain transfer polymerization. Polymer. 2006;47(16):5909-18.

37. Hummers Jr WS, Offeman RE. Preparation of graphitic oxide. Journal of the American Chemical Society. 1958;80(6):1339-1339.

38. Donkers EHD. Block copolymers with polar and non-polar blocks. Doctoral dissertation, PhD thesis, Technical University Eindhoven, The Netherlands. 2006

39. Datsyuk V, Kalyva M, Papagelis K, Parthenios J, Tasis D, Siokou A, et al. Chemical oxidation of multiwalled carbon nanotubes. Carbon. 2008;46(6):833-40.

40. Skrabania K, Miasnikova A, Bivigou-Koumba AM, Zehm D, Laschewsky A. Examining the UV-vis absorption of RAFT chain transfer agents and their use for polymer analysis. Polymer Chemistry. 2011;2(9):2074-83.

41. Bourlinos AB, Gournis D, Petridis D, Szabó T, Szeri A, Dékány I. Graphite oxide: Chemical reduction to graphite and surface modification with primary aliphatic amines and amino acids. Langmuir. 2003;19(15):6050-5.

42. Ham HT, Choi YS, Jeong N, Chung IJ. Single wall carbon nanotubes covered with polypyrrole nanoparticles by the miniemulsion polymerization. Polymer. 2005;46(17):6308-15.

43. Morrison RT, Boyd RN. Organic chemistry. Allyn and Bacon, Boston. 1973;631(666):668-9.

44. Lu Q, Keskar G, Ciocan R, Rao R, Mathur RB, Rao AM, et al. Determination of carbon nanotube density by gradient sedimentation. The Journal of Physical Chemistry B. 2006;110(48):24371-6.

45. Zou J, Liu L, Chen H, Khondaker SI, McCullough RD, Huo Q, et al. Dispersion of pristine carbon nanotubes using conjugated block copolymers. Advanced Materials. 2008;20(11):2055-60.

46. Nakashima N, Tomonari Y, Murakami H. Water-soluble single-walled carbon nanotubes via noncovalent sidewall-functionalization with a pyrene-carrying ammonium ion. Chemistry Letters. 2002;31(6):638-9.

47. Chen J, Liu H, Weimer WA, Halls MD, Waldeck DH, Walker GC. Noncovalent engineering of carbon nanotube surfaces by rigid, functional conjugated polymers. Journal of the American Chemical Society. 2002;124(31):9034-5.

48. Ehli C, Rahman GA, Jux N, Balbinot D, Guldi DM, Paolucci F, et al. Interactions in single wall carbon nanotubes/pyrene/porphyrin nanohybrids. Journal of the American Chemical Society. 2006;128(34):11222-31.

49. Haddon R. Magnetism of the carbon allotropes. 1995. 249-255

50. Kim KK, Yoon S, Choi J, Lee J, Kim B, Kim JM, et al. Design of dispersants for the dispersion of carbon nanotubes in an organic solvent. Advanced Functional Materials. 2007;17(11):1775-83.

51. Assali M, Leal MP, Fernández I, Baati R, Mioskowski C, Khiar N. Non-covalent functionalization of carbon nanotubes with glycolipids: Glyconanomaterials with specific lectin-affinity. Soft Matter. 2009;5(5):948-50.

52. Guldi DM, Rahman GA, Jux N, Balbinot D, Hartnagel U, Tagmatarchis N, et al. Functional single-wall carbon nanotube nanohybrids associating SWNTs with water-soluble enzyme model systems. Journal of the American Chemical Society. 2005;127(27):9830-8.

53. Mazinani S, Ajji A, Dubois C. Morphology, structure and properties of conductive PS/CNT nanocomposite electrospun mat. Polymer. 2009;50(14):3329-42.

54. Ra EJ, An KH, Kim KK, Jeong SY, Lee YH. Anisotropic electrical conductivity of MWCNT/PAN nanofibre paper. Chemical Physics Letters. 2005;413(1):188-93.

55. Spitalsky Z, Tasis D, Papagelis K, Galiotis C. Carbon nanotube–polymer composites: Chemistry, processing, mechanical and electrical properties. Progress in Polymer Science. 2010;35(3):357-401.

56. Baker SC, Atkin N, Gunning PA, Granville N, Wilson K, Wilson D, Southgate J. Characterisation of electrospun polystyrene scaffolds for three-dimensional in vitro biological studies. Biomaterials. 2006;27(16):3136-3146.

Chapter 4: Conclusion and Future Outlook

4.1 Conclusion

The degree of functionalization of the esterification of the RAFT and ATRP agents with their respective pyrenes was calculated to be 51.5% for DIBTC-Py and 67.0% for HEBrIB-Py using ^{13}C and ^{1}H NMR. Therefore, the degree of functionalization for the ATRP macroinitiator synthesis was better, making this a more desirable macroinitiator for use in this study. Upon polymerization, the proof that the PS chains were indeed functionalized with pyrene moieties was introduced by the UV/Vis responses which clearly showed that the pyrene groups, which absorb UV light between wavelengths of 310-350 nm, had been transferred from the macroinitiators to the PS chains in all cases. Two chain lengths were targeted for each macroinitiator. The shorter chain created using the RAFT and the ATRP approaches produced SEC results showed a $\overline{M_n}$ of 1.86×10^3 g/mol and 1.29×10^4 g/mol and a Đ of 1.14 and 1.19 for DIBTC-Py-PS and HEBrIB-Py-PS respectively. Although there is no large difference in the polydispersity, a much higher average molecular weight was obtained in the ATRP mediated polymerization of styrene than in the RAFT version. DIBTC-Py-PS and HEBrIB-Py-PS of longer PS chain lengths showed an average molecular weight of 6.46×10^3 g/mol and 3.25×10^4 g/mol and a dispersity of 1.24 and 1.29 respectively. This larger actual molecular weight for the ATRP versions in both targeted chain lengths compared to the RAFT versions is hypothesized to be as a result of the higher efficiency of polymerization of styrene that this specific ATRP initiator introduces compared to the DIBTC RAFT agent. The Đ difference was slightly broader for the ATRP versions, but not significantly so. The ATRP mediated polymerization of styrene is more efficient in creating the pyrene-end terminated controlled PS chains of both chain lengths since it showed a higher degree of functionalization during the macroinitiator synthesis as well as a higher obtained molecular weight of PS than the RAFT mediated polymerization indicated. ATRP also produces a negligible amount of PS homopolymer compared to RAFT polymerization.

The success of the noncovalent interactions between the synthesised pyrene-functional chains and the pristine MWNTs is deduced from the NMR results of the noncovalent MWNT/PyPS hybrids which show a broadening and a weakening in pyrene and PS proton signals, which is an indication of adsorption of the pyrene-functionalized PS chains onto the MWNTs leading to shielding from the MWNT surface protons and thus a diminished NMR response for the pyrene-functionalized PS chains. This effect was noticeable in the obtained NMR data. TGA data, in which the overall degree of functionalization of the MWNTs can be determined as a

function of weight loss over the temperature range, indicates the success of the functionalization. The noncovalent interaction of DIBTC-Py-PS with the MWNTs shows a larger weight loss than its ATRP counterpart. Therefore, this reaction seems to have been the most effective in noncovalently functionalizing the MWNTs through π-π stacking of the pyrene-capped PS with the MWNT surface. The noncovalent immobilization of the HEBrIB-Py-PS onto the MWNT surface only showed a weight loss of 10.07% indicating a very low degree of macroinitiator formation due to a low density of π-π stacking along the nanotubes. The surface of the MWNTs has remained intact which can be seen by the UV/Vis/NIR spectra in which the functionalized MWNT/PyPS hybrids show the same pattern of response as the pristine MWNTs do. The fluorescence data indicates a defined quenching of the emission decay and excitation signals which arise due to the transfer of energy between the MWNTs and the pyrene-functionalized PS chains which are in close enough proximity for electron transfer to occur between them due to the π-π stacking interactions. Therefore it is clear that the pristine MWNTs have indeed been noncovalently functionalized.

The effect of the different PS chain lengths on the noncovalent functionalization of the MWNTs was not significantly different. The polydispersity was somewhat broader for the longer chain HEBrIB-PS-PS than for the shorter version, although this is to be expected when synthesising a polymer of high molecular weight. The UV/Vis analyses showed no large difference between the two chain lengths, except in intensity which can be ascribed to a difference in quantity of pyrenes per amount of PS formed. This is also realised in the fluorescence spectra. The intensity of π-π stacking interactions is affected by the steric accessibility of the π-system to the CNT surface as well as the electronic structure of the π-system involved.[2] As a result it is expected that the longer chain length PyPS complexes will not adsorb noncovalently to the MWNT surfaces as efficiently as the shorter chain complexes do due to steric hindrance. The longer chain MWNT/PyPS has much lower intensities than the lower chain length version in both the excitation and emission spectra. This is due to fewer pyrene molecules which have been able to interact with the MWNT surface as a consequence of the longer PS chains introducing steric hindrance which in turn means that the degree of quenching observed upon excitation in the MWNT/PyPS will be lowered. Similar results are acquired for the two chain lengths of DIBTC-Py-PS and the resultant MWNT/PyPS hybrids. The UV/Vis spectra again only differed in the intensity of the detector response where the lower chain length compound had a higher intensity than the longer chain length version did. The TGA data indicated that less DIBTC-Py-PS of the longer chain length was lost in the corresponding hybrid MWNT/PyPS compared to the shorter version, which

seems to indicate that the extent of pyrene interaction was influenced by steric hindrance of the longer PS chains. Similar fluorescence results to those obtained for the ATRP compounds are observed for the RAFT versions. The intensity of the emission and excitation spectra is lower for the longer chain length versions. From the TGA results, the calculated pyrene molecules attached per MWNTs reconfirm this. According to the obtained values, the short chain PyPS indicated higher values of PyPS per MWNT than the longer chain PyPS did. Thus confirming that in this study, steric hindrance introduced by longer styrene chains influenced the efficacy of non-covalent pyrene-MWNT π-π stacking in a marginally detrimental manner. However, these TGA results also indicate that the DIBTC version of the MWNT/PyPS contained a larger amount of adsorbed PyPS per MWNT than the ATRP hybrids. Therefore, although the macroinitiator synthesis and subsequent polymerization of styrene was more effectively performed by the ATRP approach, it was found in this study that the adsorption of the pyrene-functional PS onto the pristine MWNTs showed to be more favourable in the DIBTC approach than the ATRP method. This is, however, most probably only due to the slightly longer PS chains of the ATRP hybrids which introduced more steric hindrance than the respective RAFT versions did.

In general the HEBrIB-Py-PS and DIBTC-Py-PS compounds behaved similarly with regard to the characteristic UV signals of the pyrene moiety being present, the degree of polymerization which affected various detector intensities as well as their capability to form the noncovalent MWNT/PyPS hybrid nanocomposites through π-π stacking of the pyrene-terminated PS chains. The largest differences between the two approaches, however, were seen in higher degree of functionalization determined from the NMR spectra of the ATRP macroinitiator compared to the RAFT version. This showed that the esterification of HEBrIB with pyrenebutanoic acid was a more successful approach in this case than the RAFT. Therefore, although it is a more technically challenging process due to the stringent reaction conditions, the ATRP approach is in this regard, a more effective one.

The covalent functionalization of the MWNTs was done as a means of comparison. The FT-IR spectrum of MWNT-DIBTC showed the successful attachment of the RAFT agent[1] onto the nanotubes since the DIBTC compound contains bonds of characteristic stretching vibrations that the MWNTs do not possess. This was not possible in the immobilization of HEBrIB which does not consist of significantly different bonds to those found along the oxidized MWNT surface. As such FT-IR was an effective means of qualitative analysis for

the covalent immobilization of the RAFT agent but not of the ATRP initiator. Therefore, TGA was essential to determining the HEBrIB immobilization onto the MWNTs. The TGA data indicated that 7.5% of the MWNT-HEBrIB product weight had decomposed, indicating the weight represented by the surface-immobilized HEBrIB. This value was substantially less than that of the immobilization of the DIBTC onto the MWNTs which showed a 45.21% weight loss in the macroinitiator. Therefore, it is evident that in this study, the immobilization of DIBTC was more efficient than the HEBrIB immobilization. In the case of DIBTC a miniemulsion polymerization system was used to graft the PS chains directly onto the MWNT surface using the multifunctional MWNT macroinitiator. The ATRP grafting was done in solution. The results show that the RAFT miniemulsion process was more efficient in grafting the chains directly to the MWNT surface. This is due to a higher degree of functionalization with the RAFT and the consequently greater number of initiation sites. This was shown by TGA after the grafted MWNTs were purified of the free PS by filtration and the subsequent isolation of the MWNTs through centrifugation and redispersion of the nanotube deposit in THF in a series of recovery steps.

Since there are much fewer active sites in the ATRP immobilized MWNTs than in the RAFT version, the amount of PS present in the respective products is expected to be much less for the ATRP version than for the RAFT. The TGA data confirms this since the % weight loss at 600°C for the MWNT-DIBTC-PS and for MWNT-HEBrIB-PS is 94.75 % and 29.23% respectively which represents the loss of the DIBTC-PS and HEBrIB-PS. Although the % yield of MWNT-HEBrIB was higher 96.5% whereas the % yield of MWNT-DIBTC was 54.0%, it can be concluded that the efficiency of the covalent surface-initiated grafting of PS was more effective via the RAFT route than the ATRP route in this instance as a result of the degree of immobilization of the respective initiators.
As a result it was found that where the covalent functionalization is concerned, the RAFT approach was a more favourable one in that a larger amount of DIBTC was immobilized along the MWNT surface leading to a higher PS grafting density in the covalent MWNT-DIBTC-PS than in the MWNT-HEBrIB-PS.

The composites were dispersed in a 20 w/v% PS in chloroform solution and analysed for the degree of dispersion which the MWNTs exhibited as a function of MWNT functionalization. It was noted during the preparation procedure that the solution stability of the functionalized

MWNTs was improved relatively to the pristine MWNTs which were seen to settle at the bottom of the test tube after a few days. This was translated into the TEM images. These showed that upon functionalization of the MWNTs (covalently and noncovalently) that the MWNTs were more dispersed in the PS matrix and did not appear as clustered or bundled aggregates as the pristine MWNTs did in the PS.

Upon electrospinning the solutions of the covalent and noncovalent composites it was found that the produced fibres ranged in colour depending on their composition. The PS homopolymer fibres which were free from MWNTs were a white colour whereas incorporation of pristine MWNTs changed the colour to grey. The functionalized MWNTs all showed a much darker grey or black colour of the fibres therefore suggesting the successful inclusion of MWNTs into the fibres as a result of the increased dispersion of the MWNTs within the PS matrix due to their compatibilization with the PS.

The fibre diameter distributions were analysed by analysis of the obtained SEM images. The obtained fibre diameters were in the micrometre range. This is expected to be as a result of the higher viscosity of the 20 w/v% electrospinning PS solution used in this study since the molecular weight of the PS chains was larger. The high viscosity leads to a decreased elongation of the fluid jet during electrospinning leading to relatively large fibre diameters.[4-6]

The average fibre diameters for the MWNTs functionalized by HEBrIB were found to be larger than those for the DIBTC functionalized MWNTs. Referring back to the results obtained from TGA for these composites, the calculated amounts of PyPS molecules adsorbed onto each MWNT surface was determined to be higher for the DIBTC composites than for the HEBrIB composites in both the covalent and noncovalent forms as well as for the short and long chained versions. This is most likely due to the longer PS chains presented by the ATRP composites which introduce steric bulk and hinder the effective adsorbance of the PyPS onto the MWNT surface. This leads to the conclusion that a higher amount of PyPS adsorption per MWNT leads to a greater degree of dispersion of the individual MWNTs in the DIBTC composites which results in a higher conductivity and chain entanglement in the electrospinning solutions which in turn produced electrospun fibres of a smaller diameter than its HEBrIB counterparts.

The TEM images of the microtomed nanofibres set in resin, however, showed that the noncovalently functionalized MWNTs migrated to the outside the PS fibres during electrospinning and were seen to be dispersed within the vicinity around the fibres as a result of the TEM sample preparation. The noncovalent functionalized MWNTs also tend to agglomerate on the surface of the fibres. The reason for this is not clear and requires further

investigation. Despite this observation, it is clear that the type of compatibilization (covalent and noncovalent) as well as the grafted chain lengths have a dramatic effect on the electrospun fibre morphology.

The noncovalent functionalization of MWNTs, and the electrospinning of such nanocomposite solutions, holds great potential for the synthesis of polymer-carbon nanotube nanofibres of superior properties which are maintained through an undamaged carbon nanotube electronic structure.

4.2 Future Outlook

The incorporation of noncovalently functionalized MWNTs into a PS matrix and the subsequent electrospinning of a solution thereof can be extended to other polymeric systems, particularly to those polymers which are commonly electrospun with covalently functionalized MWNTs. An interesting observation from this study was that despite the successful compatibilization of the MWNTs, these tended to localize on the surface of the nanofibres during the electrospinning process. The reason behind why the MWNTs are located on the surface of the polymer nanofibres instead of being embedded within the fibres is not clear and as such would be an area of potential study and research. Furthermore, such nanocomposites can be tested for their electrical properties as well as their mechanical and thermal capabilities.

4.3 References

1. Etmimi HM, Tonge MP, Sanderson RD. Synthesis and characterization of polystyrene-graphite nanocomposites via surface RAFT-mediated miniemulsion polymerization. Journal of Polymer Science Part A: Polymer Chemistry. 2011;49(7):1621-32.

2. Britz DA, Khlobystov AN. Noncovalent interactions of molecules with single walled carbon nanotubes. Chemical Society Reviews. 2006;35(7):637-59.

3. Mazinani S, Ajji A, Dubois C. Morphology, structure and properties of conductive PS/CNT nanocomposite electrospun mat. Polymer. 2009;50(14):3329-42.

4. McKee MG, Wilkes GL, Colby RH, Long TE. Correlations of solution rheology with electrospun fibre formation of linear and branched polyesters. Macromolecules. 2004;37(5):1760-7.

5. Das S, Wajid AS, Bhattacharia SK, Wilting MD, Rivero IV, Green MJ. Electrospinning of polymer nanofibres loaded with noncovalently functionalized graphene. Journal of Applied Polymer Science. 2012.

6. Ki CS, Baek DH, Gang KD, Lee KH, Um IC, Park YH. Characterization of gelatin nanofibre prepared from gelatin–formic acid solution. Polymer. 2005;46(14):5094-102.

Appendix A: FT-IR spectra for covalent functionalization of MWNTs

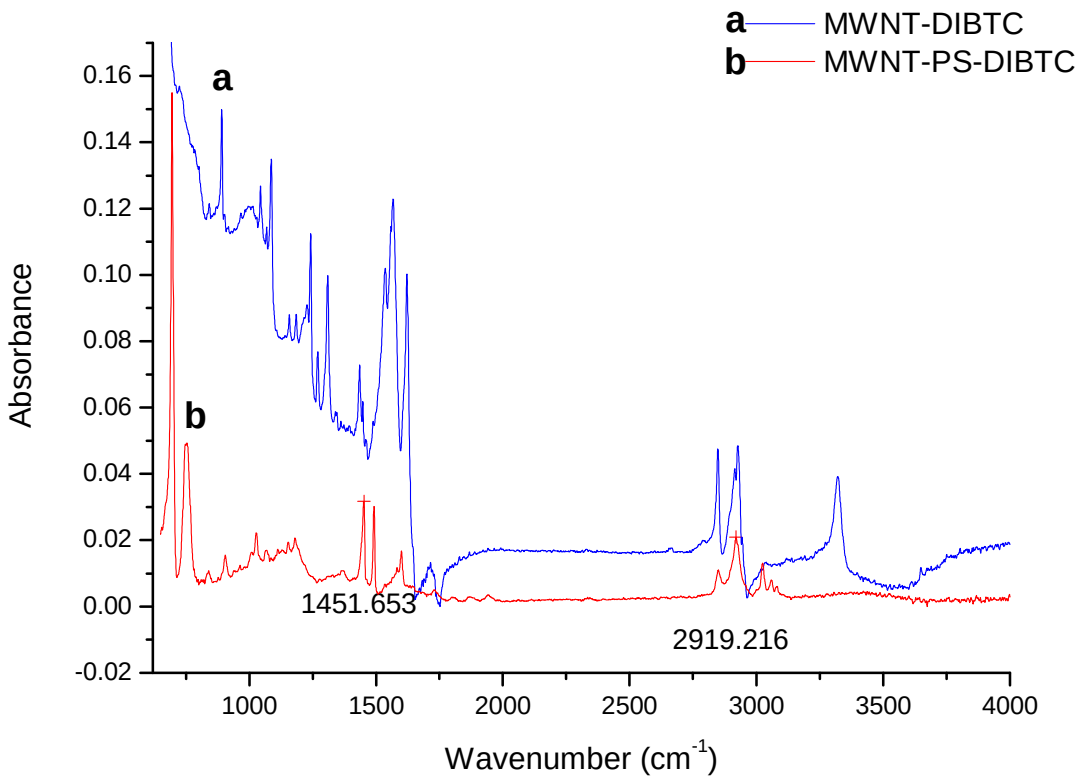

Figure A.1: FT-IR spectra of (a) MWNT-DIBTC and (b) MWNT-PS-DIBTC

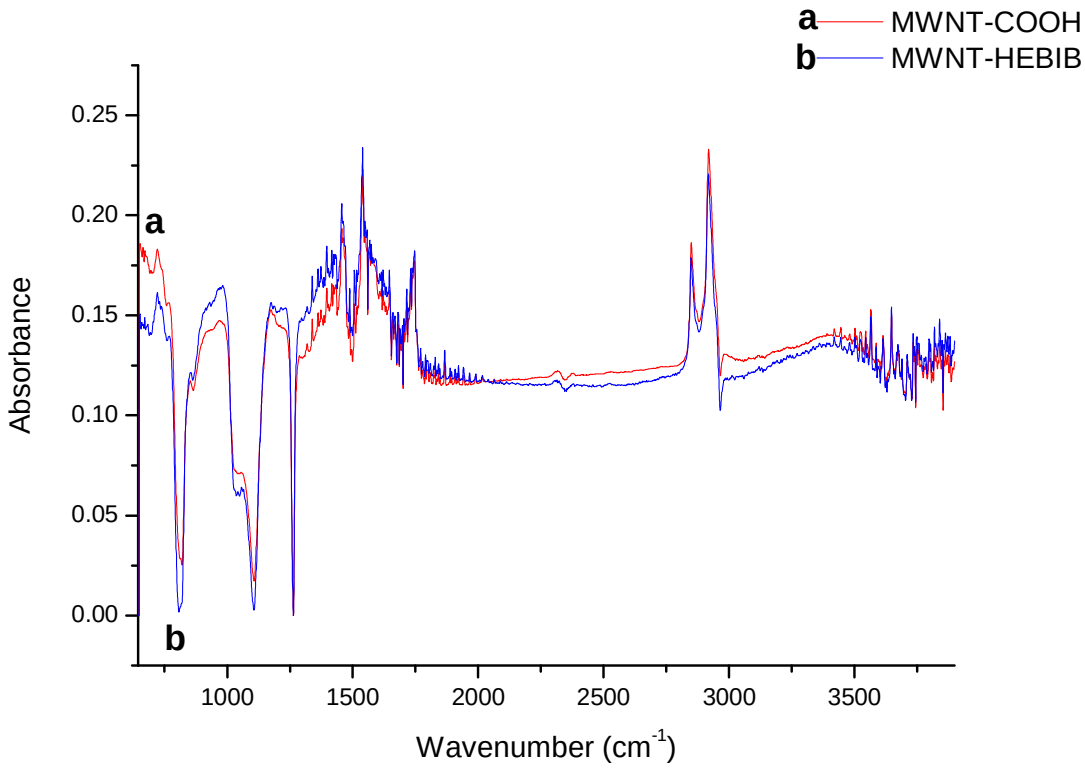

Figure A.2: FT-IR spectra of (a) oxidized MWNTs, and (b) HEBrIB-MWNTs

Appendix B: NMR spectra

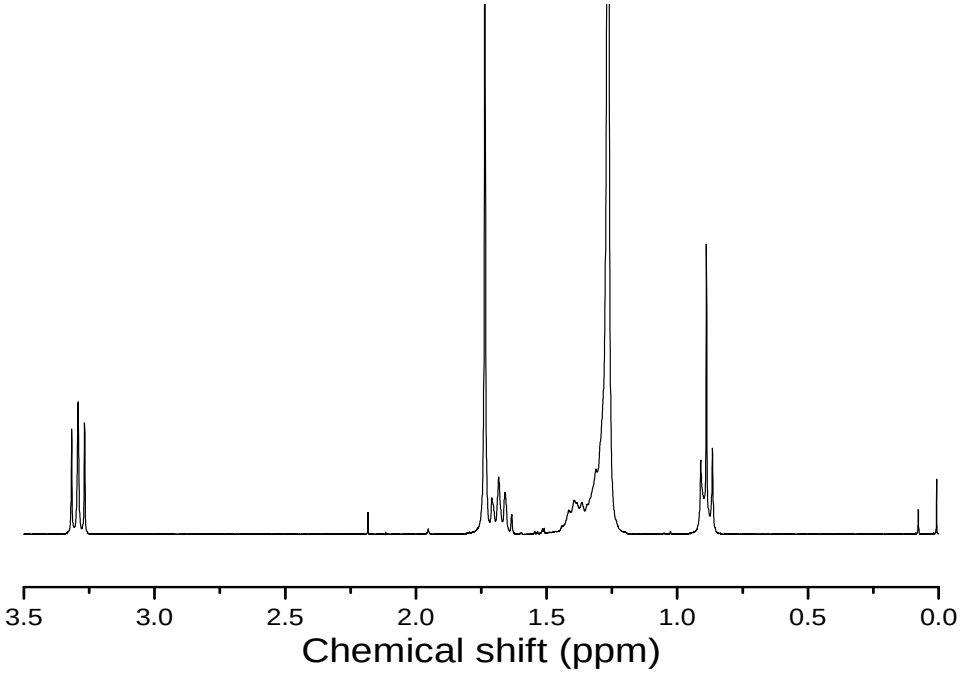

Figure B.1: ^{1}H NMR spectrum of DIBTC in $CDCl_3$

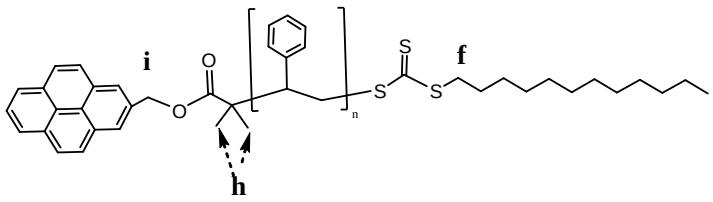

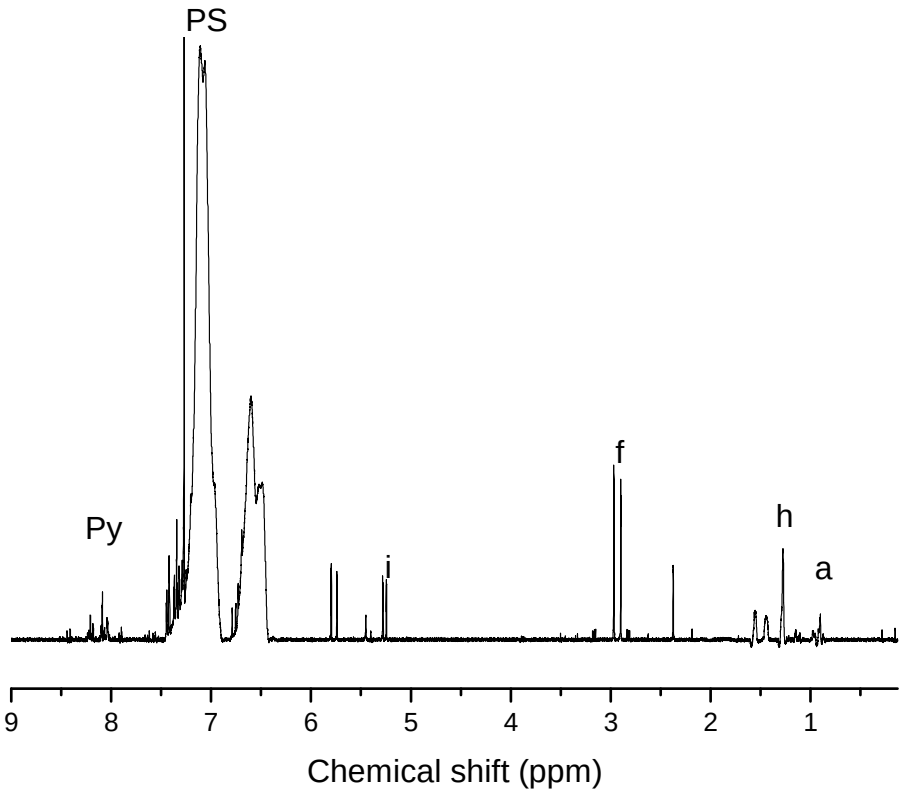

Figure B.2: ^{1}H NMR spectrum of DIBTC-PS-Py of15 000 g/mol targeted PS chain length in $CDCl_3$

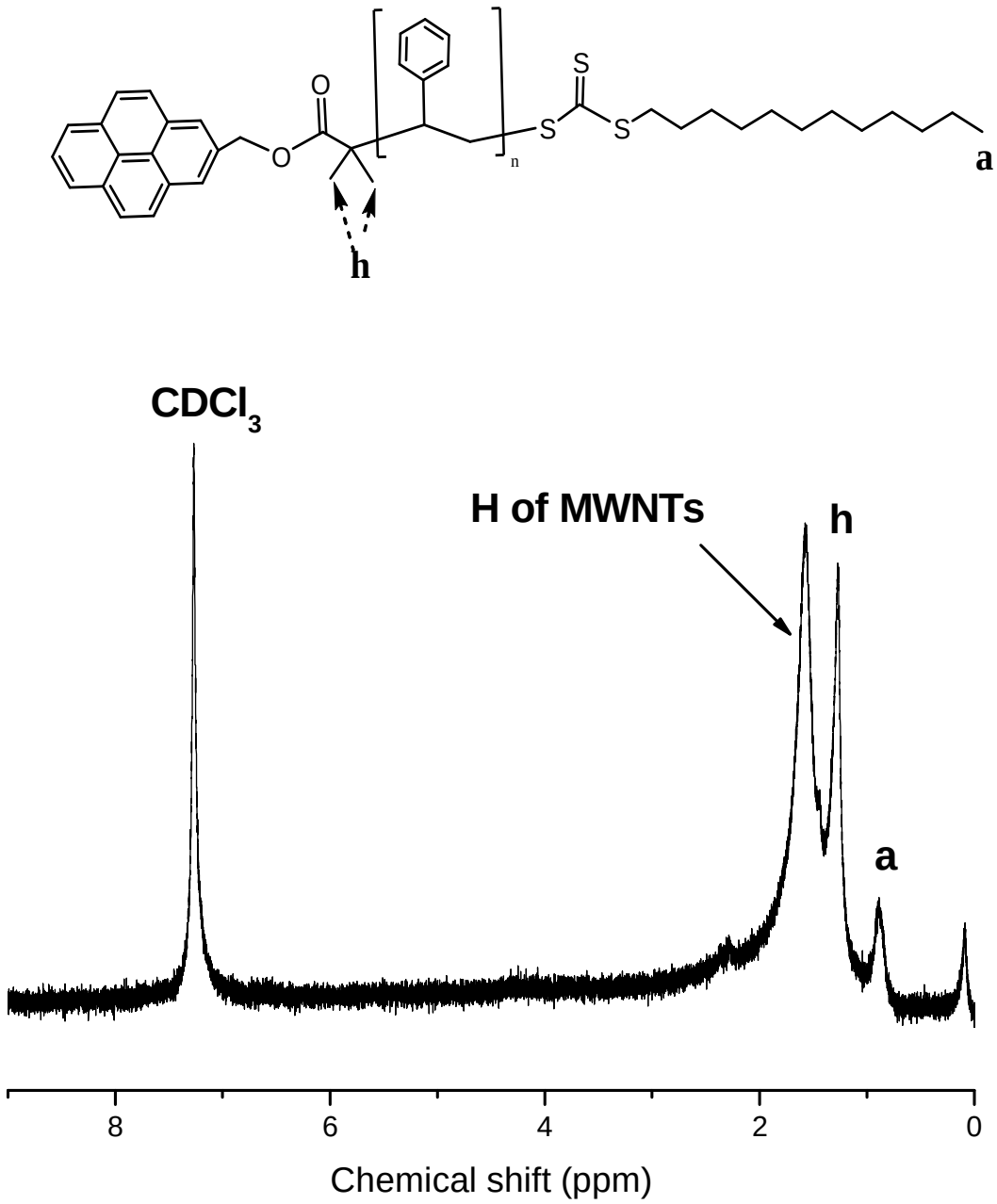

Figure B.3: ^{1}H NMR spectrum of MWNT/PyPS (DIBTC 15 000 g/mol) in $CDCl_3$

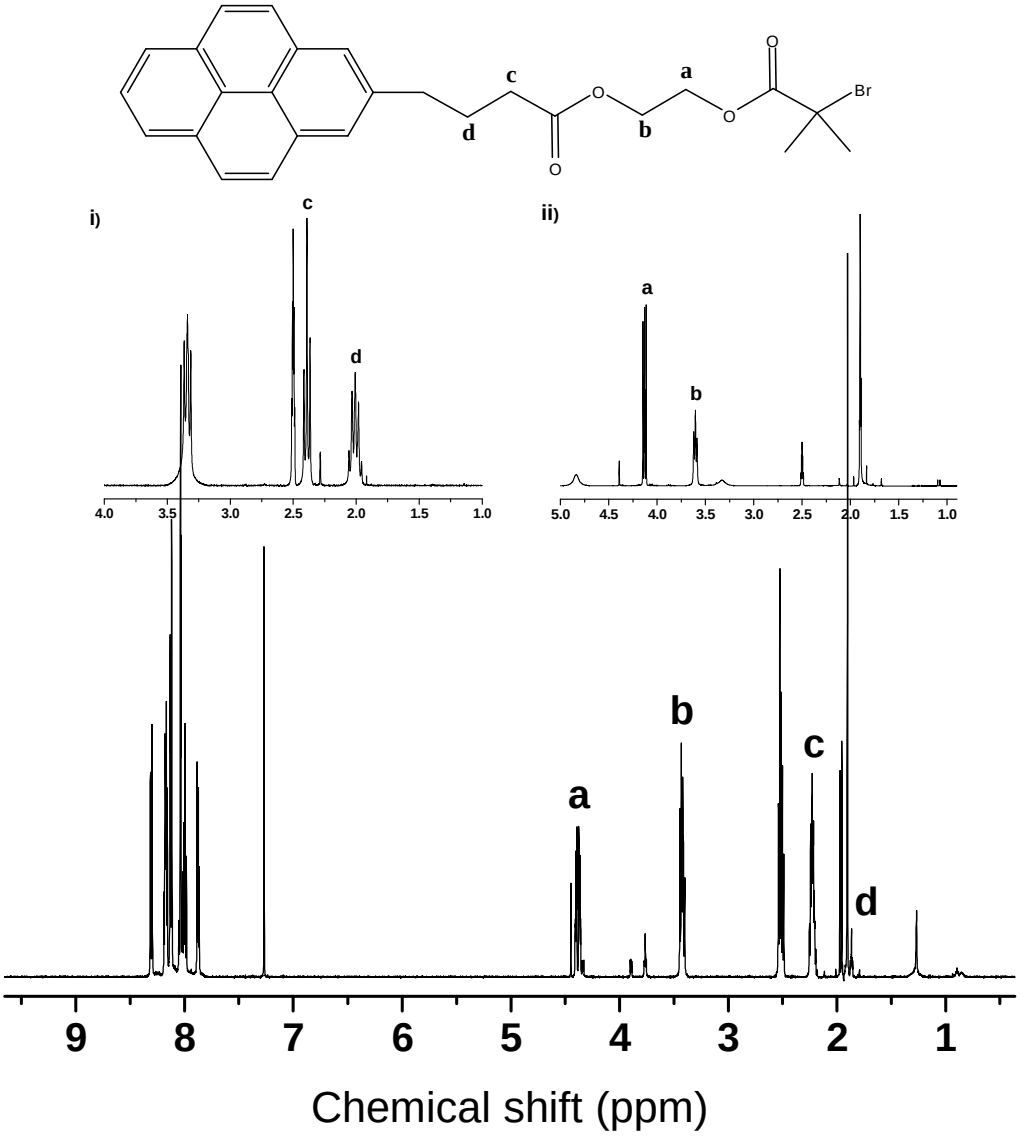

Figure B.4: ^{1}H NMR spectrum for HEBrIB-Py where the peak "a" corresponds to the two protons shown in the skeletal structure and shift from 4.13 ppm in (i) the ^{1}H NMR spectrum of pyrenebutyric acid to 4.39 ppm. Peaks "b" and "c" represent the protons most affected by the esterification and shift from 3.60 ppm in (i) to 3.43 ppm and from 2.39 ppm in (ii) the ^{1}H NMR spectrum of HEBrIB to 2.23 ppm. Peak "d" is also seen to shift from 2.01 ppm in (i) to 1.87 ppm as a result of the esterification.

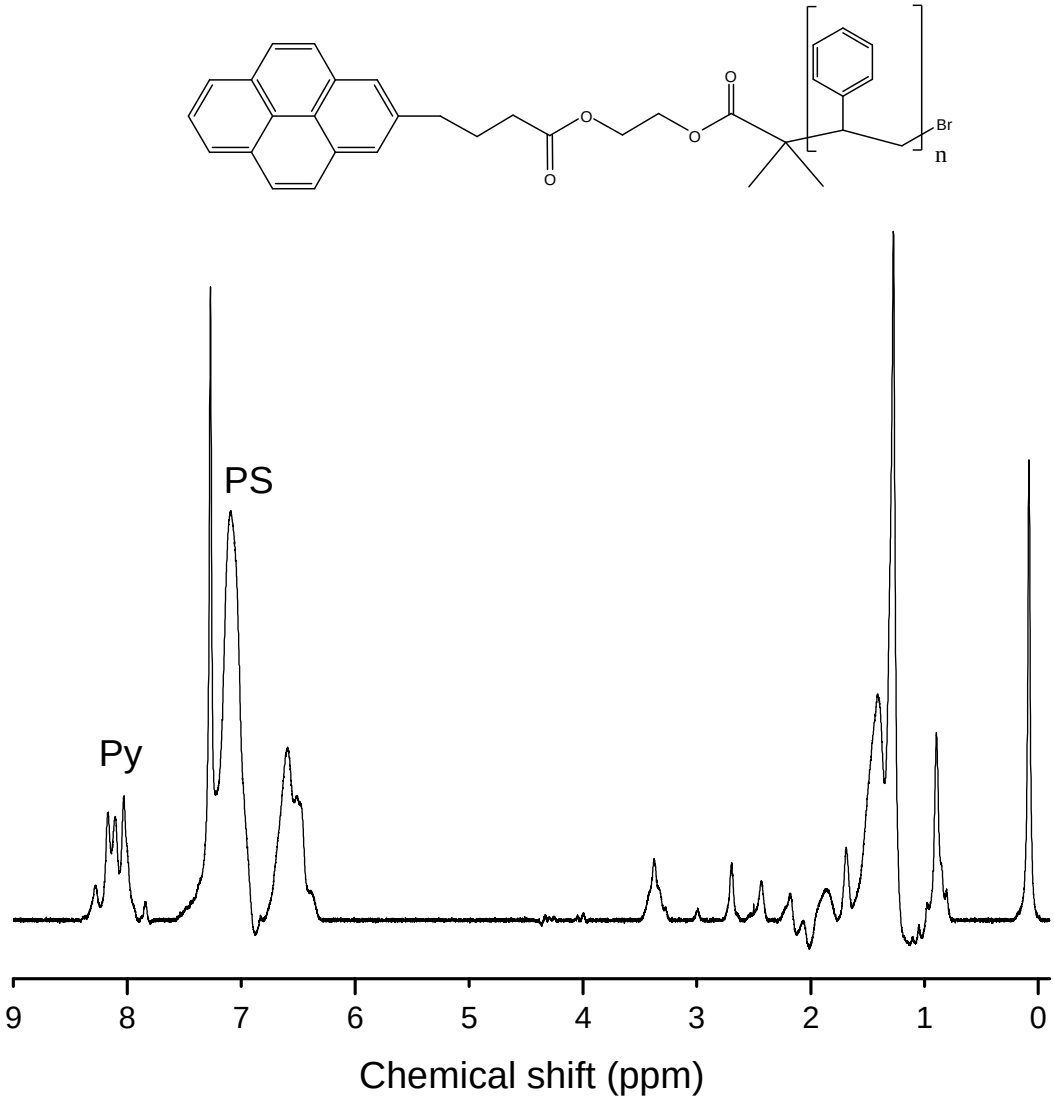

Figure B.5: ^{1}**H NMR spectrum of HEBrIB-Py-PS of 5 000 g/mol chain length**

Appendix C: Calculations for the quantitative attachment of PyPS onto MWNTs

For MWNT/PyPS prepared via DIBTC with a Mw of 1 858 g/mol (figure 3.6)using TGA data (figure 3.7)

Average MWNT parameters:

Diameter: 40 nm

Length: 1.25 µm

Density[1]: 2.14 g/cm^3

Amount of MWNTs left over after TGA analysis (according to figure 3.7): 100 g-24.5 g=75.5 g

$$V = \pi r^2 l$$

$$V = \pi(2 \times 10^{-6}\ cm)^2(1.25 \times 10^{-4}\ cm)$$

$$V = 1.57 \times 10^{-15}\ cm^3$$

$$Mass\ per\ nanotube = \ 2.14\ g/cm^3 \times 1.57 \times 10^{-15} cm^3 = 3.36 \times 10^{-15}\ g$$

$$Amount\ of\ nanotubes\ in\ 75.5\ g = \frac{75.5\ g}{3.36 \times 10^{-15}\ g} = 2.247 \times 10^{16}$$

$$Moles\ of\ PyPS\ in\ 24.5\ g = \frac{24.5\ g}{1\ 858\ g/mol} = 1.319 \times 10^{-2}\ mol$$

[1]Density is a model estimation value based on theoretical values for MWNTs similar in dimension to those used in this work as calculated by Lu *et al.*{{176 Lu, Qi 2006}}

$$Number\ of\ PyPS\ molecules = 1.319 \times 10^{-2}\ mol \times 6.022 \times 10^{23} = 7.941 \times 10^{21}$$

$$\therefore there\ are\ \frac{7.941 \times 10^{21}\ PyPS}{2.247 \times 10^{16}\ MWNTs} = \mathbf{3.534 \times 10^{5}\ molecules\ of\ PyPS\ per\ MWNT}$$

Appendix D: Fibre diameter distributions of PS nanocomposite fibres

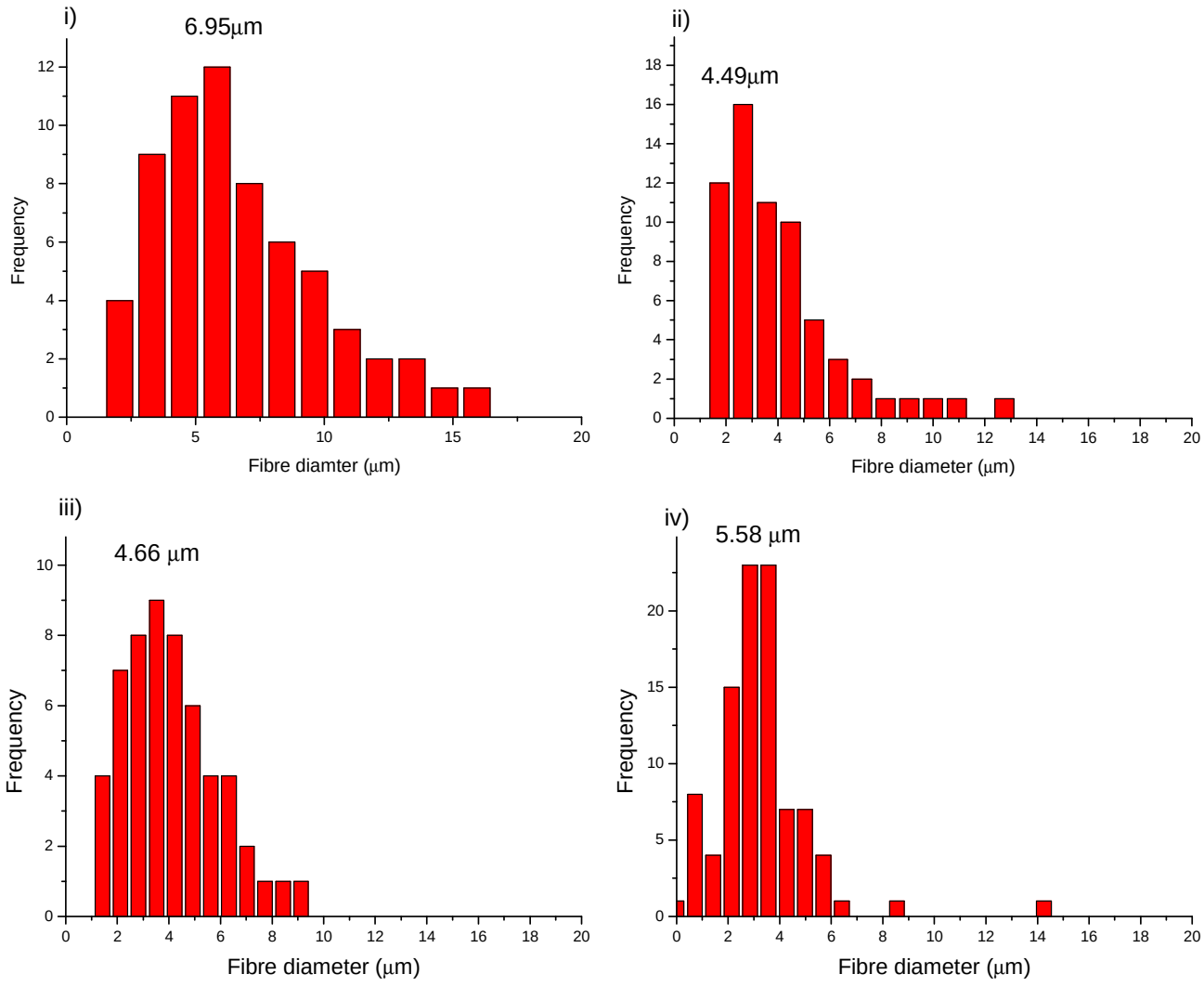

Figure D.1: Fibre diameter distribution with average diameter indicated of (i) PS homopolymer, (ii) 2wt % pristine MWNTs, (iii) 4 wt% pristine MWNTs and (iv) 6 wt% pristine MWNTs in a 20 w/v% PS in chloroform electrospinning solution.

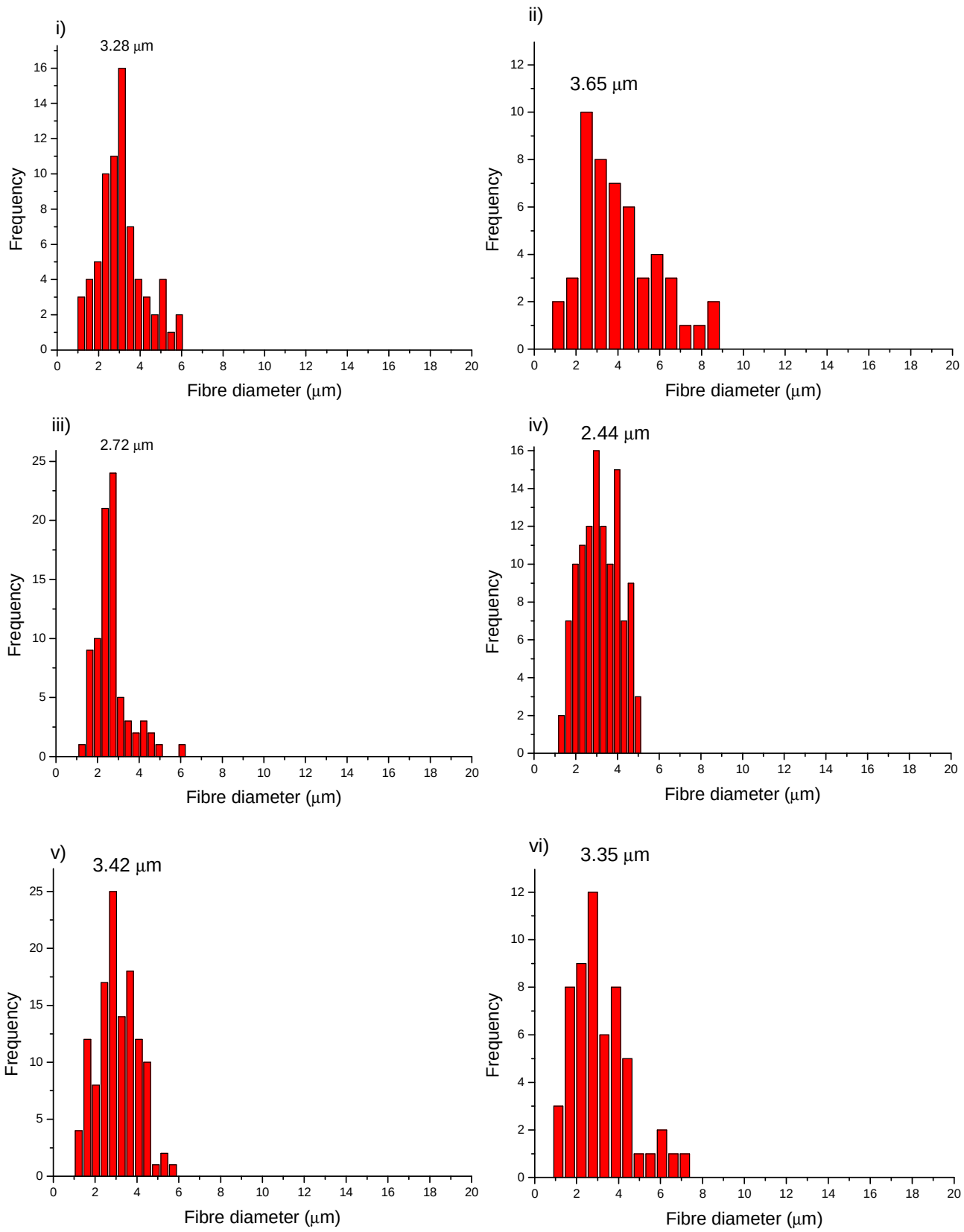

Figure D.2:Fibre diameter distribution with average diameter indicated of (i) 4 wt% MWNT-DIBTC-PS, (ii) 6 wt% MWNT-DIBTC-PS, (iii) 4 wt% MWNT/PyPS (DIBTC 5 000), (iv) 6 wt% MWNT/PyPS (DIBTC 5 000), (v) 4 wt% MWNT/PyPS (DIBTC 15 000) and (vi) MWNT/PyPS (DIBTC 15 000) in a 20 w/v% PS in chloroform electrospinning solution.

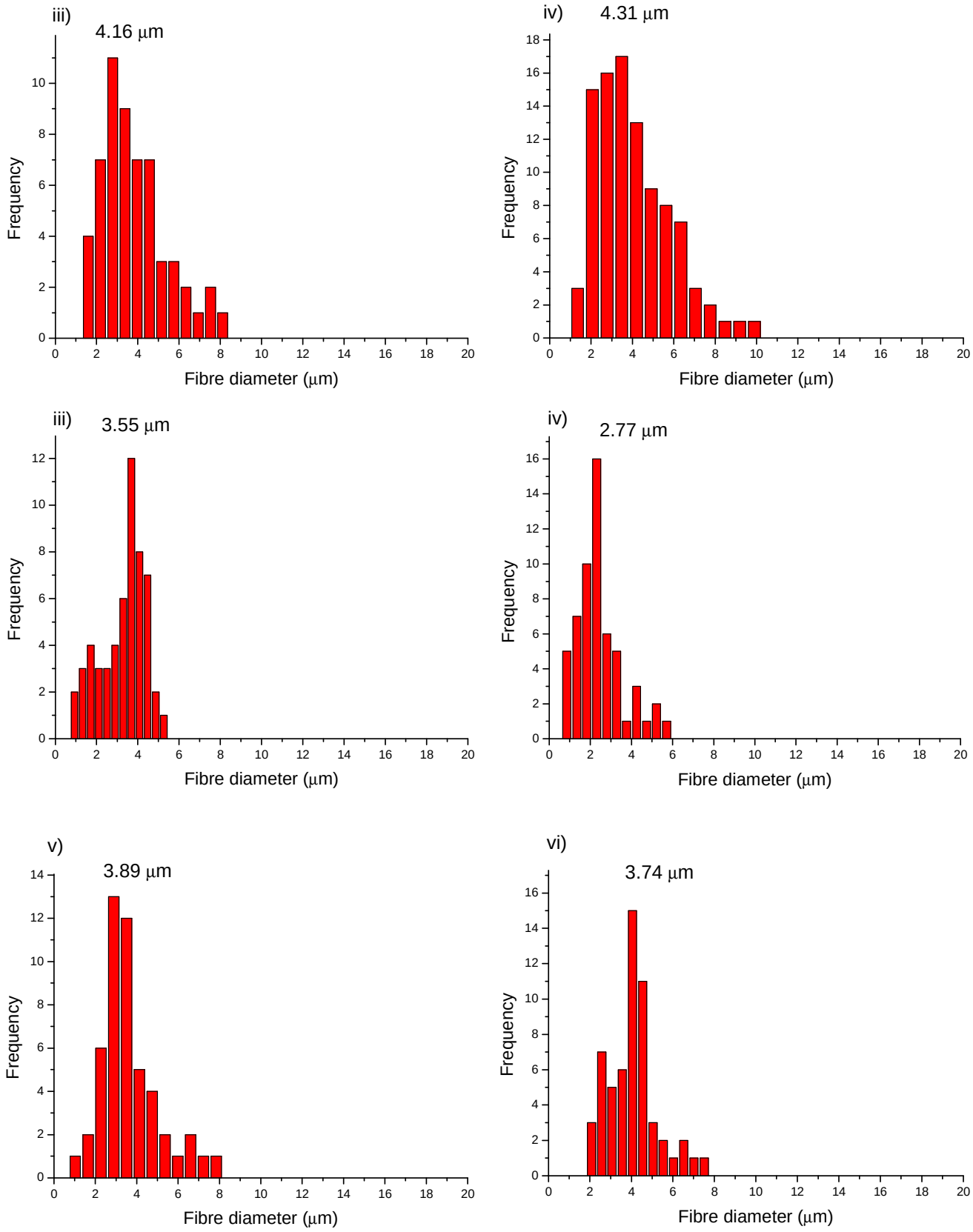

Figure D.3: Fibre diameter distribution with average diameter indicated of (i) 4 wt% MWNT-HEBrIB-PS, (ii) 6 wt% MWNT-HEBrIB-PS, (iii) 4 wt% MWNT/PyPS (HEBrIB 5 000), (iv) 6 wt% MWNT/PyPS (HEBrIB 5 000), (v) 4 wt% MWNT/PyPS (HEBrIB 15 000) and (vi) MWNT/PyPS(vi) MWNT/PyPS (HEBrIB 15 000) in a 20 w/v% PS in chloroform electrospinning solution.

Appendix E: SEM results of the PS nanocomposite prepared with 2 wt% pristine MWNTs

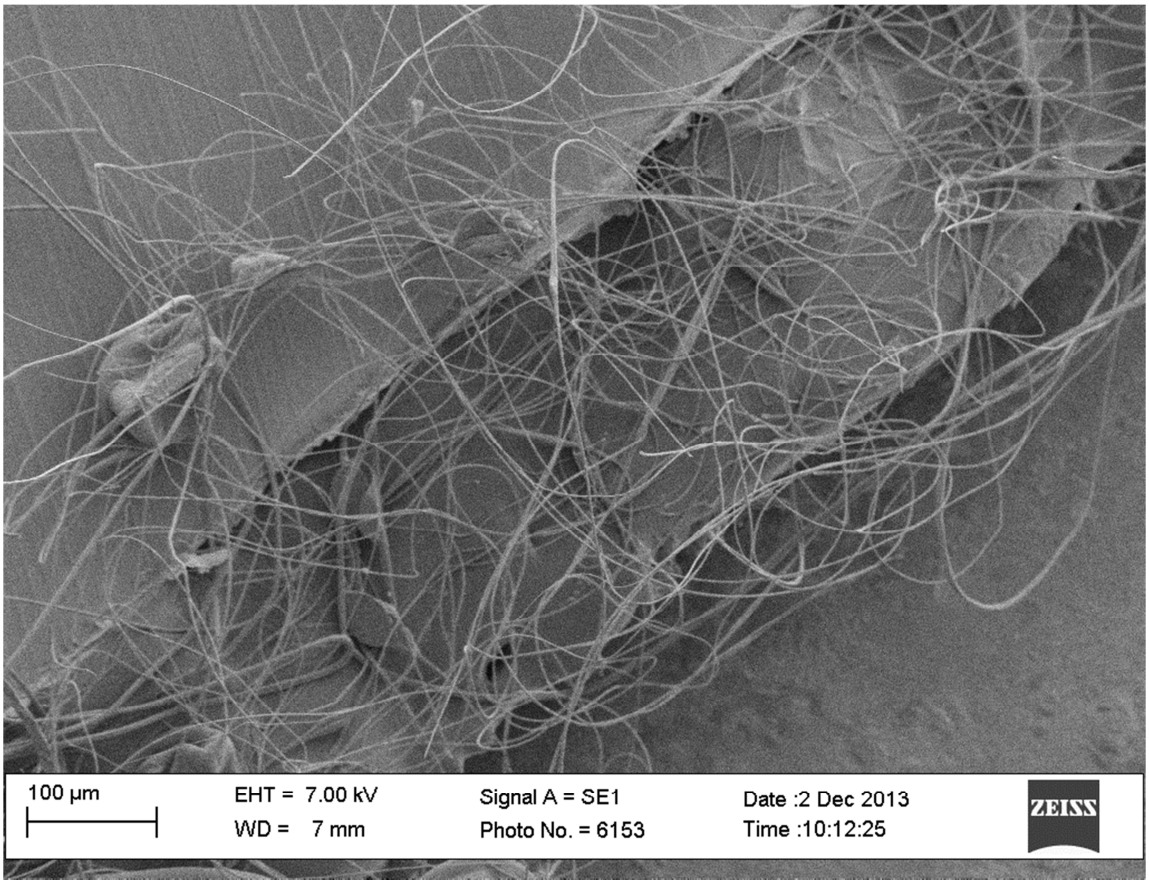

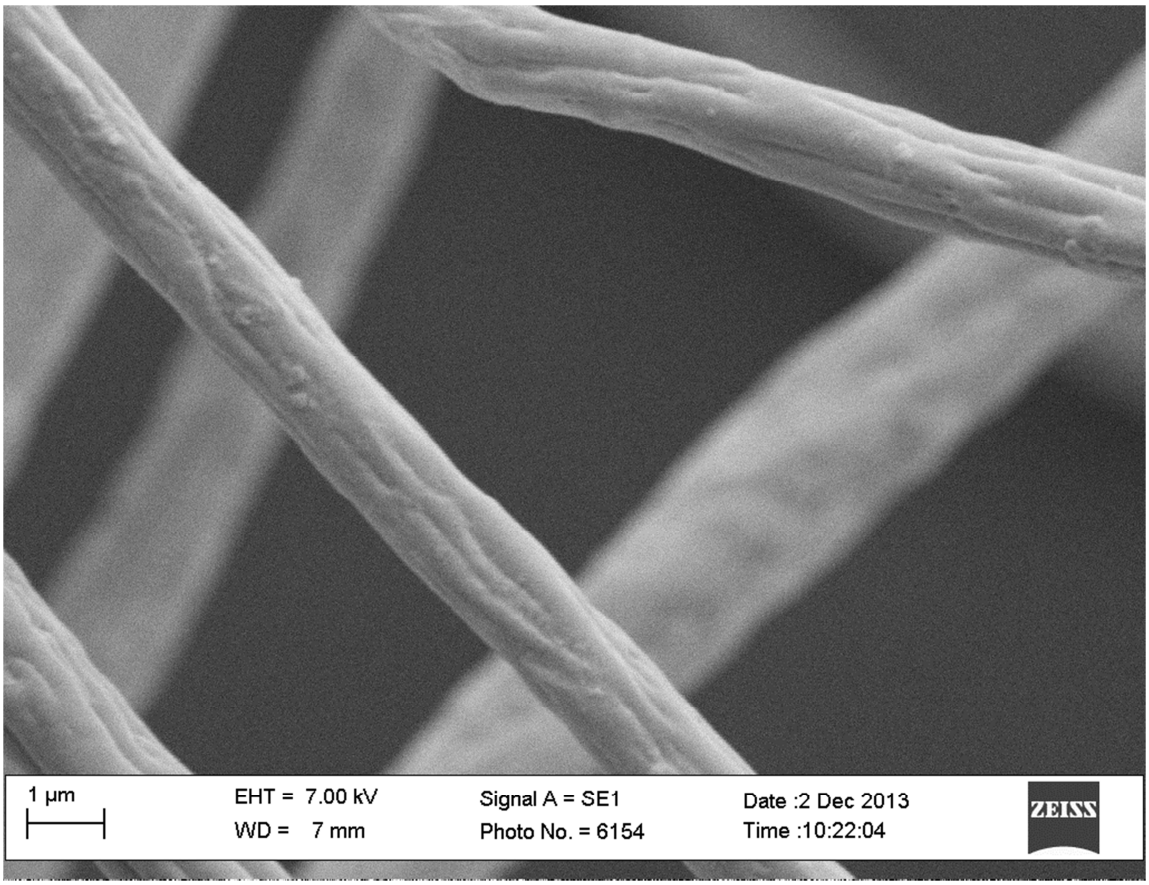

Appendix F: UV/Vis spectra for HEBrIB-Py-PS of chain length 15 000 g/mol

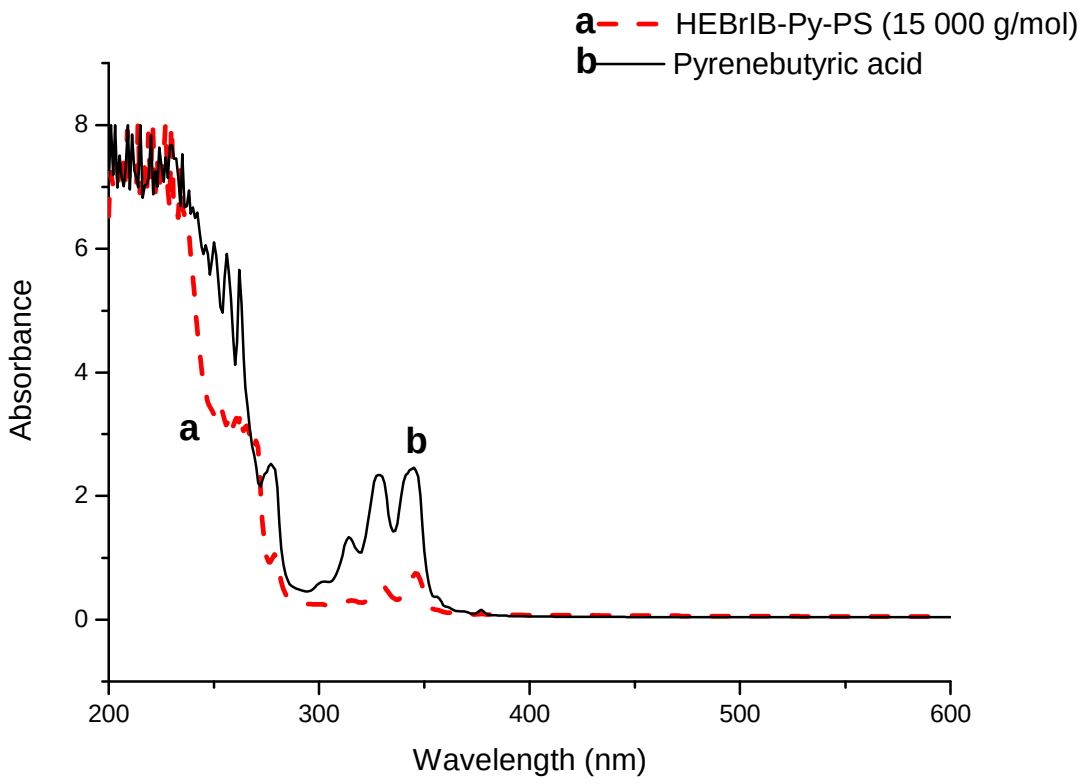

Figure D.1: UV/Vis spectrum of HEBrIB-Py-PS of 15 000 g/mol targeted styrene chain length in chloroform